Doctoral Dissertation

Designed Synthesis of Functional Hydrazone-Linked Covalent Organic Frameworks

Zhongping LI

Supervisor : Yuki NAGAO

Advanced Science and Technology

Japan Advanced Institute of Science and Technology

School of Materials Science

September 2019

Abstract

COFs are novel porous crystalline materials that are constructed by organic building units into regular structures with atomic precision through organic chemical reactions. Various reactions have been used to develop different type of COFs, such as B-O, C-N, and C-C linkages. The B-O based COFs were the first example of crystalline frameworks in 2005. Various structures and functions of these COFs were developed in the last few years. However, B-O based COFs are vulnerable in humid conditions, which limited their application in a wide field. To improve the stability of these frameworks, C-C and C-N linkage COFs including imine, azine, hydrazone, and phenazine-linked frameworks, were gradually developed. The C-C and C-N based COFs usually show excellent chemical stability. Compared to imine, azine and phenazine linkage, the hydrazone COFs have active N-H units on the walls, which can provide wide applications. For example, active N-H units of frameworks can enhance carbon dioxide uptake. Moreover, N atoms of N-H units showed sp^2 hybridization to give non-planar linkages for frameworks, which can weaken fluorescence quenching through strong π-π interaction that is derived from adjacent layers. The hydrazone linked COFs are useful to design light-emitting material and molecule sensing. This research work focused on the design and synthesis of functional hydrazone-linked COFs. Various novel hydrazone-linked COFs including hexagonal and tetragonal structure are synthesized. All new crystalline hydrazone-linked COFs were characterized using elemental analysis, Fourier transform infrared spectroscopy (FT IR), electronic absorption spectroscopy, field emission scanning electron microscopy (FE SEM), and powder X-ray diffraction measurements (PXRD).

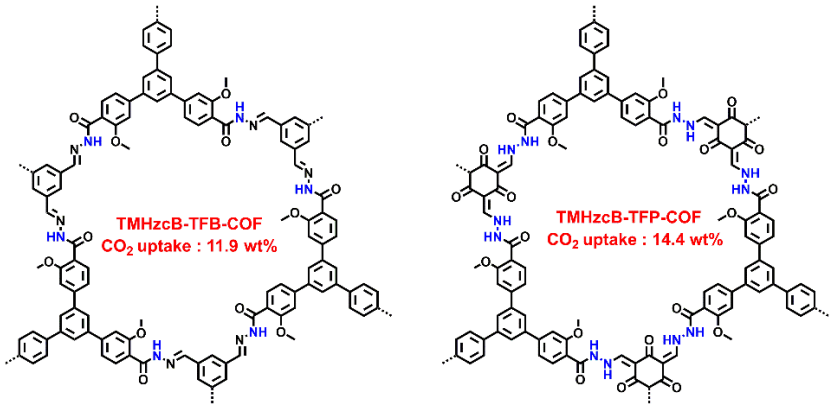

Scheme 1. TMHzcB-TFB-COF and TMHzcB-TFP-COF structures for carbon dioxide adsorption.

In chapter 2, the microporous hydrazone-linked COFs, TMHzcB-TFB-COF and TMHzcB-TFP-COF (Scheme 1) were synthesized through the condensation of 1,3,5-tris(3'-methoxy-4'-hydrazinecarbonylphenyl)benzene (TMHzcB) and 1,3,5-triformylbenzene (TFB)/triformylphloroglucinol (TFP) under solvothermal conditions. These COFs showed high crystallinity, permanent micropores, excellent thermal and chemical stability, and abundant heteroatom activated sites on the walls. Interestingly, TMHzcB-TFP-COF showed good carbon dioxide uptake of 14.4 wt% at 273 K and 1 bar.

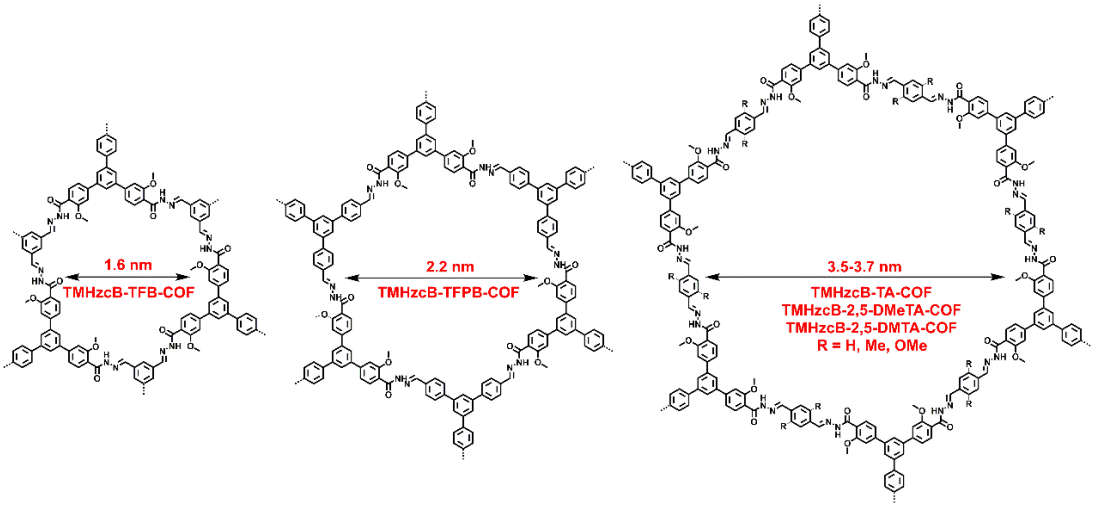

Scheme 2. Structure of light-emitting hydrazone-linked COFs.

In chapter 3, a series of light-emitting hydrazone-linked COFs was successfully synthesized (Scheme 2). These COFs not only showed excellent porosity but also displayed good stability in organic solvents, water, acid and base conditions for 1 day at the room temperature. The pore size of

hydrazone-linked COFs can be tunable from micropore (1.3 nm) to mesopore (3.7 nm) through changing different symmetrical linkers or knots. The light-emitting activity of COFs can be improved through introducing flexible building units or functional active groups decoration including methoxy and methyl groups. The luminescence can be tunable from blue to green luminescence as a result. Notably, COF-TMHzcB-2,5-DMeTA showed the highest fluorescence quantum yield over 19.5 % at solid state, which is higher than most reported azine, imine, and hydrazone based COFs.

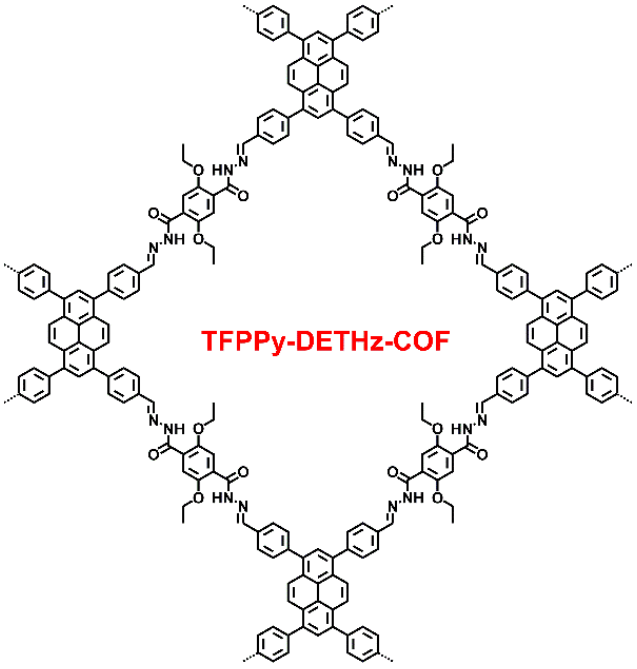

Scheme 3. Structure of TFPPy-DETHz-COF.

In chapter 4, hydrazone-linked COF, TFPPy-DETHz-COF (Scheme 3), was successfully constructed through the Schiff-base condensation reaction under solvothermal conditions. The N-H bond in linkage on the walls can be deprotonated by fluoride anion via acid-base reaction to form an anionic species, which can eliminate the nitrogen-related fluorescence quenching pathway. The addition of fluoride anion eliminates the photoinduced electron transfer pathway and directly improves the light-emitting activity. Surprisingly, the emission is switched on in the presence of fluoride anion and its intensity is enhanced in a linear proportion to the amount of fluoride anion. The absolute fluorescence quantum yield increases to 17%, which is 3.8-fold as high as that

of as-synthesized TFPPy-DETHz-COF. In contrast, other halogen anions, including chloride, bromide, and iodide, retain inactive. The detection limit of fluoride anions can be down to a ppb level.

Various novel hydrazone-linked COFs with high porosity, crystallinity, and stability, including hexagonal and tetragonal structure, can be designed and synthesized. The pore size of COFs can be adjustable from micropores (1.6 nm) and mesopores (3.7 nm), which also enriches the diversity of the structure. Moreover, fluorescence COFs showed the highest quantum yield than most reported COFs through changing flexible units and auxiliary chromophore. I also used the pinpoint surgery on the N−H unit of the hydrazone-linked COFs and the first example of COFs for anion sensing. The investigated results displayed in this thesis demonstrate functional hydrazone-linked COFs that open a new phase for not only high adsorptive media but also light-emitting materials for chemical sensing. The active N-H sites can be possibly applied in the removal and separation of molecules through hydrogen bond interaction in the future.

Keyword: Covalent organic frameworks, carbon dioxide, light-emitting, pinpoint surgery and anion sensing.

Table of Contents

Table of Contents

Chapter 1

General Introduction

1.1 Covalent organic frameworks

Covalent organic frameworks (COFs) are a new class of crystalline porous polymers that enable the elaborate integration of organic building blocks into regular structures with atomic precision by strong covalent bonds. Since boronate-ester linked COFs have been successfully designed and synthesized in 2005,[1] large amounts of COFs have been developed with different topological and chemical structures. Comparing to traditional crystalline porous polymers, such as metal organic frameworks (MOFs) or coordination polymers (CPs), COFs are constructed through strong covalent bonds with light elements, such as boron, carbon, oxygen, hydrogen and nitrogen, which endow COFs with various merits including low densities, permanent porosity and high thermal stability.[1-3] The skeleton and pore of COFs can be precisely pre-designed into various geometrical structures, while the porous structure can also be further tuned by using post-synthesis methods. According to the configuration of frameworks, COFs can be classified into two- (2D) or three-dimensional (3D) structures. In 2D COFs, the covalently bonded growth of frameworks is restricted over 2D to form sheets, which stack to form layered structures and to construct periodically aligned π columns. In contrary, 3D COFs develop their frameworks via tetrahedral knots into a 3D extended structure. In addition, 2D COFs are usually pre-designed and synthesized to achieve different structures and functions upon the use of different building blocks. Over the past decade, COFs have been quickly explored and they showed a great potential in applications, such as gas storage and separation, catalysis, chemical sensors, proton conductivity, energy conversion and storage, optoelectronics and semiconductors.[2-7]

1.2 Design principles

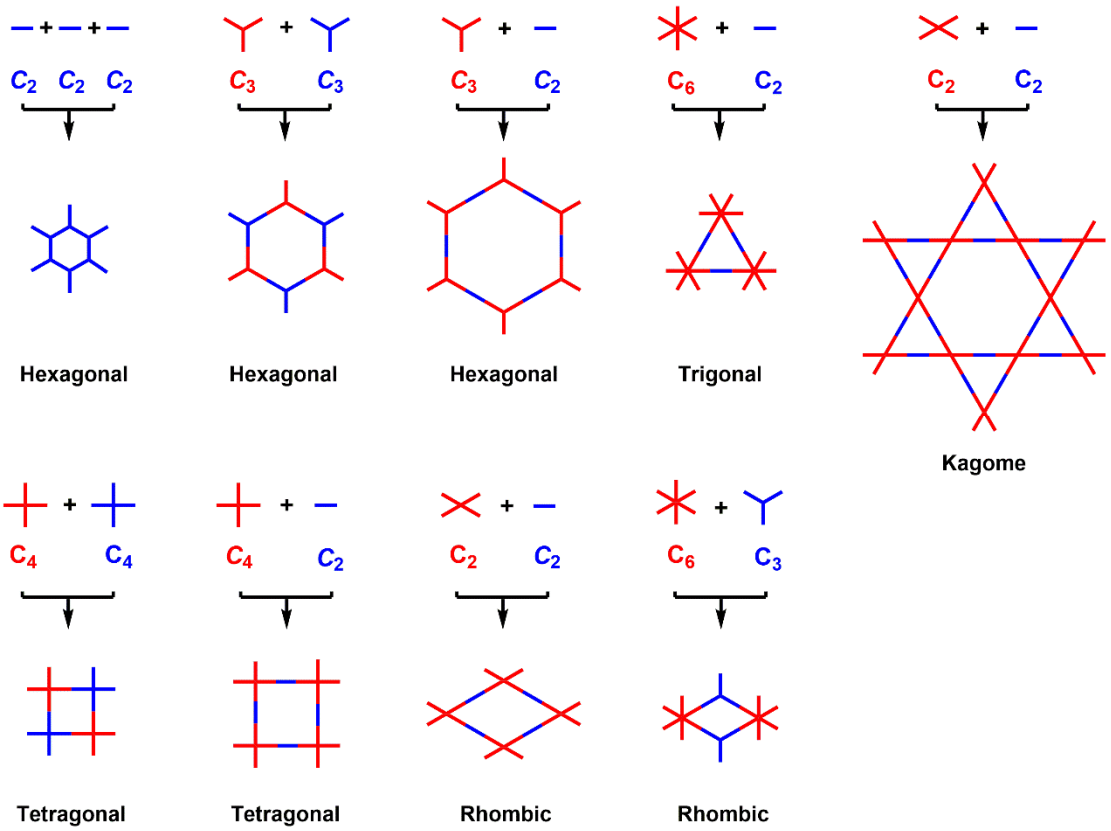

Figure 1. Topology diagram for designing 2D COFs.[2-3, 5]

The skeleton and pore of COFs can be precisely pre-designed using topology diagram-directed formation of polygon skeletons (Figure 1). This is a unique feature of COFs. With great efforts on design and synthesis, COFs with various topologies have been developed. Especially, the geometry of building blocks should be in an appropriate combination that enables the extension of frameworks and provides COFs with highly ordered structures.[3-5] The hexagonal structures can be designed via a combination of C_2 + C_2 + C_2, or C_3 + C_2 symmetric building blocks.[1,8] A C_3 + C_3 combination can also offer a hexagonal 2D COFs.[9-13] The combination of C_6 + C_2 symmetric units can achieve trigonal COFs.[14-15] Tetragonal structures can be designed through the geometry combination of C_4 + C_2 or C_4 + C_4 building blocks.[16-20] A rhombic skeleton can be designed with the combination of C_6 + C_3-symmetric building units.[21] The combination of C_2 + C_2 building blocks is unique as it can yield two

different topology; one is the rhombic topology with only one kind of pore[22-24] and another is the Kagome-type dual-pore topology that consists of one central hexagonal mesopore surrounded by six trigonal small pores.[25-27]

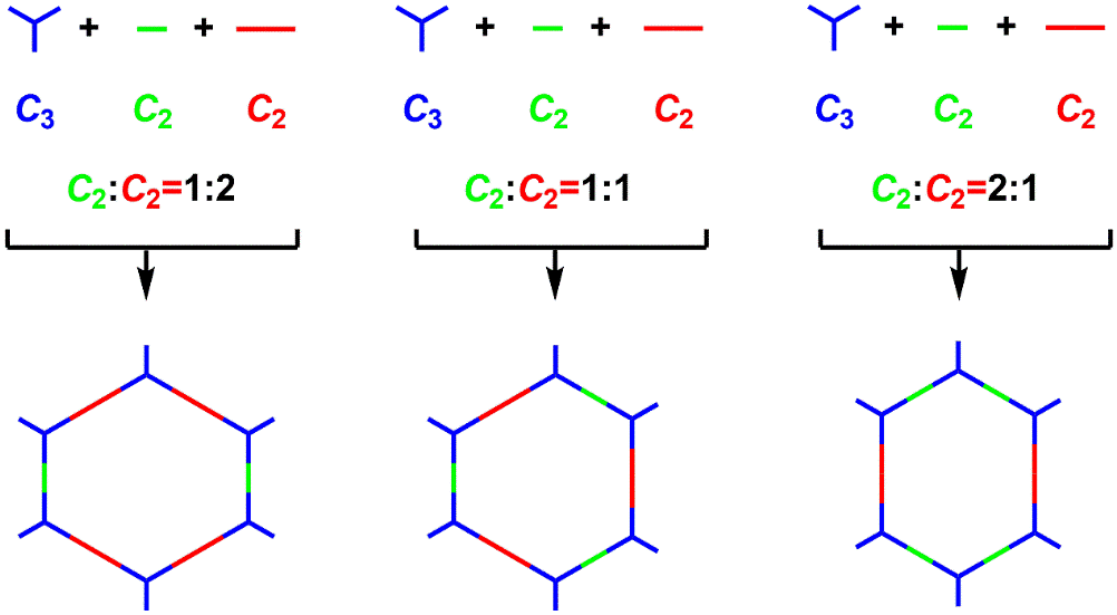

Figure 2. Multi-component (MC) topology diagram for designing hexagonal COFs with different ratio of two building blocks.[28]

The findings of multiple-component topology diagram for the design of skeleton and pore greatly increase the diversity of COFs.[28] For example, with one C_3-symmetric building block as knot and two C_2-symmetric linkers can yield three different hexagonal COFs by using different ratios (1/2, 1/1, or 2/1) of the two linkers (Figure 2).

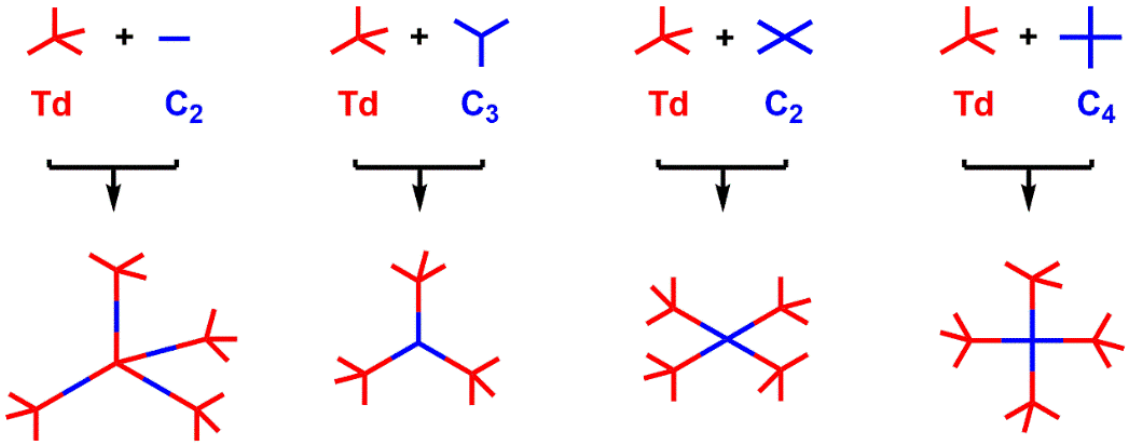

Figure 3. Topology diagram for designing 3D COFs.[29-33]

The tetrahedral units (T_d) is an essential unit in order to design 3D COFs.

Upon combination with other building blocks with C_2, C_4 or C_3 geometries, a variety of 3D COFs with different topologies have been designed.[29-33] The existence of T_d symmetric building blocks directs the growth of 3D COFs other than 2D COFs.

In short, topology diagram provides the base of the COF field as it determines not only the dimensionalities (2D or 3D) but also defines both skeleton and pore. The diversity of geometry combinations is the primary factor that offers abundant structures of skeleton and pore, which further leads to the development of a molecular platform for designing multifunctional frameworks.

1.3 Synthetic reaction

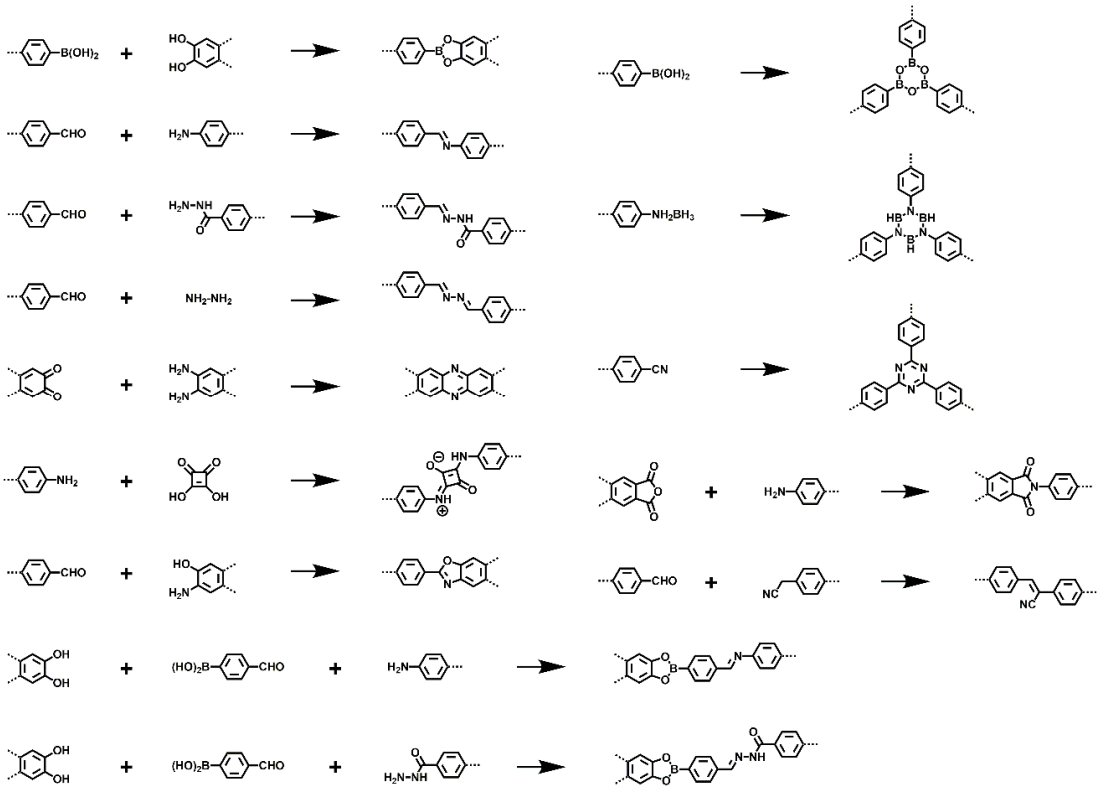

Figure 4. Diversity of linkages for directly constructing COFs.

In order to build COFs with high ordered structures, reversible reactions are typically employed as they endow the condensation systems with self-healing ability to repair structural defects.[3-8] To date, a variety of reversible reactions

have been developed for the synthesis of COFs. For example, boroxine, boronate-ester, borosilicate, triazine, imine, hydrozone, borazine, squaraine, azine, phenazine, imide, double-stage and sp^2-carbon linkages have been explored for the synthesis of crystalline porous COFs (Figure 4).

Building blocks with boronic acid groups can be either self-condensed or condense with catechol to afford boroxine- and boronate ester-linked COFs.[1,8] These reactions are highly reversible, leading to the generation of COFs with well-ordered structures. The self-healing process is helpful for achieving a high Brunauer-Emmett-Teller (BET) surface area.[8,14-18] Nevertheless, these COFs are usually unstable in the presence of water, acids or base owing to the decomposition of boronate ester and boroxine linkages.

Schiff base reactions have been developed for the synthesis of COFs through the condensation of aldehyde and amine building blocks. Nitrogen-containing linkages, including imine,[10-13,19-31] azine,[20, 36-38] hydraozne,[34-35] and phenazine[38] have also been explored for the synthesis of various COFs. Condensation of hydrazine and aldehyde yields azine-linked COFs, which usually have small pore size owing to the shortest linker of hydrazine.[20, 36-37] The hydrazone-linked COFs can be synthesized from the condensation of aromatic hydrazines with aldehydes.[34-35] The linkages including boronate ester, boroxine, imine and hydrazine, have been developed for the construction of COFs with different topologies, e.g., hexagonal, tetragonal and rhombus, to yield materials with high crystallinity and high porosity.[39] Phenazine linkage formed by ring-fusion reaction of quinone and diamine offers fully π conjugated COFs that are inaccessible to other linkages. The phenazine-linked COFs show high crystallinity and stability.[40] Benzoxazole linkage has been shown for the synthesis of stable COFs through Schiff base followed by oxazole ring formation reactions. [41]

Owing to the poor reversibility of imide linkage, imide-linked COFs have been constructed through the condensation of amines and dianhydrides at high temperatures, which may enable self-repair of defects.[42] The

self-condensation of nitrile groups in the presence of $ZnCl_2$ as catalyst at high temperature over 400 °C can yield covalent triazine frameworks (CTFs).[43] Although CTFs possess excellent thermal and chemical stability, they usually lack crystallinity.

Condensation of squaric acid and amines enables the synthesis of squaraine-linkage COFs that consists of zwitterion skeleton.[44] The condensation reaction between diol and trialkyl borate in the presence of base catalyst forms ionic spiroborate-linked COFs.[45]

The Knoevenagel polycondensation reaction of 1,4-phenylene diacetonitrile and aromatic aldehyde yields sp^2 carbon-conjugated covalent organic frameworks (sp^2c-COFs).[46-48] The sp^2c-COF features fully sp^2-carbon-linked skeletons that are ultra-high stable under various conditions.

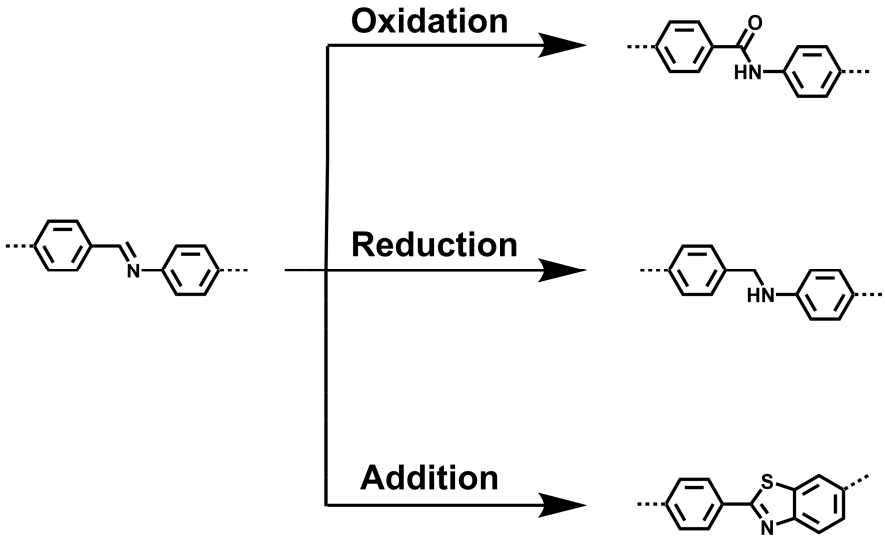

Figure 5. Transformation of imine linkages through post-synthesis reactions.[49-51]

Some linkages are quite difficult to be directly synthesized because there are lots of chemical reactions that do not allow a self-healing process. Since imine linkage can be further transformed into other linkages, the imine-linked COFs have been converted into corresponding COFs with different linkages including amide and benzothiazole (Figure 5).[49-51]

Various reversible reactions in organic chemistry can enrich the linkages of COFs, while combination of different building units enables the control over

pore shape and size. These advantages offer a great potential in the synthesis of COFs and the exploration of their functions. In order to synthesize high quality COF crystallites, many reaction factors, including the concentration of building units, type and amount of catalyst, reaction time and temperature, have to be carefully screened; quality control of COFs has not been seriously considered in many literatures.

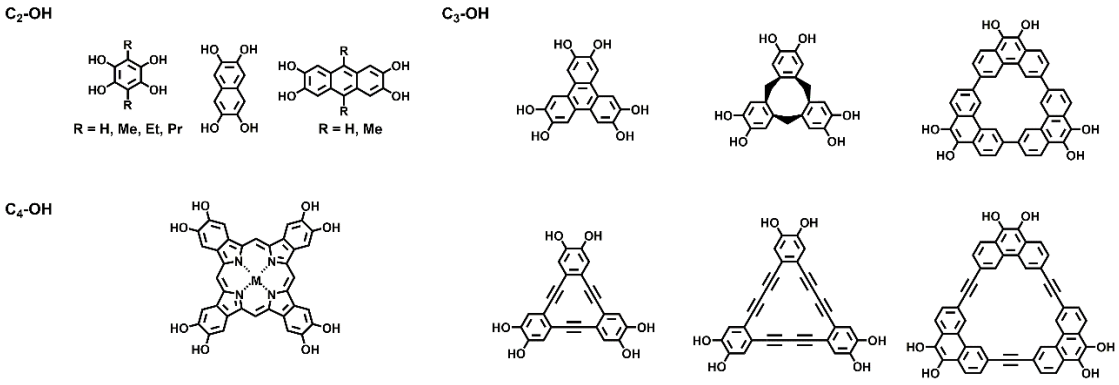

Figure 6. Typical building blocks with hydroxy group.

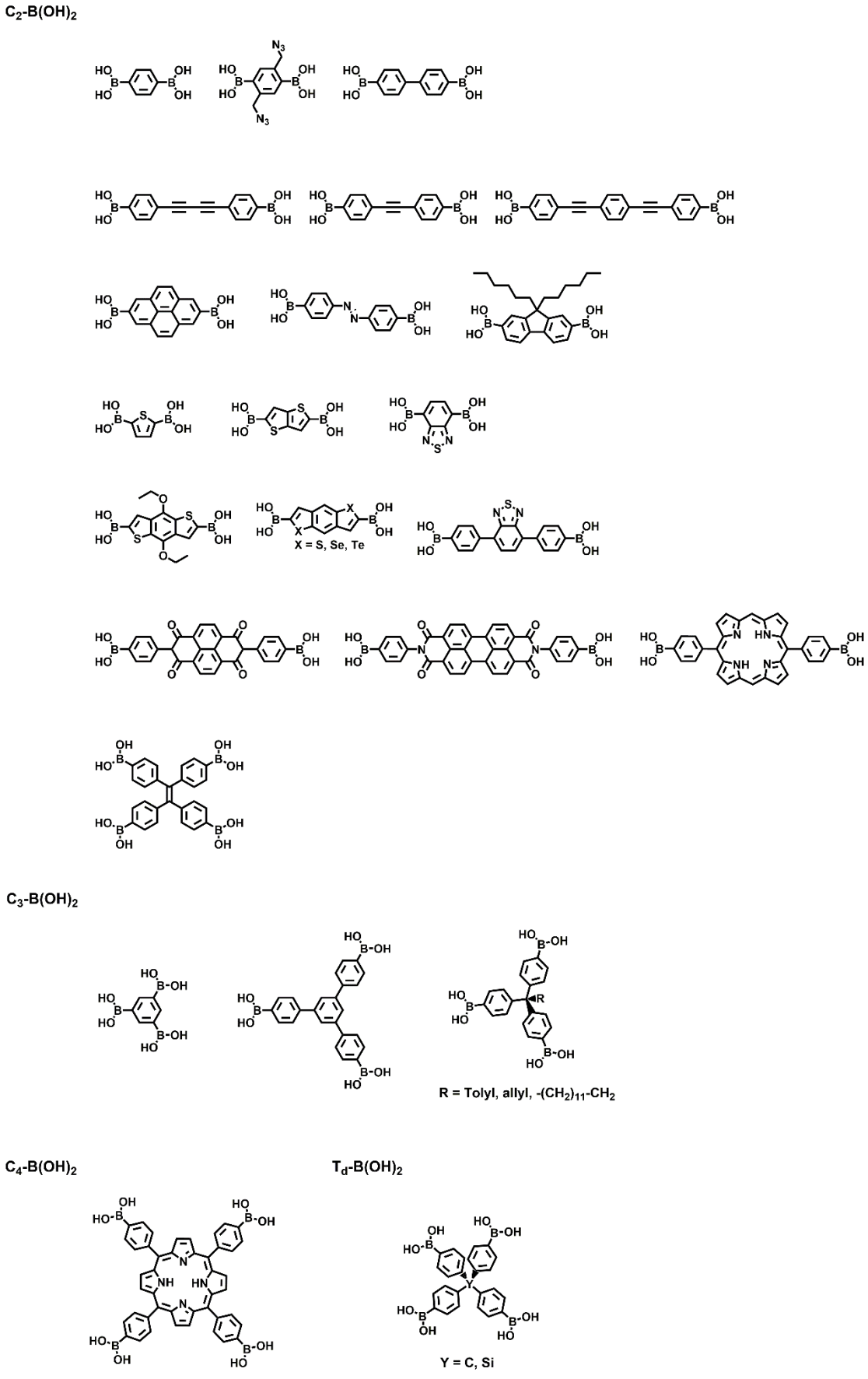

Figure 7. Typical building blocks with boric acid units.

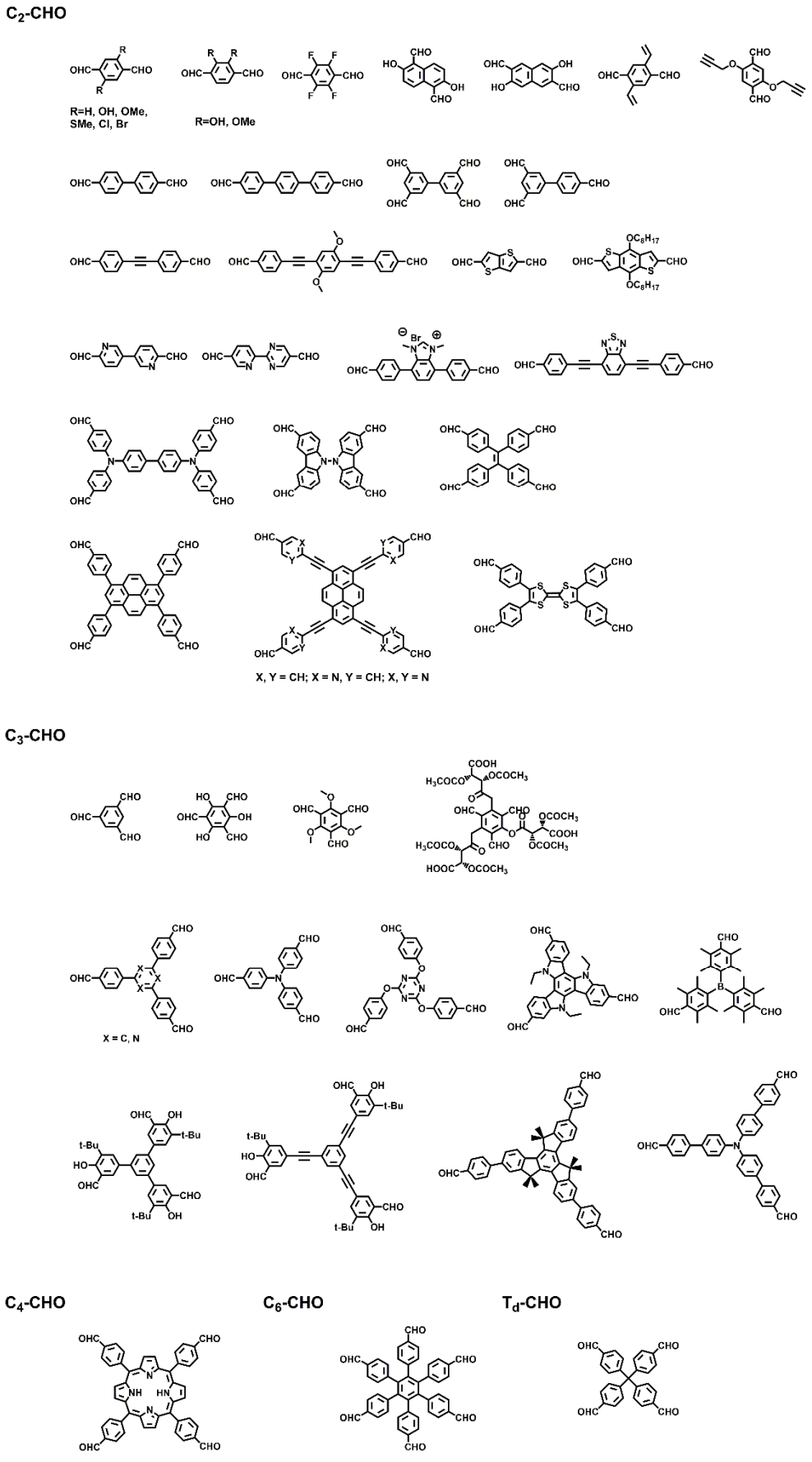

Figure 8. Typical building blocks with aldehyde group.

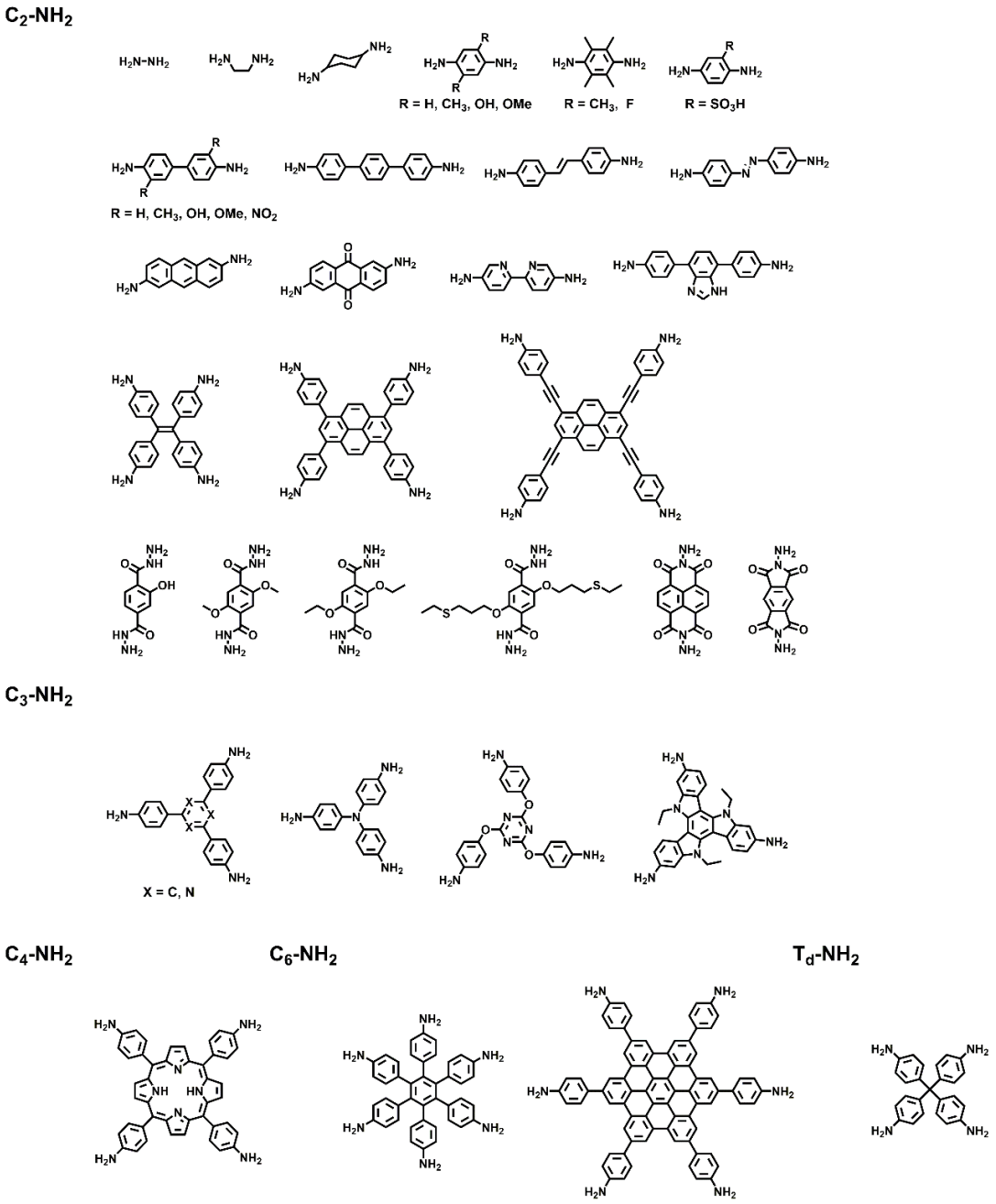

Figure 9. Typical building blocks with amino-group.

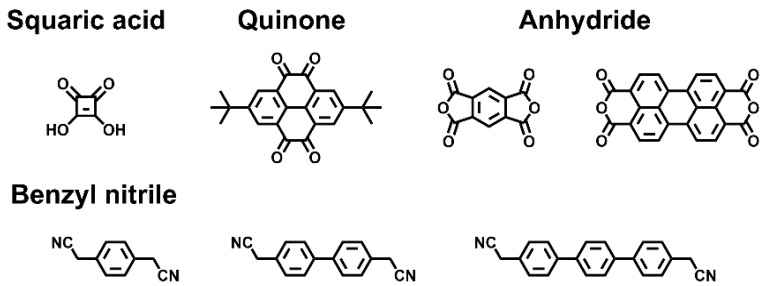

Figure 10. Typical building blocks with square acid, quinone, anhydride and benzyl nitrile group.

1.4 Synthetic methods

The synthesis of COFs usually requires a solvothermal condition, thus thermodynamic equilibrium is crucial to the synthesis of high-quality crystalline COFs. In detail, the reaction conditions, including solvent, catalyst, temperature and pressure, should be totally considered in the synthetic package. Microwave method has been developed for shortening the solvothermal reactions. Different from bulk synthesis, substrates (e.g., metal surface or graphene) have been used for growing COF monolayers or films.

1.4.1 Solvothermal synthesis

In 2005, Yaghi and coworkers designed and synthesized the first example of COFs with boronate ester and boroxine linkages under solvothermal conditions.[1] The protocol for a solvothermal synthesis is shown as follow. A Pyrex vial was added with monomers and solvents, catalyst, and the resulting mixture was degassed through freeze–pump–thaw cycles. The vial was sealed under low pressure and kept at a designated temperature (25-180 °C) for the growth of crystalline COFs as a precipitate in the reaction system.

Selecting a suitable solvent is important as the solvent affects the self-healing, crystal nucleation and lattice growth during the condensation process.[36] COFs have been produced in various solvents such as *o*-dichlorobenzene (o-DCB), 1-methyl-2-pyrrolidone (NMP), dimethylacetamide (DMAc), dimethylformamide (DMF), tetrahydrofuran (THF), 1,4-dioxane, 1,3,5-trimethylbenzene (mesitylene), *p*-xylene, *n*-butanol, ethanol and toluene. For example, azine-linked COF (ACOF-1) can be constructed through hydrazine and 1,3,5-triformylbenzene in many solvents including 1,4-dioxane, the mixture of 1,4-dioxane and mesitylene, mesitylene and ethanol, while the dioxane system yields the highest BET surface area and crystallinity.[36]

1.4.2 Microwave synthesis

To synthesize high quality frameworks, microwave-assisted solvothermal method was reported by Wei and co-workers.[52] Microwave-assisted solvothermal synthesis has some inherent merits compared to traditional solvothermal method. For example, it provides a rapid way to produce high crystalline COFs, whose porosity is usually higher than that of the one obtained under solvothermal conditions. In a word, microwave-assisted solvothermal synthesis is an effective method to produce high-quality COFs.

1.4.3 Ionothermal synthesis

In 2008, Thomas and co-workers reported that ionothermal synthesis of crystalline CTFs.[53] The cyano groups of aromatic units can be cyclization to yield a crystalline framework in molten zinc chloride at a temperature over 400 °C. In this case, the molten zinc chloride serves as solvent as well as catalyst that promotes the partially reversible trimerization reaction. However, the harsh reaction conditions limit its generality for synthesizing high crystalline CTFs.

1.4.4 Mechanochemical synthesis

The mechanochemiscal (MC) method was used to construct various COFs with thermal and chemical stabilty.[54] The new method can provide solvent-free, rapid and room-temperature synthesis. However, COFs that were constructed through this method usually showed lower porosity and crystallinity than that were formed by solvothermal synthesis. The reason is the lack of self-healing ability during the polymerization in MC method. The method also needs further study and improvement for the synthesis of COFs.

1.4.5 Surface-supported synthesis

COFs are usually bulk materials that are not soluble in any organic solvents and water. Hence, COFs powders are very difficult to be fabricated into films

and devices for application. COFs thin films on the surface of substrate can solve these perplex. Many efforts have been devoted to grow COF films on different substrates. Single layer graphene (SLG) was exploited to produce COF-5 thin films.[55] The crystalline structure of COF-5 films was confirmed by x-ray diffraction analysis. The thickness of COF-5 films can be controllable at level of 195 ± 20 nm as determined by FE SEM images.

2D COF films with controllable thickness can be also achieved through vapor-assisted conversion.[56] On glass substrate, the thickness of 2D COF films can be tuned from a few hundred nanometres to several microns. This approach can facilitate the synthesis of COF thin films for applications. Surface-supported synthesis has demonstrated for the synthesis of COF materials with different structures.

1.5 Functional application

COFs allow the precise integration of organic units to create predesigned skeleton, which provides a platform for designing structured organic materials and exploring functions. With the broad diversity of building units, linkages and pores, COFs can be developed to achieve various specific functions.

With the above structural features that are inaccessible to other materials, COFs have been developed to show various functions including semiconducting, heterogeneous catalysis, gas adsorption, light emitting and molecular sensing, electron transfer, energy storage etc. Here I selected the topics of catalysis, gas adsorption, light emitting and sensing.

1.5.1 Heterogeneous catalysis

Catalysts are important for organic transformation to synthesize daily products, chemical intermediates and medicines. Over half century, heterogeneous catalysts have attracted a wide attention because of their easy separation from the reaction mixture and recyclability. Many COFs are stable in water and organic solvents, which provide a possibility of developing

heterogeneous catalysts. The channel environment can be also predesigned and is easy to be further modified. There are three strategies in designing COFs as heterogeneous catalysts, including (1) COFs skeleton design, (2) COFs loaded with metals and (3) post-modification of COFs pores.

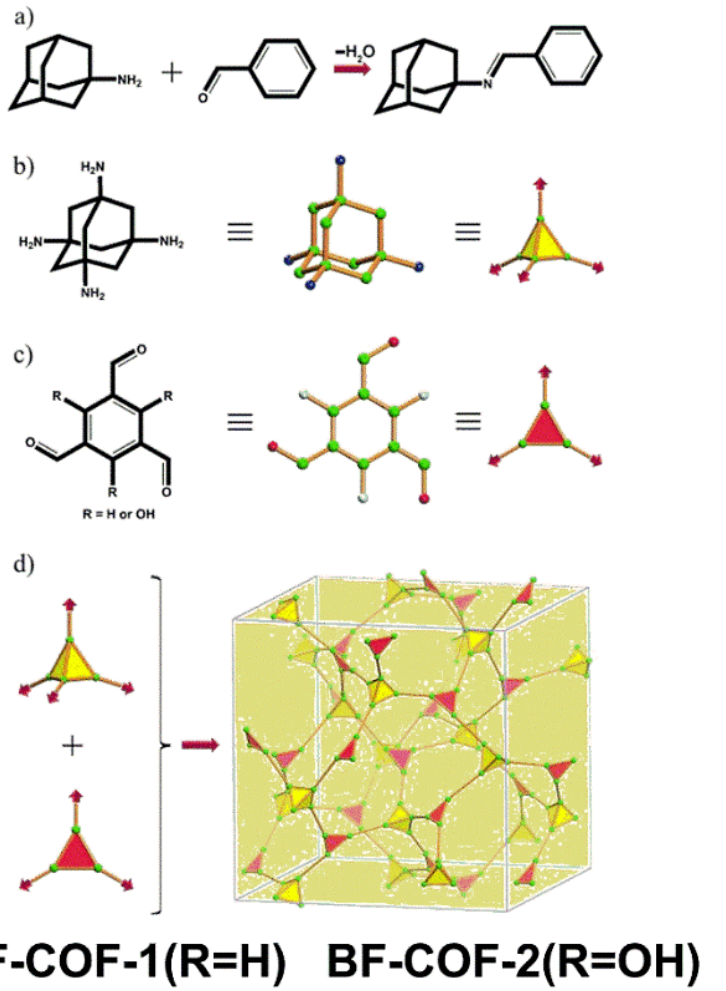

Figure 11. Design of 3D microporous COFs. (a) Model reaction of 1-adamantanamine and benzaldehyde to synthesize N-(1-adamantyl) benzaldehyde imine. (b) Structure of 1,3,5,7-tetraaminoadamantane (TAA) as a tetrahedral building unit. (c) Structure of 1,3,5-triformylbenzene (R = H, TFB) or triformylphloroglucinol (R = OH, TFP) as a triangular building unit. (d) Condensation of tetrahedral and triangular building units to give a 3D network with the symbol ctn (BF-COF-1 or BF-COF-2).[57]

Microporous 3D COFs, BF-COF-1 and BF-COF-2, were constructed by using tetrahedral alkyl amine, 1,3,5,7-tetraaminoadamantane (TAA), combined with 1,3,5triformylbenzene or triformylphloroglucinol.[57] Using the nitrogen atoms of C=N linkages as base sites, BF-COFs are active to catalyze

Knoevenagel reactions (96% conversion for BF-COF-1 and 98% for BF-COF-2). Moreover, these two COFs with small pores (8.3 Å for BF-COF-1 and 8.1 Å for BF-COF-2) are only accessible to small substrates, such as benzaldehyde (6.1 × 8.7 Å), malononitrile (4.5 × 6.9 Å), leading to a size selectivity.

Imine-linked COFs contain nitrogen atoms that can coordinate with metal species to form catalytic sites. For example, Wang and co-authors transformed COF-LZU1.[58] COF-LZU-1@Pd by coordinating Pd (II) ions at the imine bonds. It can catalyse Suzuki-Miyaura coupling reaction effectively. The open 1D channel of COF-LZU-1@Pd promises the reaction between the substrate and reactant. COF-LZU-1@Pd did not show obvious loss in performance after several cycles.

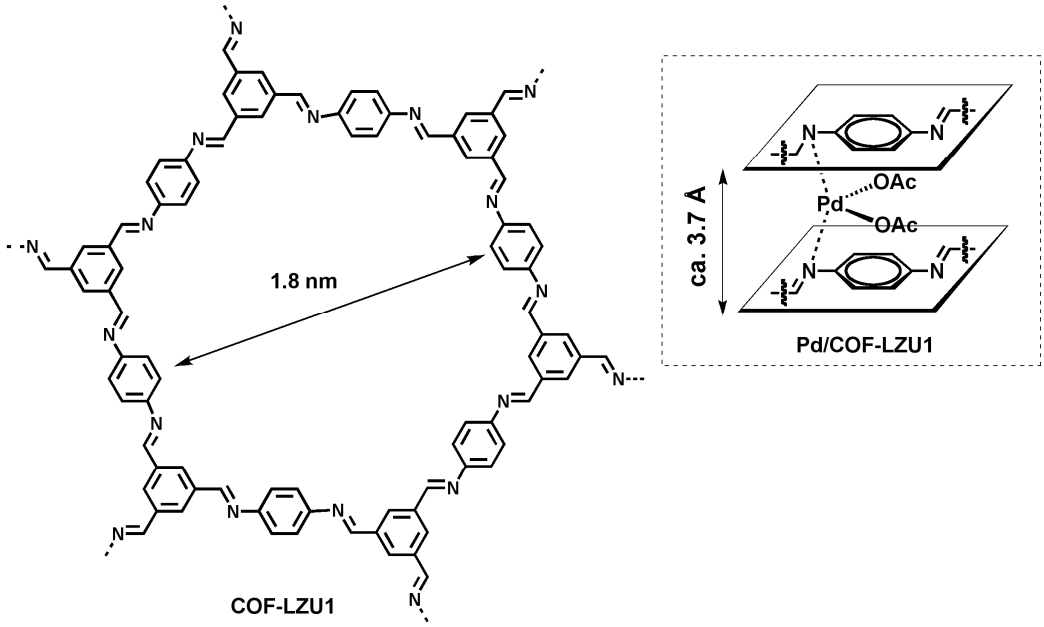

Figure 12. Structure of COF-LZU1 and Pd/COF-LZU1.[58]

COFs with metal nanoparticles in the pores have been synthesized as catalysts. In situ generation of Pd nanoparticles in imine-linked COFs with predesigned Pd-anchoring bipyridine building blocks enables the synthesis of heterogeneous catalyst Pd@TpBpy COF.[59] The Pd@TpBpy COF can be used as heterogeneous catalyst for the synthesis of biologically and

pharmaceutically important 2-substituted benzofurans from 2-bromophenols and terminal alkynes via a tandem process with high catalytic performance and turnover number up to 1101 (Figure 13).

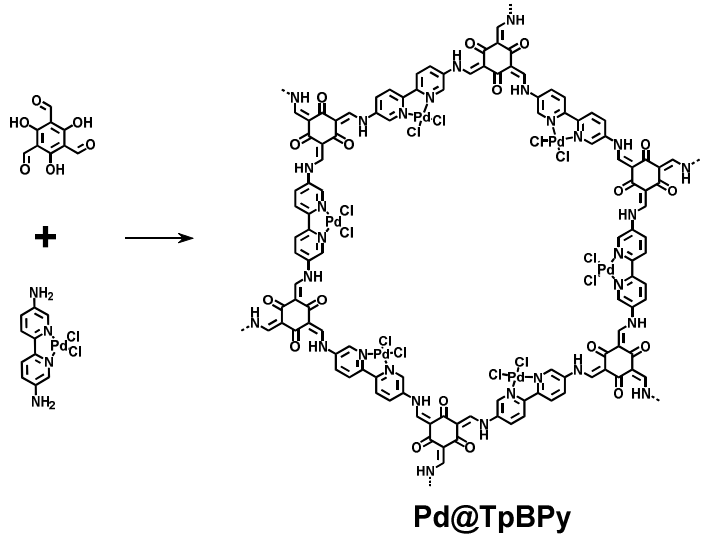

Figure 13. Synthesis and design of TpBpy COF.[59]

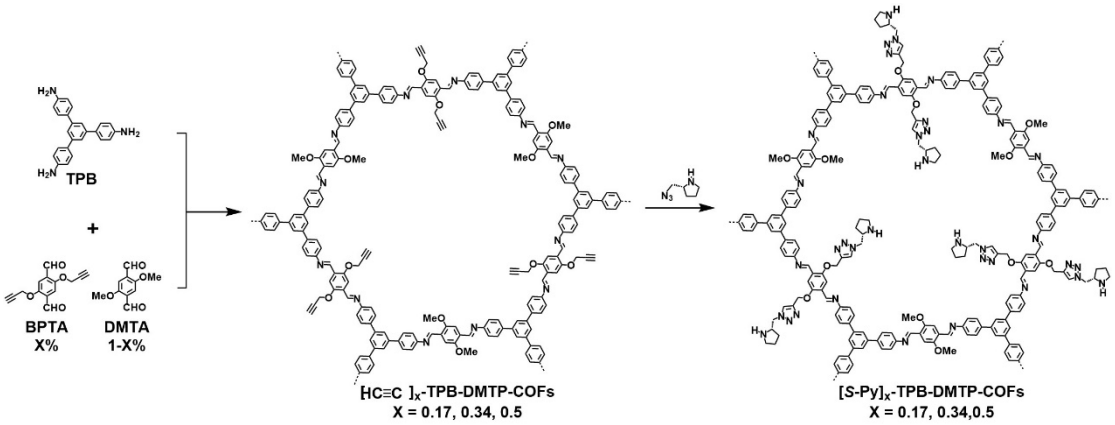

Figure 14. Introduce catalytic sites into skeleton through pore surface engineering.[60]

Pore surface engineering of COFs enables a precise and effective introduction of active sites into the skeletons to catalyze various chemical reactions. Our group has demonstrated the strategy for the first time.[60] We designed and synthesized TPB-DMTP-COF (Figure 14) with a high porosity (BET surface area of 2105 m^2 g^{-1}) and a pore size of 3.26 nm. It exhibits excellent chemical stability in harsh conditions such as aqueous NaOH (14 M) and HCl (12 M) solutions and boiling water. Its high stability originates from the

methoxy groups that trigger resonance effects to soften the polarization of C=N bonds. Methoxy groups can reduce the charge repulsions between the layers. With these advantages of TPB-DMTP-COF, we synthesized a series of chiral [(S)-Py]x-TPB-DMTP-COFs by integrating chiral pyrrolidine groups on the pore walls through click reaction. The resulting [(S)-Pyr]$_x$-TPB-DMTP-COFs showed high crystallinity, porosity, and chemical stability. They showed excellent conversion and selectivity, good recyclability in catalysing asymmetric Michael addition reactions.

1.5.2 Carbon dioxide capture and separation

Carbon dioxide (CO_2) is the primary greenhouse gas that increases with enlarging population and continuing industrial development. Serious global environmental problems caused by carbon dioxide have attracted great public concerns. COFs allow the atomically precise integration of organic building blocks into long-ordered 2D layers or 3D networks, enabling an overall control over skeleton structure, pore, and topology. To date, two strategies have been developed to improve the carbon dioxide uptake capacity. Especially, regulating porosity has proven to be an effective way to enhance the adsorption ability. Another approach is the incorporation of functional groups into the pore walls that can also enhance the selectivity of CO_2/N_2.

Constructing COFs with a high BET surface area and small pore size provides an effective way to enhance the carbon dioxide capture.[36] The azine-linked COFs are promising to construct small pores owing to the shortest length of azine bond among all the linkages. 2D azine-linked ACOF-1 was synthesized through the condensation between hydrazine hydrate and 1,3,5-triformylbenzene (Figure 15a).[36] ACOF-1 possesses a high surface area of 1176 $m^2\ g^{-1}$ and a pore size of 0.94 nm. According to the carbon dioxide adsorption measurements, ACOF-1 exhibits a carbon dioxide uptake of 17.6 wt% at 273 K and 1 bar. The ideal adsorption selectivity of CO_2/N_2 was 40 at 273 K as evaluated on the basis of initial slope in the relative pressure range

from 0 to 0.1 bar. COF-JLU2 condensed from hydrazine hydrate and 1,3,5-triformylphloroglucinol has a small pore of 0.96 nm (Figure 15b).[37] Interestingly, COF-JLU2 exhibits a remarkable carbon dioxide uptake of 21.7 wt% at 273 K and 1 bar, with a CO_2/N_2 selectivity up to 77, which is much higher than that of ACOF-1. The excellent carbon dioxide uptake and separation originates from their inherent micropores and pore walls decorated with dense nitrogen and oxygen atoms. Another azine-linked HEX-COF1 with a surface area of 1200 $m^2 g^{-1}$ and a pore size of 1 nm (Figure15c) exhibits a carbon dioxide uptake capacity of 20.0 wt% at 273 K and 1 bar.[61] These azine-linked COFs exhibit excellent carbon dioxide uptake owing to their small pores and the presence of dense CO_2-philic nitrogen atoms on the walls.

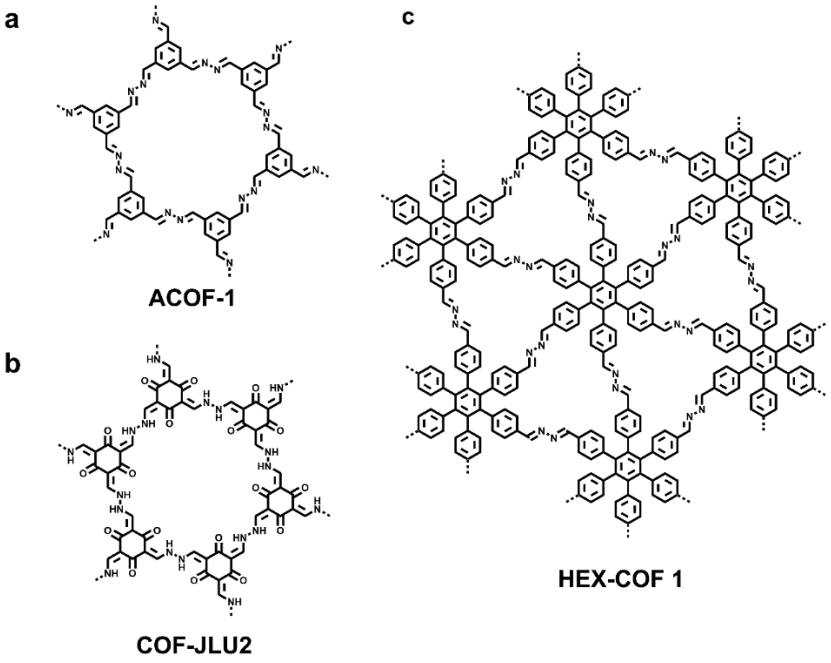

Figure 15. Structures of azine-linked COFs.[36-37, 61]

3D-Py-COF was constructed by condensation of tetra(p-aminophenyl)methane with 1,3,6,8-tetrakis(4-formylphenyl)pyrene (Figure 16a).[62] Although 3D-Py-COF has a high surface area (1290 $m^2 g^{-1}$) and a small pore size, its carbon dioxide uptake capacity of 15.3 wt% was lower than those of azine-linked COFs due to its low nitrogen content. Figure 16b shows two double-stage linked 3D DL-COF-1 and DL-COF-2 (boroxine

and imine) in Figure 16b.[63] The BET surface areas of DL-COF-1 and DL-COF-2 are 2259 and 2071 m^2 g^{-1}, respectively. The pore size distribution profiles demonstrated a pore size of 1.36 nm for DLCOF-1 and of 1.28 nm for DL-COF-2. Both COFs show large carbon dioxide uptake capacities. Especially, DLCOF-1 shows carbon dioxide uptake capacity of 26.7 wt% at 273 K and 1 bar, which is the highest one among all COFs reported to date.

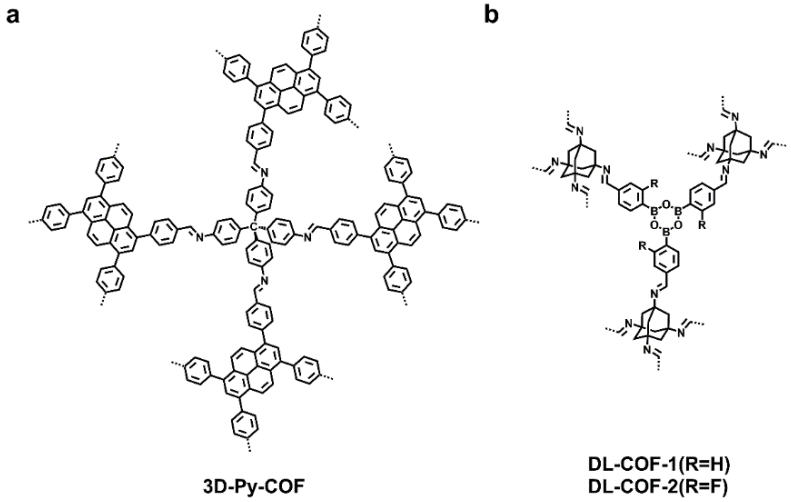

Figure 16. 3D COFs's structure for carbon cioxide adsorption.[62-63]

Pore surface engineering of COFs can precisely and effectively introduce functional sites into skeletons. using pore surface engineering strategy can convert a conventional 2D COF into a specific one with outstanding carbon dioxide adsorption and separation property. For example, functionalization with carboxylic acid group provides an opportunity to enhance carbon dioxide uptake and the selectivity.[64] The conventional imine-linked porphyrin COFs was functionalized with carboxylic acid units via ring opening reaction (Figure 17, $[HO_2C]x$-H_2P-COFs, x = 25, 50, 75, and 100%). As the content of the carboxylic acid is increased, the carbon dioxide capture capacity and selectivity increase rapidly. Indeed, $[HO_2C]_{100}$-H_2P-COFs exhibits an excellent carbon dioxide adsorption capacity of 17.4 wt% at 273K and 1 bar, which is 2.8-fold higher than that of the precursor $[HO_2C]_0$-H_2P-COFs. Especially, the CO_2/N_2 selectivity of $[HO_2C]_{100}$-H_2P-COF calculated by ideal absorbed solution

theory (IAST) is 18-fold greater than that of pristine COFs for the 15/85 CO_2/N_2 flue gas mixture at 298 K and 0.1 k bar. Furthermore, there are no significant decline in uptake capacity for $[HO_2C]_{100}$-H_2P-COFs after ten cycles, which indicates the complete regeneration and excellent cycling performance of the COF for carbon dioxide capture.

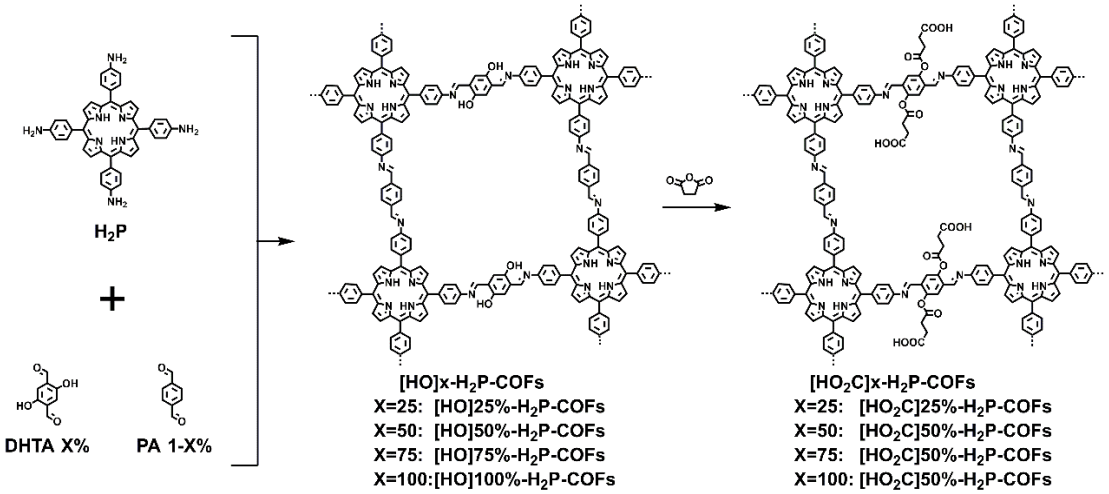

Figure 17. Imine-linked porphyrin COFs functionalized with carboxylic acid units via ring-opening reaction.[64]

To enhance the affinity toward carbon dioxide, 4-phenylazobenzoyl (PhAzo) group with CO_2-philic and N_2-phobic features has been integrated into the pore walls of $[HO]_{X\%}$-TAPH-COFs (X = 25, 50, 75 and 100) through acylation reaction (Figure 18).[65] The $[N{=}N]_{25\%}$-TAPH-COFs exhibits an excellent carbon dioxide uptake capacities up to 207 mg g^{-1} at 273 K and 1 bar, which is 3-fold more than that of $[HO]_{25\%}$-TAPH-COF.

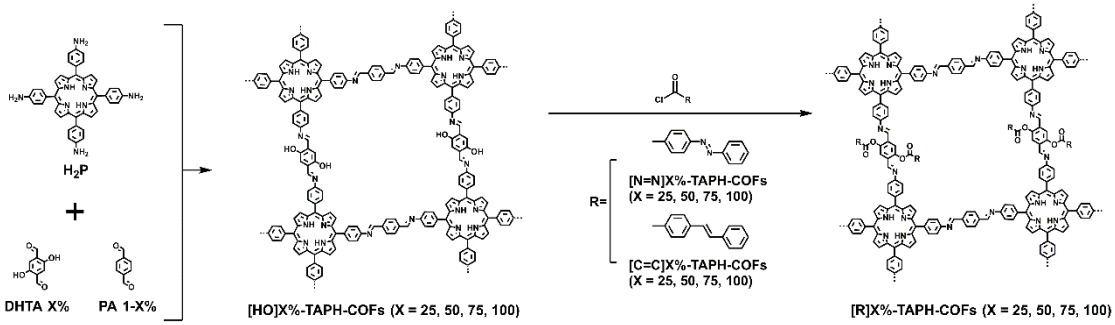

Figure 18. Imine-linked porphyrin COFs functionalized with 4-phenylazobenzoyl (PhAzo) group via acylation reaction.[65]

Click reaction has been developed for pore-wall surface engineering to

anchor diverse functional groups. For example, click reaction between ethynyl groups on the pore walls and functionalized azide compounds generates various functionalized porphyrin COFs ($[HC{\equiv}C]_x$-H_2P, x = 25, 50, 75 and 100%) (Figure 19).[66] These COFs show the generality of pore-wall surface engineering for modifying COFs with a diverse of functional groups (Et, MeOAc, EtOH, AcOH and $EtNH_2$) ranging from hydrophobic to hydrophilic units and from basic to acidic moieties with tunable loading contents. Introducing the functional groups such as ester unit (MeOAc), carboxylic acid groups (AcOH), hydroxyl groups (EtOH) and amino groups ($EtNH_2$) to the walls greatly enhances the carbon dioxide uptake capacity compared to those of the precursor $[HC{\equiv}C]_x$-H_2P-COFs. The $[EtNH_2]_{50\%}$-H_2P-COF with amino groups exhibits the highest uptake capacity of 15.7 wt% at 273 K and 1 bar.

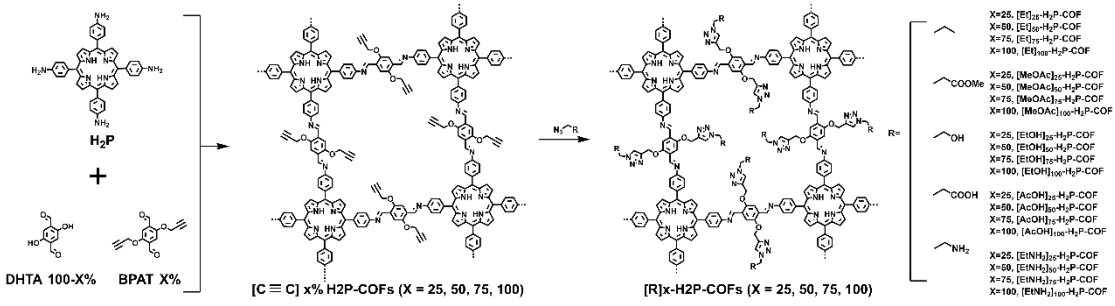

Figure 19. Imine-linked porphyrin COFs functionalized with ester (MeOAc), carboxylic acid (AcOH), hydroxyl (EtOH) and amino ($EtNH_2$) groups on the pore walls via click reaction.[66]

The immobilization of ionic units into COFs was fulfilled through the Williamson ether reaction between (2-bromoethyl)triethylammonium bromide and phenol group.[67] The ionic $[Et_4NBr]_{50\%}$-Py-COF afforded an enhanced carbon dioxide uptake capacity of 16.5 wt% at 273 K and 1 bar.

Recently, 4,4',4'',4'''-(pyrene-1,3,6,8-tetrayl)tetraaniline as a neutral knot and 5,6-bis(4-formylbenzyl)-1,3-dimethyl-benzimidazolium bromide as a cationic linker were used for the construction of imine-linked positively charged PyTTA-BFBIm-iCOF in which the benzimidazolium cationic sites were exposed to the wall surface (Figure 20).[68] The ionic COF exhibits a good porosity, crystallinity and chemical stability. Although PyTTA-BFBIm-iCOF had a large

pore size of 2.03 nm, the walls with electric dipoles can enhance the carbon dioxide uptake to 17.7 wt% in 273 K and 1 bar, which is 3-fold higher than that of neutral PyTTA-TPhA-COF. In the same year, our group also reported a series of COFs with triarylamine units on the backbone, showed good carbon dioxide capture through acid-based interaction.[69]

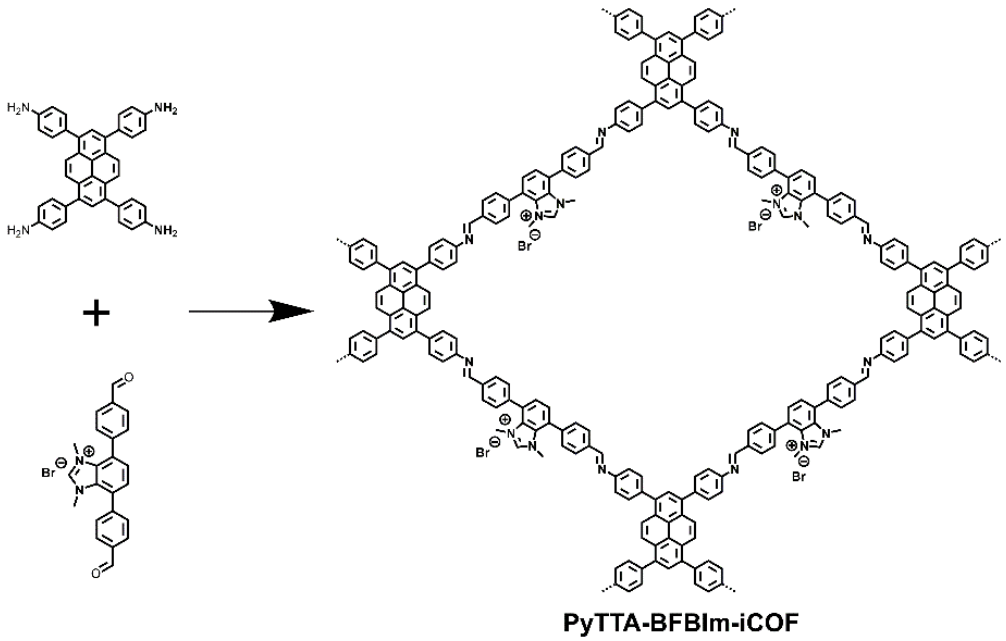

Figure 20. Imine-linked positively charged PyTTA-BFBIm-iCOF.[68]

In short, increasing porosity and integrating functional units promote the electrostatic or hydrogen bonding interactions with carbon dioxide, which form a positive force in facilitating carbon dioxide uptake and separation.

1.5.3 Light emitting and molecular sensing

COFs are robust to integrate a variety of chromophores into topologically ordered columnar π arrays and provide a unique platform for designing organic luminescent materials. Light-emitting COFs are highly dependent on their layered π structure. The light-emitting activity can be predesigned by using different knots, linkers and linkages. COFs possess permanent pores that are accessible to guest molecules while the π arrays promote exciton migration and/or energy transfer over the network, thereby enhancing the sensitivity through signal amplification. COFs are stable and insoluble so that they are

easy to be cycled. According to these characters, light-emitting COFs have a great chance to improve sensitivity, selectivity and repeatability in detection.

The first example of luminescent COF, i.e. TP-COF, was designed and synthesized with triphenylene knots and pyrene linkers by our group (Figure 21).[70] TP-COF exhibits strong blue luminescent with an emission band at 474 nm in solid, which originates from its pyrene excimer.

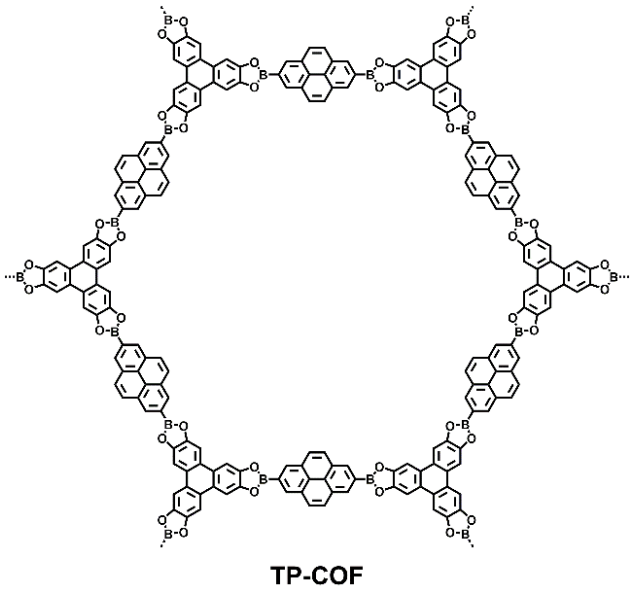

Figure 21. Structure of blue luminescence TP-COF.[70]

In 2013, the first azine linkage COF (Py-Azine COF) was constructed by condensation of 1,3,6,8-tetrakis(4-formylphenyl)pyrene with hydrazine (Figure 22).[22] Py-Azine COF shows outstanding porosity with a high surface area of 1210 $m^2\ g^{-1}$ and a pore volume of 0.72 $cm^3\ g^{-1}$. The azine-linked COF shows high stability to retain crystallinity under base and acid conditions at room temperature over one day. The Py-Azine COF in CH_3CN emits green luminescence at 522 nm upon excitation at 470 nm. The azine linkage consists of two nitrogen atoms with lone pairs that serve as open docking sites to trigger hydrogen-bonding interactions with phenol unit, which is a common backbone of nitrobenzene-based explosives. Interestingly, 2,4,6-trinitrophenol (TNP) triggers the highest quenching degree of 69%, which is much higher than those of other nitrobenzene derivatives, including 2,4-dinitrophenol (13%),

2-nitrophenol (3%), and 2-nitrotoluene (3%). This is the first example of COFs as chemical sensors, which opens an important aspect of COFs for functional material development.

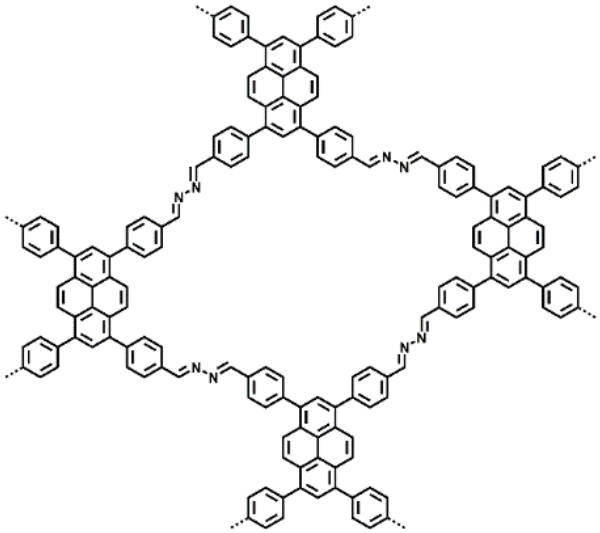

Figure 22. Structure of green fluorescence Py-Azine COF.[22]

The arrangement of molecules in H-aggregates is face-to-face that usually results in fluorescence quenching, which is observed for many π compounds. This means that two-dimensional COFs with crystalline π structures and stronger interaction between adjacent layers are hardly luminescent. COF-JLU3 with tert-butyl groups on the pore walls has been designed and successfully constructed, which can adjust the π-π interaction to reduce H-aggregates so that the luminescence can be greatly enhanced (Figure 23).[38] The novel azine-linked COF assisted by hydrogen bond features a permanent porosity with a large surface area and displayed excellent chemical and thermal stabilities. Interestingly, the COF emits a strong luminescence at 601 nm with a high absolute quantum yield of 9.91% in the solid state. COF-JLU3 with abundant heteroatom sites on the pore surface was exploited for the binding and specific sensing of metal ions via ligation. In particular, the resulting COF exhibits a selective response to copper ions and does not respond to other ions such as alkaline metal ion like Li^+ and K^+, alkaline-earth metal ion like Mg^{2+} and Ba^{2+}, transition metal ions with filled *d* shells such as

Zn^{2+}, Pb^{2+}, and Cd^{2+}. This COF is very sensitive to show a detection limit down to 0.31 μM. This is the first example of COFs that can detect a trace amount of Cu^{2+} ion in a highly selective way.

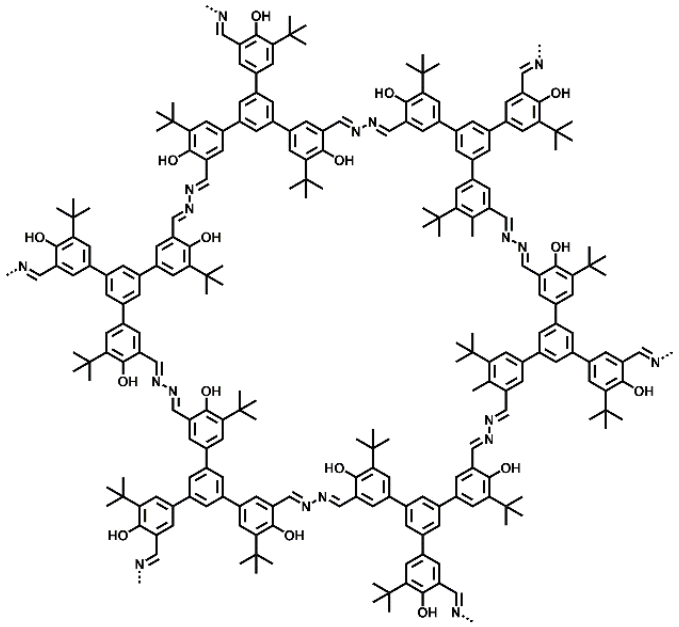

Figure 23. Structure of orange-red light emitting COF-JLU3.[38]

Covalent organic nanosheets (CONs) with few layers can be prepared by liquid-phase exfoliation of COFs. Compared to the bulk COFs, CONs not only showed an increased luminescence as a result of reduced π aggregation but also displayed an increased surface area to contact with target molecules, giving rise to an enhanced sensitivity.[71-72] For example, the imide-based CONs, TpBDH-CONs and TfpBDH-CONs, greatly increase the fluorescence intensity in both solution and solid states. These CONs exhibit an excellent performance on sensing nitro-explosive.[71] For example, the fluorescence intensity of TfpBDH-CONs was quenched by 63% at a low TNP concentration of only 5.4×10^{-5} M.

Ultrathin CONs are difficult to prepare owing to the strong π-π stacking interaction between the COF layers. The 2D imine-linked TPA-COF was designed and synthesized by using flexible C_{3v}-symmetric units, tris(4-aminophenyl)amine and tris(4-formylphenyl)amine.[72] The flexible units serve as knots that decrease the interlayer π stacking, which render TPA-COF

easily to be exfoliated into 2D CONs. FE SEM and Transmission electron microscope (TEM) revealed the layer structure. Atomic force microscope (AFM) reveals the thickness of these CONs is 3.5 ± 0.3 nm. A target two hairpin DNA was labelled with a fluorescent dye, while the fluorescence intensity of labelled DNA can be quenched by adsorption from the surface of TPA-COF nanosheets due to the π-π stacking interactions. The detection limit was down to 20 ppm, which is lower than those of most 2D nanomaterials that have been reported as fluorescence DNA sensors. The fluorescence quenching degree of the single-based mismatch DNA and random DNA is lower than that of the target DNA. The TPA-COF nanosheets thus are capable of sensing labelled fluorescence DNA in a selective manner.

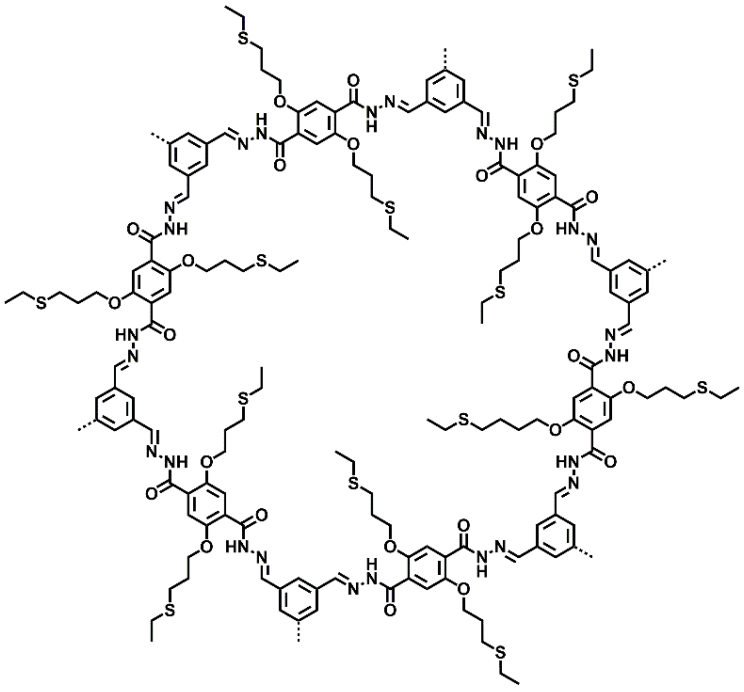

COF-LZU8

Figure 24. Structure of blue light-emitting COF-LZU-8.[73]

Aggregation-caused quenching (ACQ) turns off the fluorescence of materials. Ding and co-authors introduced a contorted non-planar structure that endows COF-LZU8 with reduced ACQ and an absolute quantum yield of 3.5% (Figure 24).[73] The long chains modified with thioether group in open 1D channels could easily react with Hg^{2+}. The fluorescence intensity was

quenched by Hg^{2+}, while other metal ions show less quenching, leading to a selective detection. The LZU-8 sample loaded with Hg^{2+} can be easily recovered to yield pristine COF by immersed into a sodium sulfide solution, enabling the reuse of LZU-COF8.

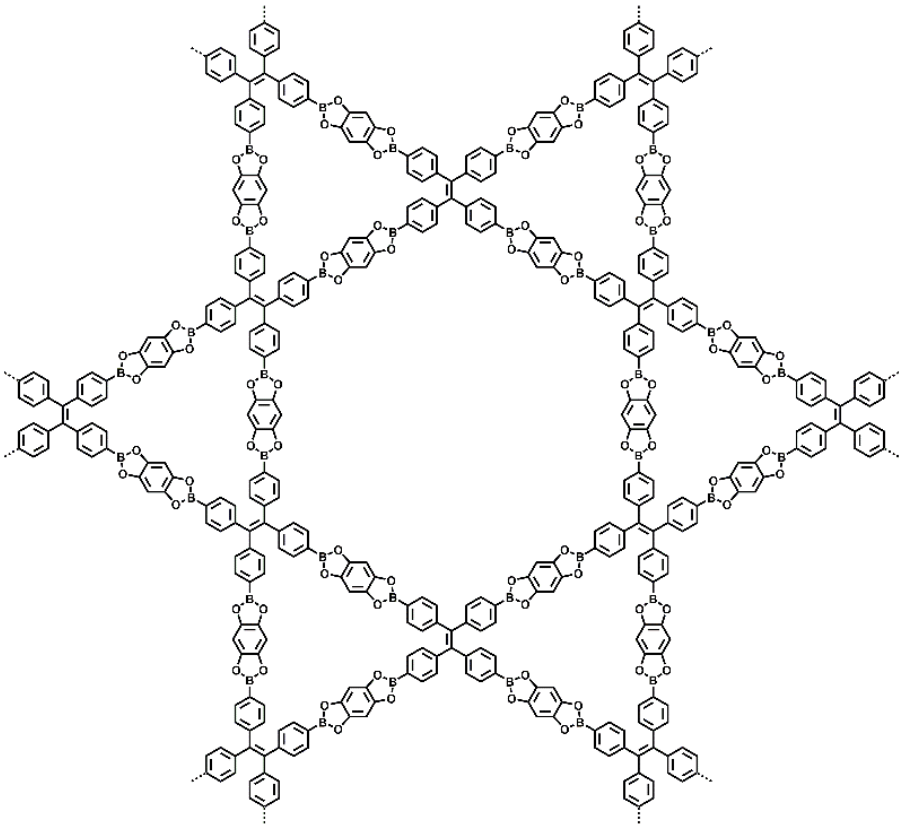

TPE-Ph COF

Figure 25. Structure of high blue luminescence TPE-Ph COF.[26]

To fully explore the potential of a highly porous structure for sensing, the rational design of COFs that allows the elimination of ACQ is necessary. Incorporation of AIE-based building blocks to the skeleton is proven to be effective to address this problem (AIE: aggregation-induced emission). The TPE-Ph COF exhibits a strong blue luminescence with AIE-active TPE units as knots (Figure 25).[26] It exhibits a high absolute fluorescence quantum yield over 30% in solid state or suspension. Compared with the model compounds with absolute fluorescence quantum yield of 15%, the TPE units are restricted in terms of rotation by the ordered 2D frameworks, which can enhance the AIE effect. Intralayer covalent bonds and interlayer noncovalent-stacking structure

synergistically work together to decrease the rotation-related thermal dissipation of photo-excited state, thus significantly enhancing the fluorescence quantum yield of TPE-Ph COF. TPE-Ph COF was linked by the boronate bond in which boron atom has an open *pz* orbital that serves as Lewis acid to interact with ammonia as Lewis base. The blue emission of TPE-Ph COF was rapidly quenched by ammonia gas at a ppm level. The fluorescence quenching rate constant k_q ($k_q = k_{SV}/\tau$)) is as high as 6.3×10^{14} M^{-1} s^{-1}, indicating an exceptional luminescence quenching owing to the facilitated exciton migration over the framework. Interestingly, 1 ppm ammonia can cause a 30% decrement of the original fluorescence intensity. These results suggest an approach to emissive COFs in which supramolecular interactions can be designed to construct detecting systems.

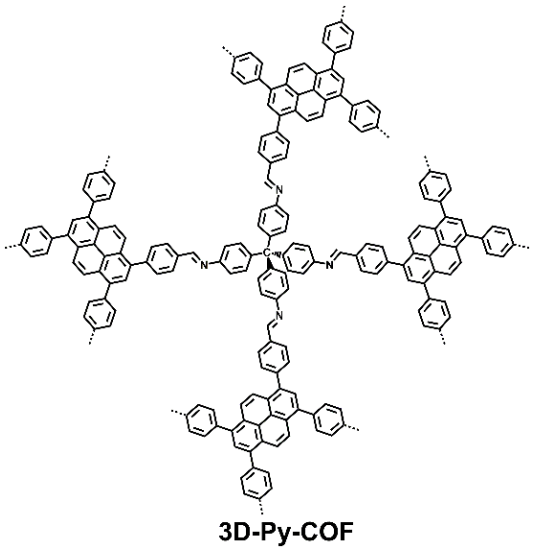

Figure 26. Structure of yellow-green luminescence 3D Py-COF.[74]

Changing the dimensionality of COFs from 2D to 3D structure is another effective way to solve the ACQ issue. 3D-Py-COF exhibits a strong yellow-green luminescence by excluding ACQ (Figure 26).[74] 3D-Py-COF in DMF showed blue fluorescence with an emission peak at 484 nm upon excitation at 408 nm. 3D-Py-COF can detect TNP-type explosives with fluorescence quenching degree as high as 75% at a concentration of 20 ppm.

The sp^2 carbon COFs (sp^2c-COFs) were linked with the carbon-carbon

double bond so that the π conjugation is extended along both the *x* and *y* directions. A series of sp^2c-COF was constructed with pyrene as knots and phenyl, biphenyl, and terphenyl as linkers, which offer sp^2c-COFs with different π lattice sizes (Figure 27).[75] The extension of π conjugation of these sp^2c-COFs is controlled by the phenyl, biphenyl, and terphenyl linkers owing to a progressed twist conformation that results in a shorter π conjugation. The sp^2c-COFs exhibited exceptional chemical stability in most organic solvents, strong acid (HCl, 12 M) and base (NaOH,14 M) conditions at 168 hours. Moreover, these COFs can also keep excellent crystallinity and porosity upon exposure to air for one year. All sp^2c-COFs showed strong red luminescence. The emission peaks of sp^2c-COFs were controlled from 606 nm to 620 nm. All COFs exhibited highly luminescent quantum yields of 6-21% in the solid state and in dispersions in organic solvents and water. The cyano groups on the walls can interact with metal ions through supramolecular interactions. Interestingly, sp^2c-COF shows a high sensitivity towards the Cu^{2+} ion with a low detection limit of only 88 ppb. The Stern-Volmer plot was used to calculate fluorescence quenching rate constant, which is as high as $4.1 \times 10^{14}\ M^{-1}\ s^{-1}$. These results indicated sp^2c-COFs can be serves as an efficient metal detector.

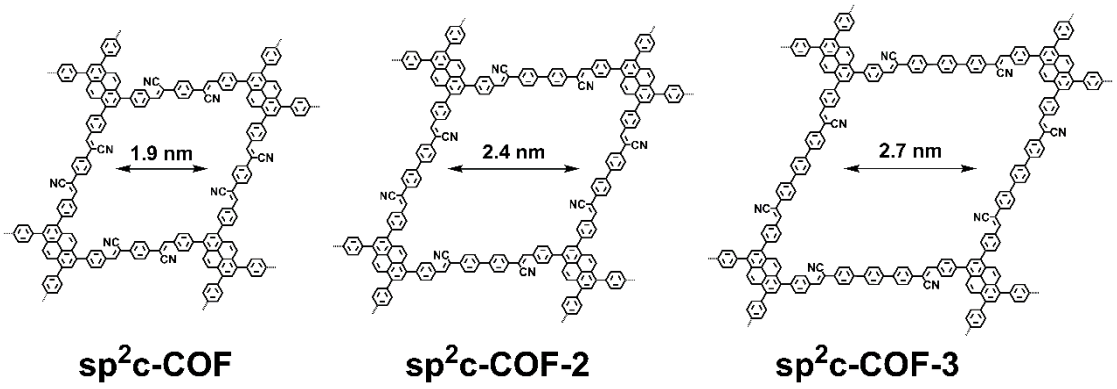

Figure 27. Structure of red luminescence sp^2c -COFs.[75]

Functional light-emitting COFs can be precisely constructed with various building units, which can promote the development of molecular recognition. The new strategy was applied for imine-based COFs through Michael

addition-elimination reaction.[76] These COFs also display good luminescence. These luminescent CONs can be prepared through the ultrasonic stripping method for sensing triacetone triperoxide (TATP) explosive through fluorescence quenching. A series of chiral COFs (CCOFs) was designed and synthesized through chiral catalytic induction by chiral 1-phenylethylamine as organic precursors.[77] Chiral luminescence CCOF-TpTab serves as a chiral carbohydrates sensor to achieve high enantioselectivity for various saccharides, including D-glucose, D-mannitol, D-sucrose, D-lactose, D-maltose, D-sorbitol, D-fructose, D-gentiobiose, D-lactobionic acid, D-glucuronic acid, and D-gluconic acid. In short, design and synthesis of light-emitting COFs for sensing target molecules have been gradually developed and improved with the development of the design principle as well as structural diversity.

1.6 Scope of this thesis

COFs are a class of porous crystalline materials that are constructed with organic building units through organic reactions. Nowadays, various reactions including B–O, C=N, and C=C linkages have been developed for synthesizing COFs. The C=N linked COFs including imine, azine, hydrazine, and phenazine-linked frameworks, usually show good chemical stability.

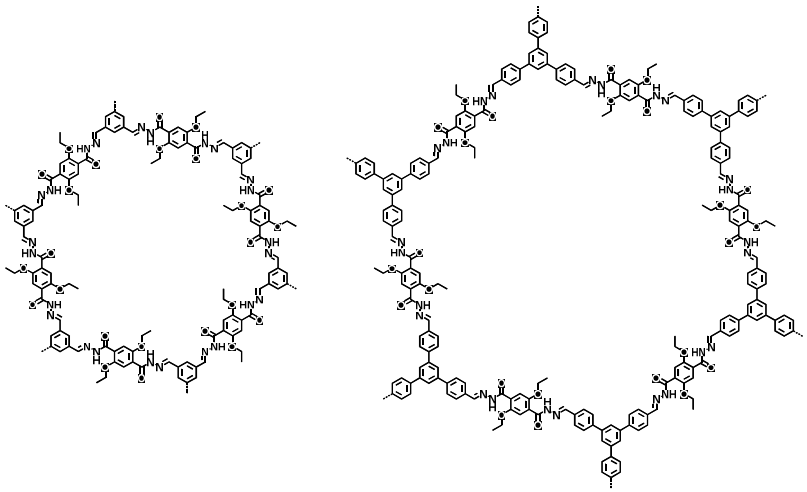

Figure 28. Structure of hydrazone-linked COFs.[34]

The hydrazone-linked COFs were firstly reported by Yaghi's group in 2011 (Figure 28).[34] However, few researchers paid attention to the hydrazone-linked COFs [34-35,78-79] because they ignore the advantages of their structure. Among COFs with imine, azine, and phenazine linkages, the COFs with hydrazone linkage possess active N-H units and rich oxygen atoms on the pore walls, which can be further explored for a wide application including carbon dioxide capture and chemical sensors. Moreover, the hydrazone linkage can give a non-planar structure of COFs, which can weaken fluorescence quenching caused by strong π-π stacking from the adjacent layers of 2D COFs. This thesis focuses on the design and synthesis of hydrazone-linked COFs and their functions.

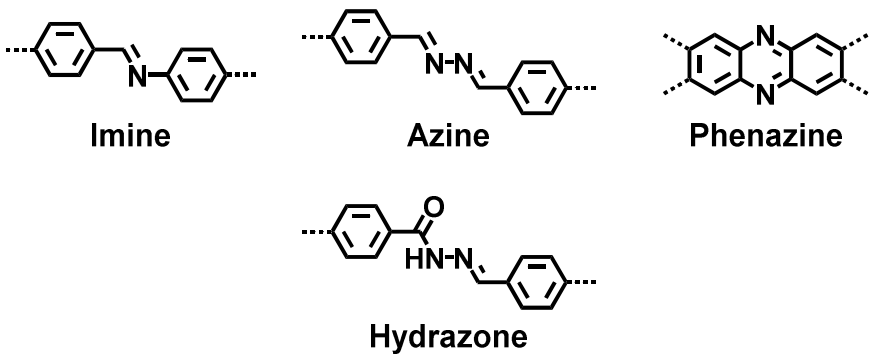

Figure 29. Structure of imine, azine, phenazine and hydrazone linkages.

In chapter 1, I reviewed the COF field by summarizing the general principle of structural design as well as illustrating synthetic methods and approaches. This chapter includes selected functions of COFs.

In chapter 2, I summarized the synthesis of two microporous hydrazone-linked COFs, TMHzcB-TFB-COF and TMHzcB-TFP-COF, through condensation of 1,3,5-tris(3'-methoxy-4'-hydrazinecarbonylphenyl)benzene (TMHzcB) and 1,3,5-triformylbenzene (TFB) / triformylphloroglucinol (TFP) under solvothermal conditions. These new COFs exhibited high crystallinity, permanent microporosity, excellent thermal and chemical stability, and abundant heteroatom sites on the pore walls. These two COFs exhibit remarkable CO_2 uptake capacity. The capacity of TMHzcB-TFP-COF can reach up to 14.4 wt% at 273 K and 1 bar.

In chapter 3, I described the synthesis of a series of light-emitting COFs. These COFs exhibited good porosity and stability. The pore size of hydrazone-linked frameworks can be tunable from 1.3 to 3.7 nm by using different linkers. The light-emitting activity of COFs can be predesigned through selecting functional groups such as fluorine, chlorine, bromine, methoxy, methyl and hydroxy on the pore walls, which tune the emission color from blue to green.

In chapter 4, I reported a new hydrazone-linked COF, TFPPy-DETHz-COF through Schiff base condensation reaction under solvothermal conditions. The N–H bond in the linkage part on the walls can be deprotonated to form an anionic species, which can eliminate the nitrogen-related fluorescence quenching pathway. The fluorescence of deprotonated COF can be improved by 3.8 fold. This pinpoint N–H cleavage is driven only by fluoride anion that switches on the fluorescence. In contrast, other halogen anions, including chloride, bromide, and iodide, retain inactive. This is the first example of COFs that serve as a functional fluorescent sensor for detecting fluoride anion.

Various hydrazone-linked COFs including hexagonal and tetragonal structure were designed and synthesized. The COFs showed good porosity. The pore size of COFs can be adjustable from micropores (1.6 nm) and mesopores (3.7 nm), which enriches the diversity of COF's structure. The hydrazone-linked COFs can be used for various applications. These microporous COFs with rich nitrogen and oxygen on the walls showed good carbon dioxide uptake. The non-planar structure of hydrazone linkage can reduce the strong interaction of adjacent layers, which can afford high luminescent materials. The light-emitting activity of COFs can be tunable through various building units and linkage. In chapter 2, various luminescence with high light-emitting activity can be controllable by building blocks. Interestingly, TMHzcB-2,5-DMETA-COF showed the highest quantum yield of 19.5%, which is higher than most reported COFs. In chapter 3, high fluorescence COF can be provided through changing the N-H of linkage into

nitrogen anions. This COF can also detect fluoride anion with high sensitivity and selectivity with a lower detection limit. The acidic and basic ions can be also recognized through an acid-base reaction. The investigated results displayed in this thesis demonstrated functional hydrazone-linked COFs that open a new phase for not only high adsorptive media, but also light-emitting materials for chemical sensing.

1.7 References

1. A. P. Côté, A. I. Benin, N. W. Ockwig, M. O'Keeffe, A. J. Matzger, O. M. Yaghi. Porous, crystalline, covalent organic frameworks. *Science*. **2005**, *310,* 1166.
2. X. Feng, X. Ding, D. Jiang. Covalent organic frameworks. *Chem. Soc. Rev*. **2012**, *41*, 6010-6022.
3. N. Huang, P. Wang, D. Jiang. Covalent organic frameworks: a materials platform for structural and functional designs. *Nat. Rev. Mat*. **2016,** *1*, 16068.
4. S. Das, P. Heasman, T. Ben, S. Qiu. Porous organic materials: strategic design and structure-function correlation. *Chem. Rev.* **2017**, *117*, 1515-1563.
5. S. Yuan, W. Wang. Covalent organic frameworks (COFs): from design to applications. *Chem. Soc. Rev*. **2013**, *42*, 548-568.
6. C. S. Diercks, O. M. Yaghi. The atom, the molecule, and the covalent organic framework. *Science*. **2017**, *355*, eaal1585.
7. J. L. Segura, M. J. Mancheñoa, F. Zamora. Covalent organic frameworks based on Schiff-base chemistry: synthesis, properties and potential applications. *Chem. Soc. Rev*. **2016**, *45*, 5635-5671.
8. S. Wan, J. Guo, J. Kim, H. Ihee, D. Jiang. A belt-shaped, blue luminescent and semiconducting covalent organic framework. *Angew. Chem. Int. Ed*. **2008**, *47*, 8826-8830.
9. A. P. Côté, H. M. El-Kaderi, H. Furukawa, J. R. Hunt, O. M. Yaghi.

Reticular synthesis of microporous and mesoporous 2D covalent organic frameworks. *J. Am. Chem. Soc.* **2007**, *129*, 12914-12915.

10. Q. Gao, L. Bai, X. Zhang, P. Wang, P. Li, Y. Zeng, R. Zou, Y. Zhao. Synthesis of microporous nitrogen-rich covalent-organic framework and its application in CO_2 capture. *Chin. J. Chem*. **2015**, *33*, 90-94.
11. D. Kaleeswaran, P. Vishnoia, R. Murugavel. [3+3] Imine and β-ketoenamine tethered fluorescent covalent-organic frameworks for CO_2 uptake and nitroaromatic sensing. *J. Mater. Chem. C*. **2015**, *3*, 7159-7171.
12. L. Xu, S. Ding, J. Liu, J. Sun, W. Wang, Qi. Zheng. Highly crystalline covalent organic frameworks from flexible building blocks. *Chem. Commun*. **2016**, *52*, 4706-4709.
13. L. Zhai, N. Huang, H. Xu, Q. Chen, D. Jiang. A backbone design principle for covalent organic frameworks: the impact of weakly interacting units on CO_2 adsorption. *Chem. Commun*. **2017**, *53*, 4242-4245.
14. S. Dalapati, M. Addicoat, S. Jin, T. Sakurai, J. Gao, H. Xu, S. Irle, S. Seki, D. Jiang. Rational design of crystalline supermicroporous covalent organic frameworks with triangular topologies. *Nat. Commun*. **2015**, *6*, 7786.
15. S. B. Alahakoon, C. M. Thompson, A. X. Nguyen, G. Occhialini, G. T. McCandless R. A. Smaldone. An azine-linked hexaphenylbenzene based covalent organic framework *Chem. Commun*. **2016**, *52*, 2843-2845.
16. X. Feng, L. Chen, Y. Dong, D. Jiang. Porphyrin-based two-dimensional covalent organic frameworks: synchronized synthetic control of macroscopic structures and pore parameters. *Chem. Commun*. **2011**, *47*, 1979-1981.
17. X. Ding, J. Guo, X. Feng, Y. Honsho, J. Guo, S. Seki, P. Maitarad, A. Saeki, S. Nagase, D. Jiang. Synthesis of metallophthalocyanine covalent organic frameworks that exhibit high carrier mobility and photoconductivity. *Angew. Chem. Int. Ed*. **2011**, *50*, 1289-1293.

18. X. Ding, L. Chen, Y. Honsho, X. Feng, O. Saengsawang, J. Guo, A. Saeki, S. Seki, S. Irle, S. Nagase, P. Vudhichai, D. Jiang. An n-channel two-dimensional covalent organic framework. *J. Am. Chem. Soc*. **2011**, *133*, 14510-14513.
19. X. Feng, X. Ding, L. Chen, Y. Wu, L. Liu, M. Addicoat, S. Irle, Y. Dong, D. Jiang. Two-dimensional artificial light-harvesting antennae with predesigned high-order structure and robust photosensitising activity. *Sci. Rep.* **2016**, *6*, 32944.
20. X. Ding, X. Feng, A. Saeki, S. Seki, A. Nagai, D. Jiang. Conducting Metallophthalocyanine 2D covalent organic frameworks: the role of central metals in controlling π-electronic functions. *Chem. Commun*. **2012**, *48*, 8952-8954.
21. S. Xu, R. Liang, T. Zhan, Q. Qia, X. Zhao. Construction of 2D covalent organic frameworks by taking advantage of the variable orientation of imine bonds. *Chem. Commun*. **2017**, *53*, 2431-2434.
22. S. Dalapati, S. Jin, J. Gao, Y. Xu, A. Nagai, D. Jiang. An azine-linked covalent organic framework. *J. Am. Chem. Soc*. **2013**, *135*, 17310-17313.
23. M. G. Rabbani, A. K. Sekizkardes, Z. Kahveci, T. E. Reich, R. S. Ding, H. M. EI-Kaderi. A 2D mesoporous imine-linked covalent organic framework for high pressure gas storage applications. *Chem. Eur. J.* **2013**, *19*, 3324-3328.
24. X. Chen, N. Huang, J. Gao, H. Xu, F. Xu, D. Jiang. Towards covalent organic frameworks with predesignable and aligned open docking sites. *Chem. Commun*. **2014**, *50*, 6161-6163.
25. T. Zhou, S. Xu, Q. Wen, Z. Pang, X. Zhao. One-step construction of two different kinds of pores in a 2D covalent organic framework. *J. Am. Chem. Soc*. **2014**, *136*, 15885-15888.
26. S. Dalapati, E. Jin, M. Addicoat, T. Heine, D. Jiang. Highly emissive covalent organic frameworks. *J. Am. Chem. Soc*. **2016**, *138*, 5797-5800.

27. Y. Mo, X. Liu, D. Wang. Concentration-directed polymorphic surface covalent organic frameworks: rhombus, parallelogram, and kagome. *ACS Nano*. **2016**, *11*, 11694-11700.

28. N. Huang, L. Zhai, D. E. Coupry, M. A. Addicoat, K. Okushita, K. Nishimura, T. Heine, D. Jiang. Multiple-component covalent organic frameworks. *Nat. Commun.* **2016**, 7, 12325.

29. H. M. El-Kaderi, J. R. Hunt, J. L. Mendoza-Cortés, A. P. Côté, R. E. Taylor, M. O'Keeffe, O. M. Yaghi. Designed synthesis of 3D covalent organic frameworks. *Science.* **2007**, *316*, 268-272.

30. F. J. Uribe-Romo, J. R. Hunt, H. Furukawa, C. Klöck, M. O'Keeffe, O. M. Yaghi. A crystalline Imine-linked 3-D porous covalent organic framework. *J. Am. Chem. Soc*. **2009**, *131*, 4570-4571.

31. Q. Fang, S. Gu, J. Zheng, Z. Zhuang, S. Qiu, Y. Yan. 3D microporous base-functionalized covalent organic frameworks for size-selective catalysis. *Angew. Chem. Int. Ed*. **2014**, *53*, 2878-2882.

32. G. Lin, H. Ding, D. Yuan, B. Wang, C. Wang. A pyrene-based, fluorescent three-dimensional covalent organic framework. *J. Am. Chem. Soc*. **2016**, *138*, 3302-3305.

33. G. Lin, Hu. Ding, R. Chen, Z. Peng, B. Wang, C. Wang. 3D porphyrin-based covalent organic frameworks. *J. Am. Chem. Soc.* **2017**, *139*, 8705-8709.

34. F. J. Uribe-Romo, C. J. Doonan, H. Furukawa, K. Oisaki, O. M. Yaghi. Crystalline covalent organic frameworks with hydrazone linkages. *J. Am. Chem. Soc*. **2011**, *133*, 11478-11481.

35. L. Stegbauer, K. Schwinghammer, B. V. Lotsch. A hydrazone-based covalent organic framework for photocatalytic hydrogen production. *Chem. Sci.* **2014**, *5*, 2789-2793.

36. Z. Li, X. Feng, Y. Zou, Y. Zhang, H. Xia, X. Liu, Y. Mu. A 2D azine-linked covalent organic framework for gas storage applications. *Chem. Commun*. **2014**, *50*, 13825-13828.

37. Z. Li, Y. Zhi, X. Feng, X. Ding, Y. Zou, X. Liu, Y. Mu. An azine-linked covalent organic framework: synthesis, characterization and efficient gas storage. *Chem. Eur. J*. **2015**, *21*, 12079-12084.

38. Z. Li, Y. Zhang, X. Feng, H. Xia, X. Liu, Y. Mu. A robust and luminescent covalent organic framework as a highly sensitive and selective sensor for detection of Cu^{2+} ion. *Chem. Commun*. **2016**, *52*, 6613-6616.

39. X. Chen, M. Addicoat, E. Jin, H. Xu, T. Hayashi, F. Xu, N. Huang, S. Irle, D. Jiang. Designed synthesis of double-stage two-dimensional covalent organic frameworks. *Sci. Rep*. **2015**, *5*, 14650.

40. J. Guo, Y. Xu, S. Jin, L. Chen, T. Kaji, Y. Honsho, M. A. Addicoat, J. Ki, A. Saeki, H. Ihee, S. Seki, S. Irle, M. Hiramoto, J. Gao, D. Jiang. Conjugated organic framework with three-dimensionally ordered stable polymer with delocalized π clouds. *Nat. Commun*. **2013**, *4*, 2736.

41. P. Wei, M. Qi, Z. Wang, S. Ding, W. Yu, Q. Liu, L. Wang, H. Wang, W. An, W. Wang. Benzoxazole-linked ultrastable covalent organic frameworks for photocatalysis. *J. Am. Chem. Soc*. **2018**, *140*, 4623-4631.

42. Q. Fang, Z. Zhuang, S. Gu, R. B. Kaspar, J. Zheng, J. Wang, S. Qiu, Y. Yan. Designed synthesis of large-pore crystalline polyimide covalent organic frameworks. *Nat. Commun*. **2014**, *5*, 4503.

43. A. Nagai, X. Chen, X. Feng, X. Ding, Z. Guo, D. Jiang. A squaraine-linked mesoporous covalent organic framework. *Angew. Chem. Int. Ed*. **2013**, *52*, 3770 -3774.

44. Y. Du, H. Yang, J. M. Whiteley, S. Wan, Y. Jin. S. Lee. W. Zhang. Ionic covalent organic frameworks with spiroborate linkage. *Angew. Chem. Int. Ed*. **2016**, *55*, 1737-1741.

45. A. I. Cooper. Conjugated microporous polymers. *Adv. Mater.* **2009**, *21*, 1291-1295.

46. X. Zhuang, W. Zhao, F. Zhang, Y. Cao, F. Liu, S. Bia, X. Feng. A two-dimensional conjugated polymer framework with fully sp^2-bonded carbon skeleton. *Polym. Chem*. **2016**, *7*, 4176-4181.

47. E. Jin, M. Asada, Q. Xu, S. Dalapati, M. A. Addicoat, M. A. Brady, H. Xu, T. Nakamura, T. Heine, Q. Chen, D. Jiang. Two-dimensional sp^2 carbon-conjugated covalent organic frameworks. *Science*. **2017**, *357*, 673-676.

48. S. Xu, G. Wang, B. P. Biswal, M. Addicoat, S. Paasch, W. Sheng, X. Zhuang, E. Brunner, T. Heine. A nitrogen-rich 2D sp^2-carbon-linked conjugated polymer framework as a high-performance cathode for lithium-ion batteries. *Angew. Chem. Int. Ed*. **2019**, *58*, 849-853.

49. P. J. Waller, S. J. Lyle, T. M. O. Popp, C. S. Diercks, J. A. Reimer, O. M. Yaghi. A chemical conversion of linkages in covalent organic frameworks. *J. Am. Chem. Soc*. **2016**, *138*, 15519-15522.

50. H. Liu, J. Chu, Z. Yin, X. Cai, L. Zhuang, H. Deng. Covalent organic frameworks linked by amine bonding for concerted electrochemical reduction of CO_2. *Chem*. **2018***, 4*, 1-14.

51. P. J. Waller, Y. S. AlFaraj, C. S. Diercks, N. N. Jarenwattananon, O. M. Yaghi. Conversion of imine to oxazole and thiazole linkages in covalent organic frameworks. *J. Am. Chem. Soc*. **2018**, *140*, 9099-9103.

52. H. Wei, S. Chai, N. Hu, Z. Yang, L. Wei, L .Wang, The microwave-assisted solvothermal synthesis of a crystalline two-dimensional covalent organic framework with high CO_2 capacity. *Chem. Commun.* **2015**, *51*, 12178-12181.

53. P. Kuhn, M. Antonietti, A. Thomas. Porous, covalent triazine-based frameworks prepared by ionothermal synthesis. *Angew. Chem. Int. Ed*. **2008**, 47, 3450-3453.

54. B. P. Biswal, S. Chandra, S. Kandambeth, B. Lukose, T. Heine, R. Banerjeet, mechanochemical synthesis of chemically stable isoreticular covalent organic frameworks. *J. Am. Chem. Soc*. **2013**, *135*, 5328-5331.

55. J. W. Colson1, A. R. Woll, A. Mukherjee, M. P. Levendorf, E. L. Spitler, V. B. Shields, M. G. Spencer, J. Park, W. R. Dichtel. Oriented 2D covalent organic framework thin films on single-layer graphene. *Science*. **2011**,

332, 228.

56. D. D. Medina, J. M. Rotter, Y. Hu, M. Dogru, V. Werner, F. Auras, J. T. Markiewicz, P. Knochel, and T. Bein. Room temperature synthesis of covalent-organic framework films through vapor-assisted conversion. *J. Am. Chem. Soc*. **2015**, 137, 1016-1019.
57. Q. Fang, S. Gu, J. Zheng, Z. Zhuang, S. Qiu, Y. Yan. 3D microporous base-functionalized covalent organic frameworks for size-selective catalysis. *Angew. Chem. Int. Ed*. **2014**, *53*, 2878-2882.
58. S. Ding, J. Gao, Q. Wang, Y. Zhang, W. Song, W. Wang. Construction of covalent organic framework for catalysis: Pd/COF-LZU1 in suzuki-miyaura coupling reaction. *J. Am. Chem. Soc.* **2011**, *133*, 19816-19822.
59. M. Bhadra, H. S. Sasmal, A. Basu, S. P. Midya, S. Kandambeth, P. Pachfule, E. Balaraman, R. Banerjee. Predesigned metal-anchored building block for in situ generation of Pd nanoparticles in porous covalent organic framework: application in heterogeneous tandem catalysis. *ACS Appl. Mater. Interfaces*. **2017**, *9*, 13785-13792.
60. H. Xu, J. Gao, D. Jiang. Stable, crystalline, porous, covalent organic frameworks as a platform for chiral organocatalysts. *Nat. Chem.* **2015**, *7*, 905-912.
61. S. B. Alahakoon, C. M. Thompson, A. X. Nguyen, G. Occhialini, G. T. McCandless, R. A. Smaldone. An azine-linked hexaphenylbenzene based covalent organic framework. *Chem. Commun*. **2016**, *52*, 2843-2845.
62. G. Lin, H. Ding, D. Yuan, B. Wang, C. Wang. A pyrene-based, fluorescent three-dimensional covalent organic framework. *J. Am. Chem. Soc*. **2016**, *138*, 3302-3305.
63. H. Li, Q. Pan, Y. Ma, X. Guan, M. Xue, Q. Fang, Y. Yan, V. Valtchev, S. Qiu. Three-dimensional covalent organic frameworks with dual linkages for bifunctional cascade catalysis. *J. Am. Chem. Soc*. **2016**, *138*,

14783-14788.

64. N. Huang, X. Chen, R. Krishna, D. Jiang. Two-dimensional covalent organic frameworks for carbon dioxide capture through channel-wall functionalization. *Angew. Chem. Int. Ed*. **2015**, *54*, 2986-2990.

65. S. Zhao, B. Dong, R. Ge, C. Wang, X. Song, W. Ma, Y. Wang, C. Hao, X. Guo, Y. Gao. Channel-wall functionalization in covalent organic frameworks for the enhancement of CO_2 uptake and CO_2/N_2 selectivity. *RSC Adv*. **2016**, 6, 38774-3878.

66. N. Huang, R. Krishna, D. Jiang. Tailor-made pore surface engineering in covalent organic frameworks: systematic functionalization for performance screening. *J. Am. Chem. Soc.* **2015**, *137*, 7079-7082.

67. B. Dong, L. Wang, S. Zhao, R. Ge, X. Song, Y. Wang, Y. Gao. Immobilization of ionic liquids to covalent organic frameworks for catalyzing the formylation of amines with CO_2 and phenylsilane. *Chem. Commun.* **2016**, 52, 7082-7085.

68. N. Huang, P. Wang, M. A. Addicoat, T. Heine, D. Jiang. Ionic covalent organic frameworks: design of a charged interface aligned on 1D channel walls and its unusual electrostatic functions. *Angew. Chem. Int. Ed*. **2017**, *56*, 4982-4986.

69. L. Zhai, N. Huang, H. Xu, Q. Chen, D. Jiang. A backbone design principle for covalent organic frameworks: the impact of weakly interacting units on CO_2 adsorption. *Chem. Commun*. **2017**, *53*, 4242-4245.

70. S. Wan, J. Guo, J. Kim, H. Ihee, D. Jiang. A belt-shaped, blue Luminescent, and semiconducting covalent organic framework. *Angew. Chem. Int. Ed*. **2009**, *48*, 3197-3207.

71. G. Das, B. P. Biswal, S. Kandambeth, V. Venkatesh, G. Kaur, M. Addicoat, T. Heine, S. Verma, R. Banerjee. Chemical sensing in two dimensional porous covalent organic nanosheets. *Chem. Sci*. **2015,** 6, 3931-3939.

72. Y. Peng, Y. Huang, Y. Zhu, B. Chen, L. Wang, Z. Lai, Z. Zhang, M. Zhao, C. Tan, N. Yang, F. Shao, Y. Han, H. Zhang. Ultrathin two-dimensional

covalent organic framework nanosheets: preparation and application in highly sensitive and selective DNA detection. *J. Am. Chem. Soc*. **2017**, *139,* 8698-8704.

73. S. Ding, M. Dong, Y. Wang, Y. Chen, H. Wang, C. Su, W. Wang. Thioether-based fluorescent covalent organic framework for selective detection and facile removal of mercury (II). *J. Am. Chem. Soc*. **2016**, *138*, 3031-3037.

74. G. Lin, H. Ding, D. Yuan, B. Wang, C. Wang. A pyrene-based, fluorescent three-dimensional covalent organic framework. *J. Am. Chem. Soc*. **2016**, *138*, 3302-3305.

75. E. Jin, J. Li, K. Geng, Q. Jiang, H. Xu, Q. Xu, D. Jiang. Designed synthesis of stable light-emitting two-dimensional sp^2 carbon-conjugated covalent organic frameworks. *Nat. Commun.* **2018**, *9*, 4143.

76. M. R. Rao, Y. Fang, S. D. Feyter, D. F. Perepichka. Conjugated covalent organic frameworks via Michael addition-elimination. *J. Am. Chem. Soc.* **2017**, 139, 2421-2427.

77. X. Han, J. Zhang, J. Huang, X. Wu, D. Yuan, Y. Liu, Y. Cui. Chiral induction in covalent organic frameworks. *Nat. Commun*. **2018**, *9*, 1294.

78. Y. Zhang, X. Shen, X. Feng, H. Xia, Y. Mu, X. Liu. Covalent organic frameworks as pH responsive signaling. *Chem. Commun*. **2016**, *52*, 11088-11091.

79. Z. Kang, Y. Peng, Y. Qian, D. Yuan, M. A. Addicoat, T. Heine, Z. Hu, L. Tee, Z. Guo, and D. Zhao. Mixed matrix membranes (MMMs) comprising exfoliated 2D covalent organic frameworks (COFs) for efficient CO_2 separation. *Chem. Mater.* **2016**, *28*, 1277-1285.

80. G. Chen, H. Lan, S. Cai, B. Sun, X. Li, Z. He, S. Zheng, J. Fan, Y. Liu, W. Zhang. Stable hydrazone-linked covalent organic frameworks containing O,N,O′-chelating sites for Fe(III) detection in water. ACS Appl. Mater. Interfaces. 2019, 1113, 12830-12837.

Chapter 2

Design and Synthesis of Hydrazone-Linked Covalent Organic Frameworks for Carbon Dioxide Capture

Abstract:

The microporous hydrazone-linked COFs, TMHzcB-TFB-COF and TMHzcB-TFP-COF were synthesized TMHzcB-TFB-COF was constructed through condensation of 1,3,5-tris(3'-methoxy-4'-hydrazinecarbonylphenyl)benzene (TMHzcB) and 1,3,5-triformylbenzene (TFB) under solvothermal condition. The TMHzcB-TFP-COF was constructed from two building blocks of 1,3,5-tris(3'-methoxy-4'-hydrazinecarbonylphenyl)benzene (TMHzcB) and triformylphloroglucinol (TFP). These new COFs exhibited high crystallinity, permanent microporosity, excellent thermal, chemical stability, and abundant heteroatom sites on the pore walls. These two COFs exhibited remarkable CO_2 uptake capacity. Notably, the CO_2 uptake capacity of TMHzcB-TFP-COF reaches 14.4 wt% at 273 K and 1 bar.

2.1 Introduction

Carbon dioxide (CO_2) is the primary greenhouse gas increasing with population and industrial development. Serious global environment problem caused by CO_2 attracts great social attentions. Higher ocean temperatures can accelerate icebergs and ice shelves to melt, which can cause sea-level rise. Nowadays, developing the new technologies and novel materials for Carbon dioxide capture is very urgent and necessary.

Porous materials such as zeolites, activated carbon, alumina, metal-organic frameworks (MOFs) and microporous organic polymers (MOPs) have been designed and developed for carbon dioxide sorbents which derived from their high surface areas and isosteric heat of carbon dioxide adsorption.[1] COFs as a class of crystalline polymers, allow atomically precise integration of organic units into long-ordered 2D layers or 3D networks, which make themselves easily controlled skeleton, pore size, and topology.[2-5] Now, the various researchers focused on to enhance carbon dioxide capture performance to solve environmental problems.[6] To date, two strategies can improve the carbon dioxide capacity of the materials efficiently. Regulating porosity such as a high surface area and a small pore size is proven to be an effective way to enhance the ability of carbon dioxide absorption. For example, an azine-linked ACOF-1 with high surface area of 1176 m^2 g^{-1} and small pore size of 0.94 nm can store up to 177 mg g^{-1} of carbon dioxide under 273 K and 1 bar.[6a] Another approach is the incorporation of special functional sites to the COF skeleton that can enhance the selectivity of carbon dioxide over nitrogen to increase the carbon dioxide uptake and decreasing nitrogen capture. The amine and acid groups were introduced into the frameworks by post-synthesis methods, which can greatly enhance carbon dioxide absorption ability. [6c, 6d]

Designing COFs not only showed micropore structurebut also possessed active units, which is an effective way to improve the ability of carbon dioxide

uptake.[6] The hydrazone linkage has abundant oxygen and nitrogen heteroatoms and active N-H units to enhance carbon dioxide capture. The micropore hydrazone-linked COFs, TMHzcB-TFP-COF and TMHzcB-TFB-COF were successfully synthesized under solvothermal conditions. These two COFs possess a high surface area and micropore structure. Moreover, abundant heteroatoms such as nitrogen and oxygen on the skeleton benefit to the carbon dioxide uptake.

2.2 Design and synthesis of COFs and Model Compounds

2.2.1. Synthesis of TMHzcB-TFB-COF

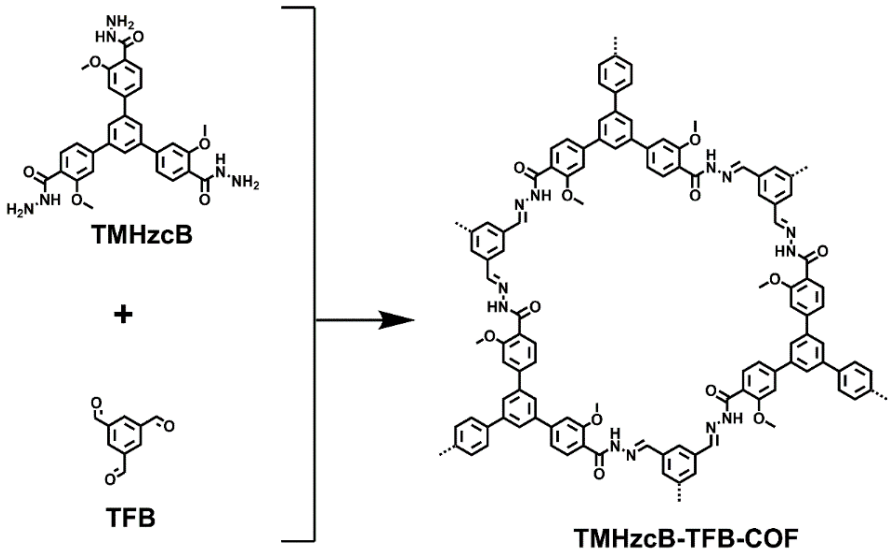

Scheme 1. Synthesis and structures of TMHzcB-TFB-COF.

TMHzcB-TFB-COF : A 10 mL Pyrex tube was charged with TMHzcB (15 mg, 0.026 mmol), TFB (4.3 mg, 0.026 mmol), dioxane (0.5 mL), mesitylene (0.5 mL) and AcOH (0.1 mL, 6 M), the mixture was sonicated for 2 minutes, degassed through three freeze-pump-thaw cycles, sealed under vacuum. The reaction was heated at 120 ºC for 168 h. The precipitate was collected and washed with tetrahydrofuran (THF) and acetone, soxhleted with THF for 12 h, dried under vacuum at 120 °C for 12 h to give the white powder (Yield 87%).

2.2.2 Synthesis of TMHzcB-TFP-COF

TMHzcB-TFP-COF : A 10 mL Pyrex tube was charged with TMHzcB (15 mg, 0.026 mmol), TFP (5.5 mg, 0.026 mmol), dioxane (0.5 mL), mesitylene (0.5 mL) and AcOH (acetic acid, 0.1 mL, 6 M), the mixture was sonicated for 2 minutes, degassed through three freeze-pump-thaw cycles, sealed under vacuum. The system was heated at 120 ºC for 168 h. The precipitate was collected and washed with THF and acetone, soxhleted with THF for 12 h, dried under vacuum at 120 °C for 12 h to give the white powder (Yield 86%).

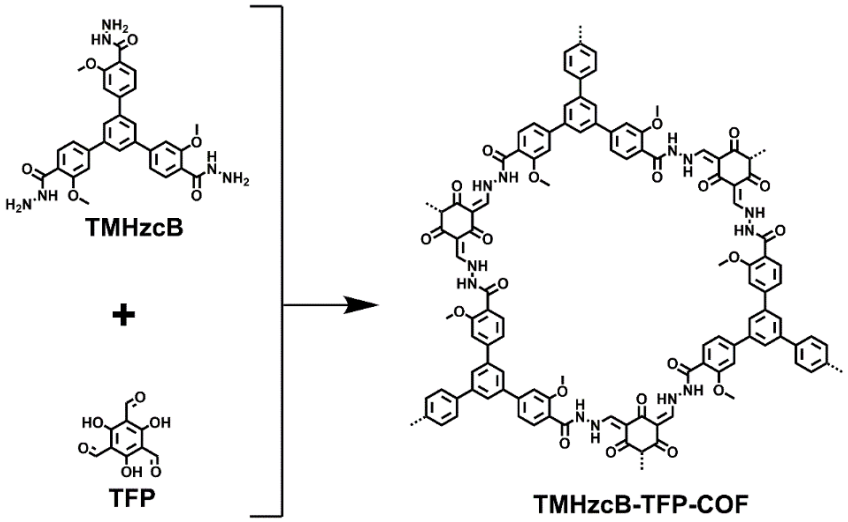

Scheme 2. Synthesis of TMHzcB-TFP-COF.

2.2.3 Synthesis of Model Compound-H

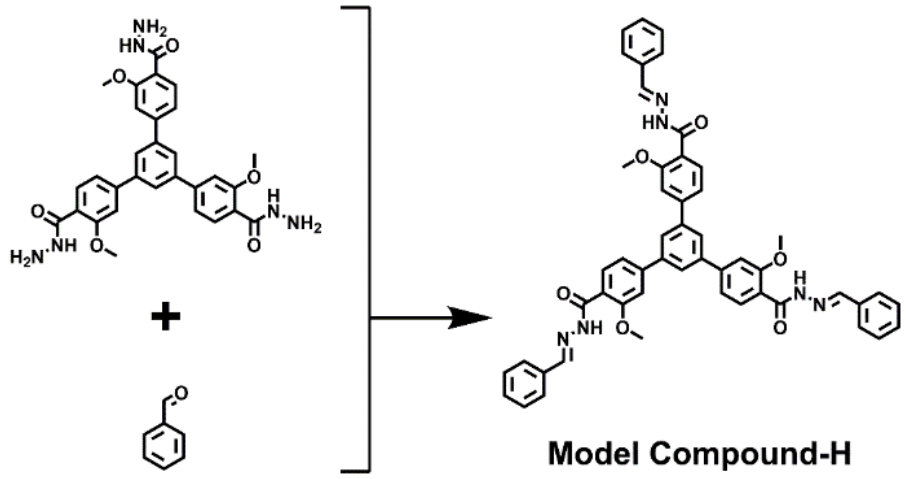

Scheme 3. Synthesis of Model Compound-H.

Model Compound-H: benzaldehyde (65 mg, 0.63 mol) and

1,3,5-tris(3`-methoxy-4`-hydrazinecarbonylphenyl)benzene **(**TMHzcB**)** (60 mg, 0.11 mmol), AcOH 0.1 mL was added in methanol 10 mL and chloroform 5 mL at room temperature with vigorous stirring about 5 minutes. The system was refluxed at 48 h, cooled down at room temperature, filtered and washed with methanol, dried under vacuum to afford Model Compound-H as white powder in 88% yield (78 mg). ^{1}H NMR ($CDCl_3$, 400 MHz): δ = 11.53 (s, 3H), 8.42 (s, 3H), 7.34-8.09 (m, 27H). 4.08 (s, 9H). ^{13}C NMR ($CDCl_3$, 500 MHz): δ (ppm) 162.51, 157.78, 148.00, 144.60, 134.84, 131.22, 130.54, 129.34, 127.56, 126.25, 122.23, 120.23, 111.57, 56.77.

2.2.4 Synthesis of Model Compound-Keto-form

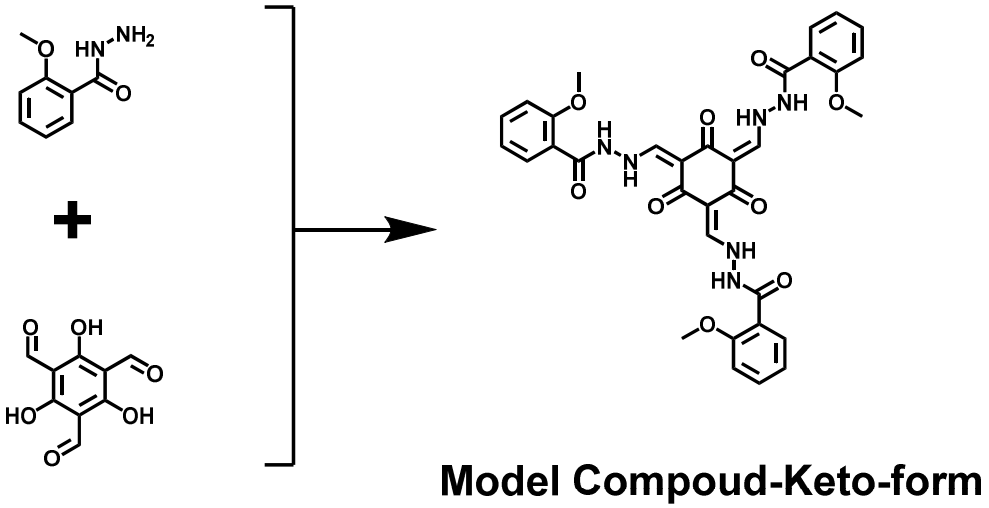

Scheme 4. Synthesis of Model Compound-Keto-form.

Model Compound-Keto-form: Triformylphloroglucinol (0.10 g, 0.48 mmol), 2-methoxybenzohydrazide (0.4 g, 2.4 mmol) and AcOH 0.1 mL was added into 45 mL methanol. Then, the mixture was under refluxing condition for 48 h. The system was cooled down to room temperature and the precipitate was collected by filtration, washed with methanol (25 mL × 3) and dichloromethane (5 mL × 3), and dried under vacuum to give an orange solid 0.30 g (Yield: 90%). ^{1}H NMR (400 MHz, DMSO) δ = 13.98 (s, 3H), 11.87 (s, 3H), 8.88 (s, 3H), 7.67 (d, 3H), 7.55 (t, 13H), 7.20 (d, 3H), 7.10 (t, 3H), 3.93 (s, 9H) ppm.

2.3 Results and discussions

2.3.1 Characterizations

The TMHzcB-TFB-COF and TMHzcB-TFP-COF were characterized by using Fourier transform infrared spectroscopy, ultraviolet-visible spectroscopy, elemental analysis, field emission scanning electron microscopy, thermogravimetric analysis, powder X-ray diffraction analysis and nitrogen adsorption.

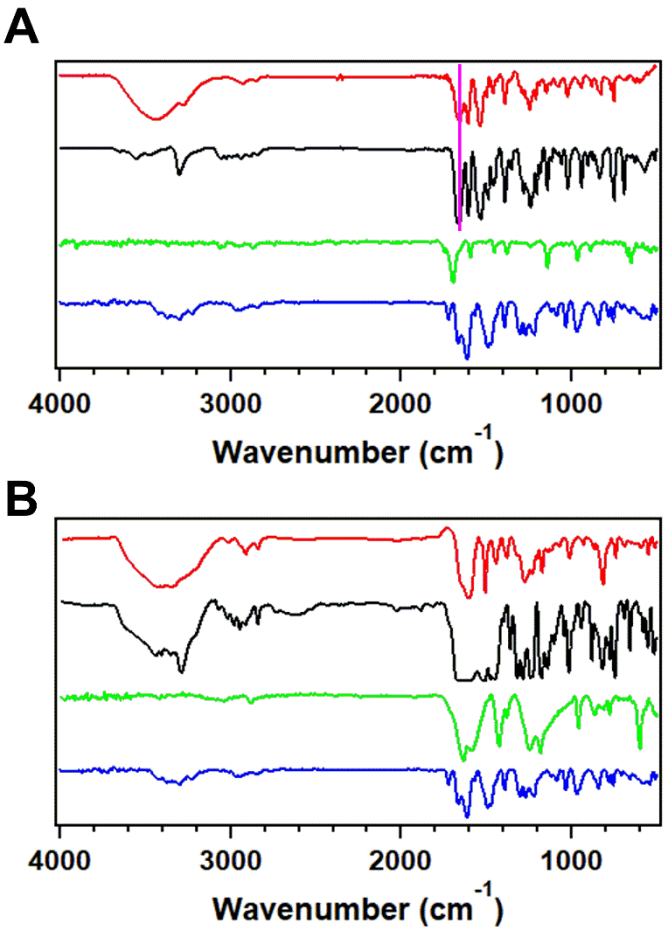

Figure 1. (A) FT-IR spectra of TMHzcB-TFB-COF (red curve), Model Compound-H (black curve), TFB, (green curve), TMHzcB (blue curve). (B) FT-IR spectra of TMHzcB-TFP-COF (red curve), Model Compound-Keto-form (black curve), TFP (green curve), and TMHzcB (blue curve).

To study structures of these COFs, I performed the FT-IR spectrum of hydrazone-linked COFs, Model Compounds, and buildings units. The FT-IR spectrum of TMHzcB-TFB-COF showed a stretching vibration band at 1665

cm^{-1} that belonged to the imine (C=N) bond, which indicated successful condensation of TMHzcB and TFB via the formation of imine bonds. Model Compound-H was synthesized through condensation of TMHzcB and benzaldehyde, and it also exhibited the imine vibration band at 1667 cm^{-1}, which is similar to the new TMHzcB-TFB-COF. The characteristic vibrational bands at 1660 cm^{-1} in the FT-IR spectrum of TMHzcB-TFP-COF were from the keto group of TFP (Figure 1B). The other keto peaks at 1618 cm^{-1} belonged to alkyl ketone (Scheme 2 and Scheme 3). The signal at 1593 cm^{-1} was contributed to carbon-carbon double bonds.

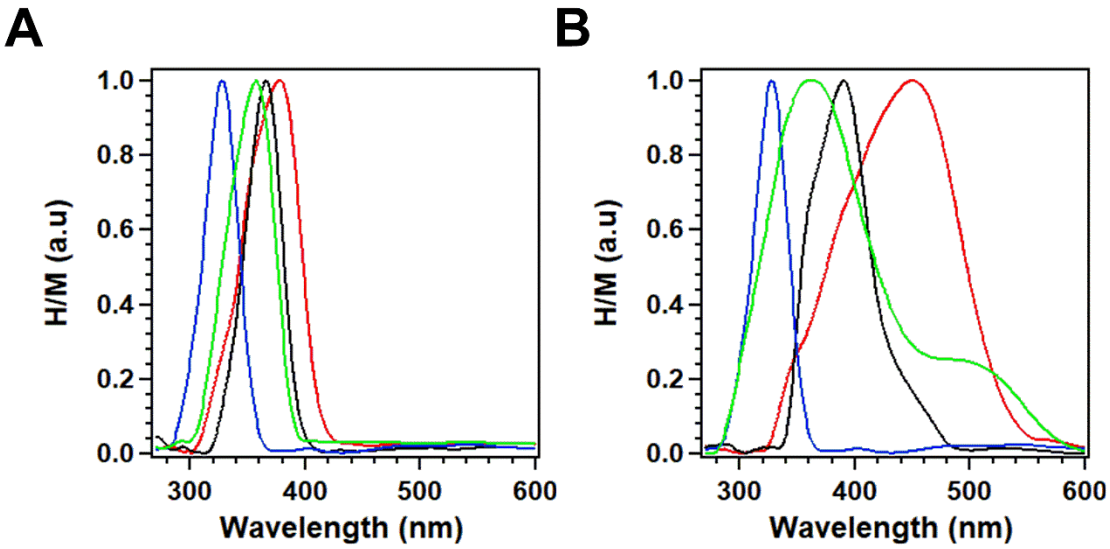

Figure 2. (A) Solid-state electronic absorption spectra of TMHzcB (blue curve), TFB (green curve), Model Compound-H (black curve), and TMHzcB-TFB-COF (red curve). (B) TMHzcB (blue curve), TFB (green curve), Model Compound-Keto-form (black curve), and TMHzcB-TFP-COF (red curve).

The TMHzcB-TFB-COF at the solid state showed an electronic absorption band at 380 nm (Figure 2A, red curve). The powders of TMHzcB (blue curve), TFB (green curve) and model compound (black curve) exhibited absorption bands at 327, 357 and 366 nm, respectively. Compared with monomers and model compound, the absorption band of TMHzcB-TFB-COF occurred obvious red-shift (Figure 2A). TMHzcB-TFP-COF also exhibited an obvious red-shift, comparing the building units of TMBHzB and TFP, and Model Compound-Keto-form (Figure 2B).

Elemental analysis of the TMHzcB-TFB-COF displayed that the C, H, and N contents were 69.09, 3.85, 10.20 %, respectively, which were close to the calculated values of 69.02, 4.46, and 12.38 % (Table 1). Comparing the calculated values of 64.46, 4.16, and 11.56 % for C, H, and N contents, the TMHzcB-TFP-COF displayed that the C, H, and N contents were 62.83, 4.51, 10.79 %, respectively (Table 1). Elemental analysis of two COFs showed a small amount of error between observed and calculated values, which is mainly due to the material being exposed to air during the test. Another reason may be little defects at the edge of the skeleton.

Table 1 : Elemental analysis of the TMHzcB-TFB-COF and TMHzcB-TFP-COF.

		C (%)	N (%)	H (%)
TMHzcB-TFB-COF	Observed Value	69.09	10.20	3.85
	Calculated Value	69.02	12.38	4.46
TMHzcB-TFP-COF	Observed Value	62.83	10.79	4.51
	Calculated Value	64.46	11.56	4.16

Field emission scanning electron microscopy (FE SEM) of TMHzcB-TFB-COF and TMHzcB-TFP-COF revealed micrometer-scale long rods (Figure. 3A and 3B).

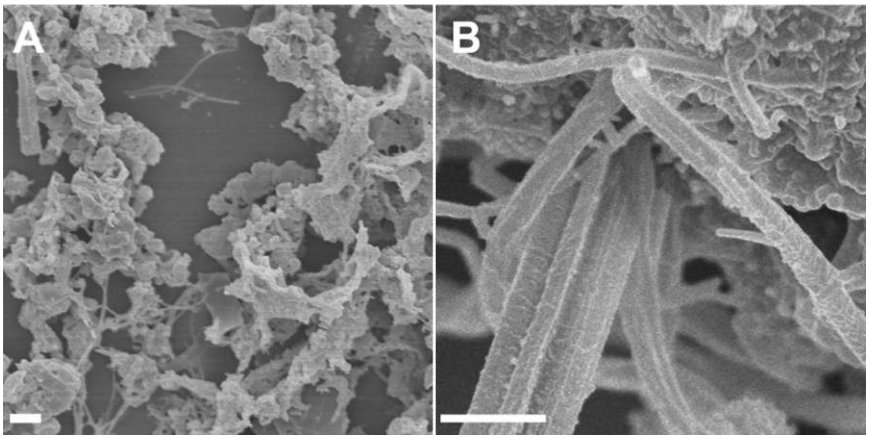

Figure 3. FE SEM Images of (A) TMHzcB-TFB-COF and (B) TMHzcB-TFP-COF (scale bar: 1 μm).

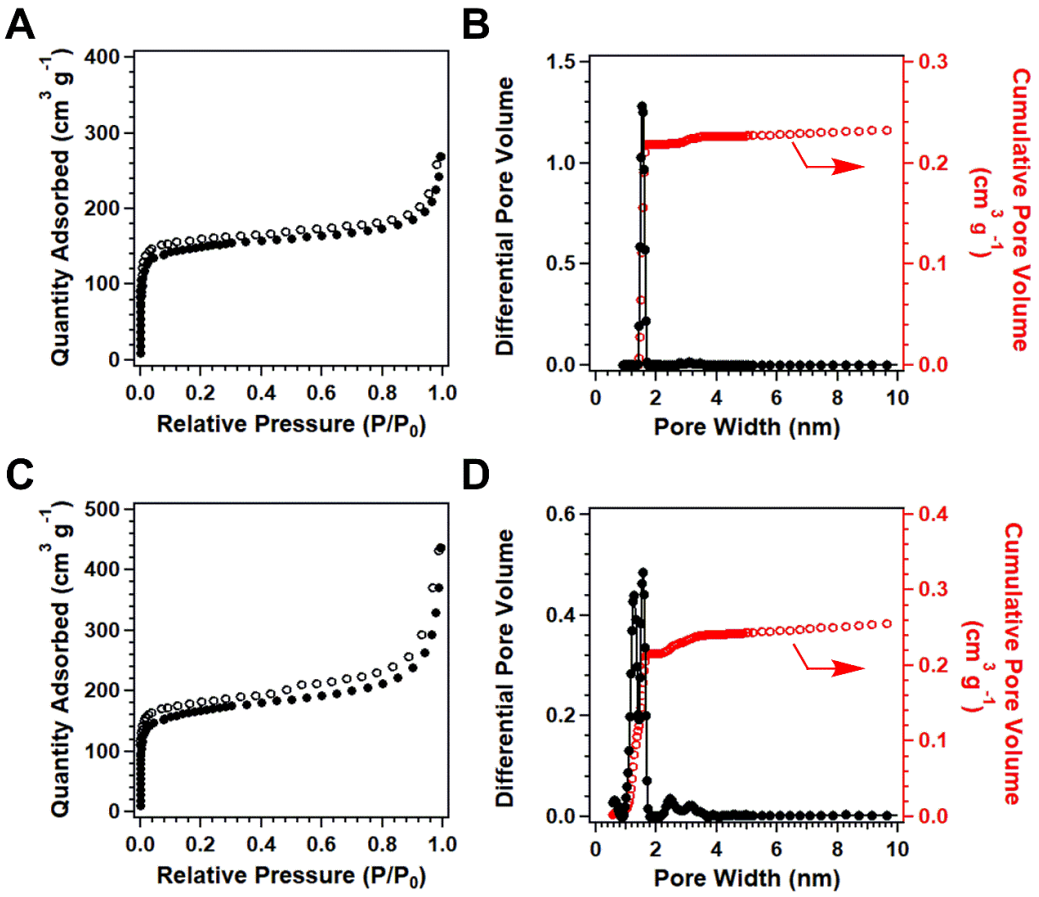

Figure 4. (A) Nitrogen sorption isotherm curve of TMHzcB-TFB-COF measured at 77 K (○: desorption, ●: adsorption). (B) Pore width distribution profile of TMHzcB-TFB-COF. (C) Nitrogen sorption isotherm curve of TMHzcB-TFP-COF. (D) Pore width distribution profile of TMHzcB-TFP-COF.

The porosity of new COFs could be evaluated by Nitrogen (N_2) adsorption-desorption isotherms at 77 K. TMHzcB-TFB-COF exhibited type-I sorption curves sorption curves (Figure 4A and Table 2), which are typical of the micropores and exhibited BET surface area of 471 $m^2\ g^{-1}$ with pore volume of 0.23 $cm^3\ g^{-1}$ (Figure 4B and Table 2). The pore size distribution was calculated by the nonlocal density functional theory method. TMHzcB-TFB-COF showed pore size of 1.6 nm. TMHzcB-TFP-COF also exhibited type-I sorption curves and BET surface area of 535 $m^2\ g^{-1}$ (Figure 4C and Table 2). TMHzcB-TFB-COF showed pore size about 1.3-1.6 nm with pore volumes of 0.25 $cm^3\ g^{-1}$ (Figure 4D and Table 2). These two COFs possess micropores, which are smaller than most hydrazone-linked COFs reported, such as COF-JLU4 (2.2 nm),[7] TFPPy-DETHz-COF (2.1 nm), COF-42 (2.8

nm),[8] COF-43 (3.5 nm),[8] and TFPT-COF (3.8 nm).[9]

Table 2: Porosity of TMHzcB-TFB-COF and TMHzcB-TFP-COF.

	BET Surface Area (m^2 g^{-1})	Pore Volume (cm^3 g^{-1})	Pore Size (nm)
TMHzcB-TFB-COF	471	0.23	1.6
TMHzcB-TFP-COF	535	0.25	1.3-1.6

I performed powder X-ray diffraction (PXRD) measurements to determine the crystalline structure of TMHzcB-TFB-COF and TMHzcB-TFP-COF. From PXRD pattern, TMHzcB-TFB-COF showed excellent crystallinity and exhibited strong PXRD peaks at 4.74°, 9.54°, 12.46°, and 25.94°, which were assigned to the (100), (200), (210), and (001) facts, respectively (Figure 5A). TMHzcB-TFP-COF also showed high crystallinity and all peaks could be clearly observed from Figure 5B.

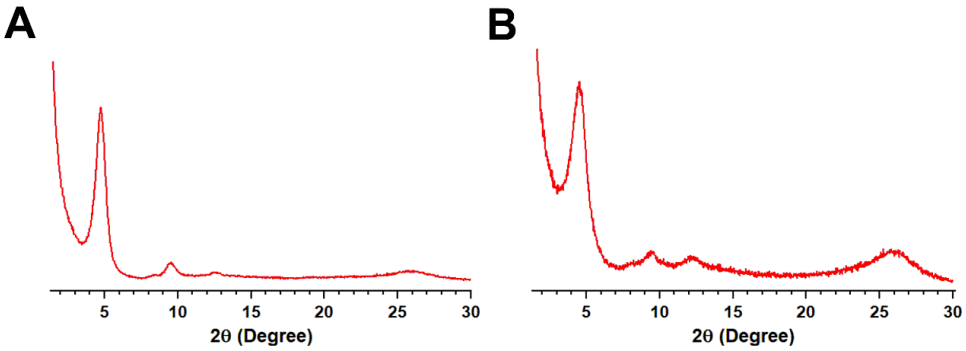

Figure 5. PXRD patterns of experimentally observed (A) TMHzcB-TFB-COF and (B) TMHzcB-TFP-COF.

As we know, the stability of the functional material is very important. The thermogravimetric analysis under the nitrogen atmosphere was investigated for new COFs. Both COFs exhibited excellent thermal stability up to 300 °C without any decomposition (Figure 6A and 6B).

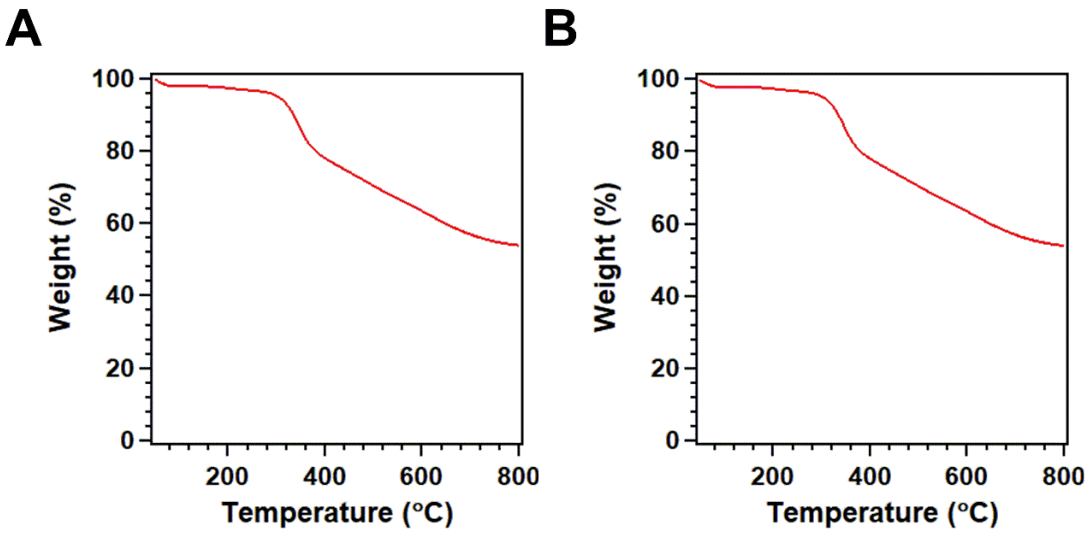

Figure 6. TGA curves of (A) TMHzcB-TFB-COF and (B) TMHzcB-TFP-COF under nitrogen atmosphere.

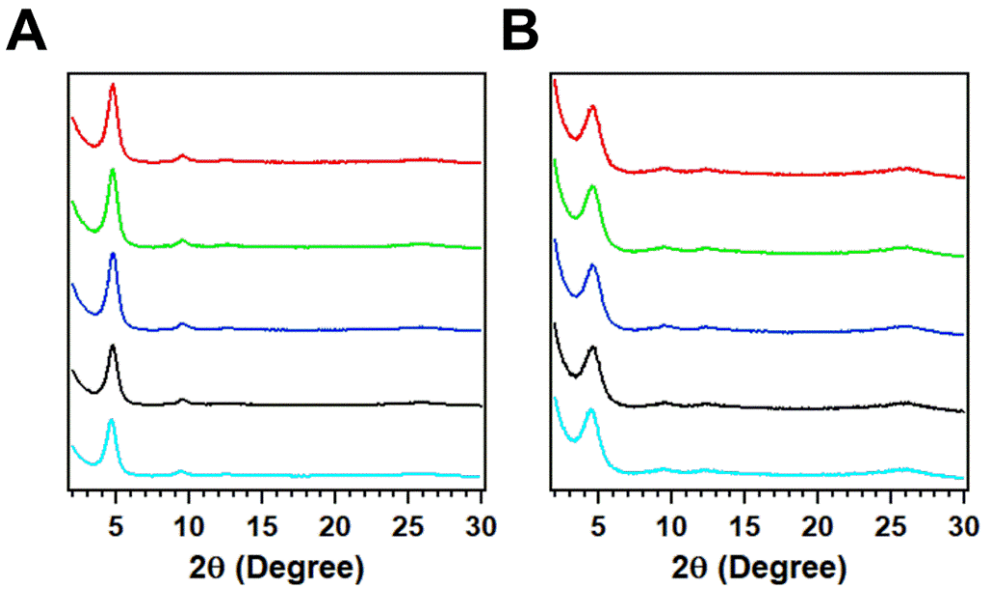

Figure 7. XRD patterns of (A) TMHzcB-TFB-COF and (B)TMHzcB-TFP-COF upon 24 h treatment in different conditions. As-synthesized COFs (red line), tetrahydrofuran (green line); water (blue line); 1M HCl (black line); 1 M NaOH (sky line).

I also checked the chemical stability of these COFs by immersing in different solvents, including tetrahydrofuran (THF), water, aqueous HCl (1 M) and NaOH (1 M) solutions at room temperature for 24 h. All samples were collected by filtered, washed with THF and water for six times, dried under vacuum for 24 h. I measured PXRD patterns of two COFs. All the samples of

TMHzcB-TFB-COF and TMHzcB-TFP-COF do not change diffraction peaks in XRD patterns without any change in the peak position, which indicated two new frameworks showed excellent chemical stability.

2.3.2 Carbon dioxide capture of COFs

These COFs have excellent microporous characteristics, excellent stability, and abundant nitrogen atoms in the skeleton, which can be used for carbon dioxide uptake. With these in mind, I investigated carbon dioxide adsorption ability of these frameworks.

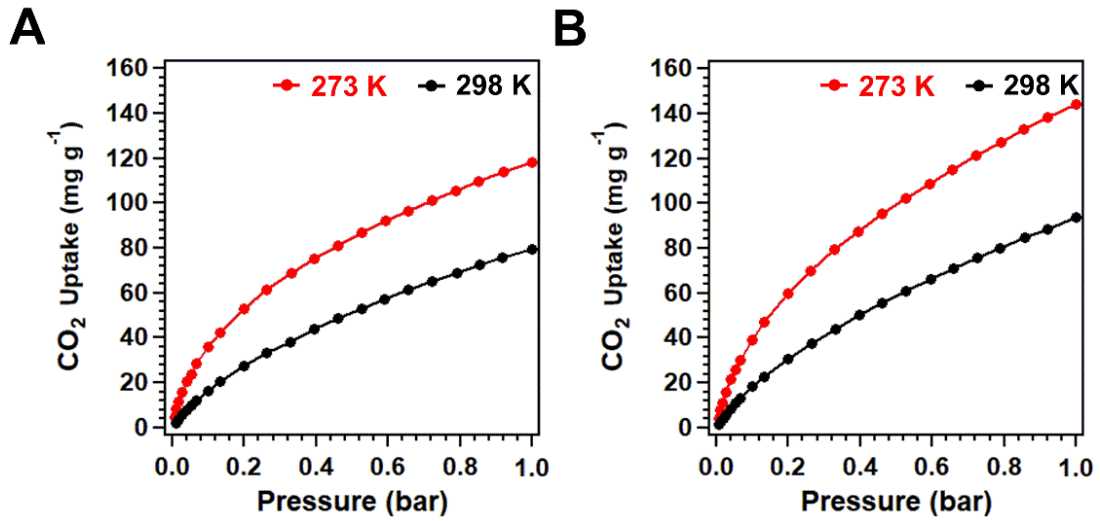

Figure 8. Carbon dioxide uptake of (A) TMHzcB-TFB-COF and (B) TMHzcB-TFP-COF under different temperature and 1 bar.

The carbon dioxide isotherms of new COFs were measured at 298 and 273 K under 1.0 bar (Figure 8). The TMHzcB-TFB-COF showed 11.9 wt% carbon dioxide uptakes at 273 K and 1 bar. Owing to smaller pore size and rich nitrogen atoms on the walls, TMHzcB-TFP-COF exhibited good carbon dioxide of 14.4 wt% at 273 K and 1 bar, which is higher than other hydrazone-linked COFs including TMHzcB-TFB-COF (11.9 wt%), COF-JLU4 (12.8 wt%),[7] and NUS-3 (6.6 wt%)[10] under the same conditions. Carbon dioxide adsorption ability of TMHzcB-TFP-COF was also better than other reported COFs, such as COF-5 (5.9 wt%),[11] COF-103 (7.6 wt%),[11] TDCOF-5 (9.2 wt%),[12] ILCOF-1 (6.0 wt%),[13] TFPA-TAPB-COF (6.1 wt%).[14] This value is lower than ACOF-1

(17.7 wt%).[6a] Isosteric heats of adsorption (Qst) for TMHzcB-TFB-COF and TMHzcB-TFP-COF were calculated based on carbon dioxide adsorption isotherms measured at 273 K and 298 K (Figure 9). Qst for TMHzcB-TFB-COF and TMHzcB-TFP-COF samples varied in the range of 28-32 KJ mol^{-1} and 27-32 KJ mol^{-1}, respectively, which which is higher than the values reported for C-N based COFs. [6a, 6b, 7, 10, 13-14.] The good carbon uptake capacity and binding by two COFs are attributed to the high porosity, the small pore size of two COFs and rich nitrogen and oxygen sites on the skeleton wall as well as the molecular sieving effects of the micropores.[6a]

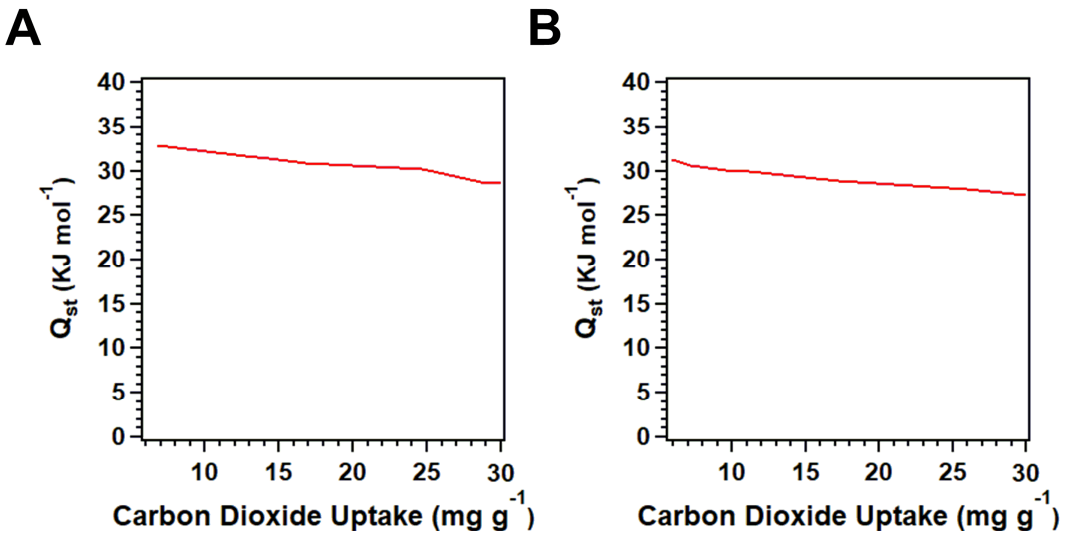

Figure 9. Isosteric heats of carbon dioxide adsorption of (A) TMHzcB-TFB-COF and (B) TMHzcB-TFP-COF.

2.4 Conclusion

In summary, two novel hydrazone-linked covalent organic frameworks, TMHzcB-TFB-COF and TMHzcB-TFP-COF, were successfully designed and synthesized under solvothermal conditions. These COFs showed permanent porosity, excellent chemical stability and micropore structure with abundant heteroatoms in the skeleton, affording to good carbon dioxide adsorption ability.

2.5 Experimental Section

2.5.1 Chemicals

The tetrahydrofuran, dioxane, mesitylene, benzaldehyde, methyl 2-methoxyacetate, hydrazine monohydrate and trifluoroacetic acid were obtained from TCI and Sigma-Aldrich. 1,3,5-triformylbenzene (TFB), Triformylphloroglucinol (TFP), 2-methoxybenzohydrazide, and 1,3,5-tris(3'-methoxy-4'-hydrazinecarbonylphenyl)benzene (TMHzcB) were synthesized using reported methods.[6a, 6b, 15]

2.5.2 Methods

Characterizations. ^{1}H NMR spectra were recorded on a Varian Mercury-400 NMR spectrometer, where chemical shifts (δ in ppm) were determined with a residual proton of the solvent as standard. Solid-state ^{13}C CP/MAS NMR spectra were recorded on a Bruker spectrometer AVANCE III 500 MH using a rotor frequency of 10 kHz. Fourier transforms Infrared (FT IR) spectra were recorded from 500 to 4000 cm^{-1} by using KBr pellets on a JASCO model FT IR-6100 spectrophotometer. Powder X-ray diffraction (PXRD) data were recorded on a Rigaku model RINT Ultima III diffractometer (Cu Kα, λ = 0.154 nm) by depositing powder on glass substrate, from 2θ = 1.5° up to 30° with 0.02° increment. TGA measurements were performed on a Mettler-Toledo model TGA/SDTA851e under Nitrogen atmosphere, which was heated from room temperature to 800 °C at a rate of 10 °C min^{-1}. Electronic absorption spectra were measured by a JASCO model V-670 spectrophotometer. The morphology of COFs was recorded on JEOL JSM-6701F. Nitrogen sorption isotherms were measured at 77 K with a Micromeritics Instrument Corporation model 3Flex surface characterization analyzer. The Brunauer-Emmett-Teller (BET) method was utilized to calculate the specific surface areas. By using the non-local density functional theory (NLDFT) model, the pore volume was derived from the sorption curve. The COFs were dried under vacuum at 120 °C

for carbon dioxane capture measurement.

2.5.3 Synthesis of building units

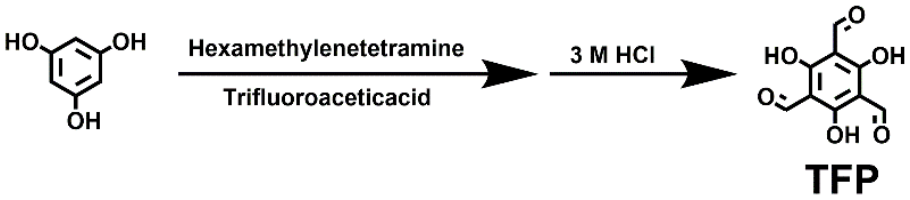

Scheme 5. Synthesis of Triformylphloroglucinol (TFP).[6b]

Triformylphloroglucinol (TFP): Trifluoroacetic acid (90 mL) was added anhydrous phloroglucinol (3.0 g, 24 mmol), and hexamethylenetetramine (7.0 g, 54 mmol) under argon atmosphere. The system was refluxed for three hours under argon atmosphere. 3M HCl 150 mL was added into the system and refluxed about two hours. The mixture was cooled down to room temperature, the reaction mixture was filtered through Celite bed. The filtrate was extracted by methylene dichloride with three times, dried over $NaSO_4$ and removed all the solvent by evaporation. The solid was washed with hot ethanol and further purified by column chromatography on silica by using methylene chloride to give a light yellow solid (yield 13%).^{1}HNMR (400 MHz, $CDCl_3$): δ = 14.12 (s, 3H),10.17 (s, 3H) ppm.

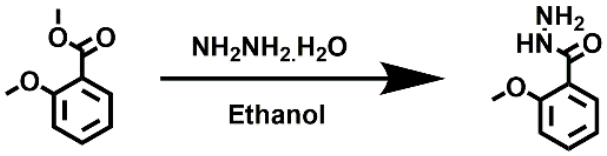

Scheme 6. Synthesis of 2-methoxybenzohydrazide.[7]

2-methoxybenzohydrazide: Methyl 2-methoxyacetate was obtained from TCI and further purified by column chromatography to give a colorless oil. The purified methyl 2-methoxyacetate (2.0 g, 0.012 mol) was added into ethanol 30 mL and hydrazine monohydrate (1.87 mL, 0.06 mol) was added into the mixture. The system was refluxed at 24 h and cooled down to room temperature overnight. The white solid was filtered and washed with ethanol, further purified by column chromatography on silica by using the mixture of hexane and ethyl acetate to give the white solid (yield 93%). ^{1}HNMR (400 MHz,

$CDCl_3$): δ = 9.46 (d, 1 H), 8.11 (dd, 1 H), 7.36 (d, 1 H), 7.03 (t, 1 H), 6.90 (d, 1 H), 4.27 (s, 2 H), 3.85 (s, 3 H) ppm.

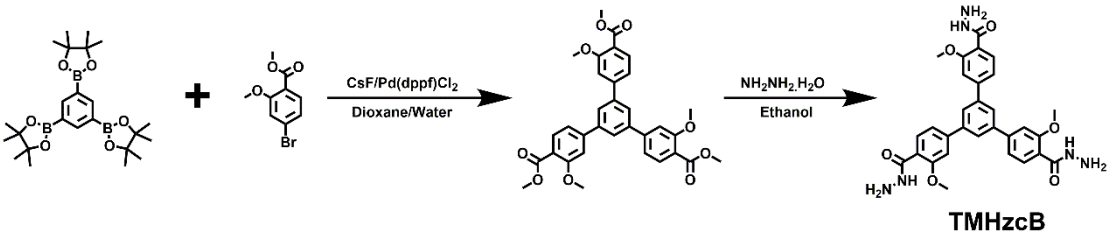

Scheme 7. Synthesis of 1,3,5-tris(3`-methoxy-4`-methoxycarbonylphenyl)benzene (TMHzcB).[15]

1,3,5-tris(3`-methoxy-4`-methoxycarbonylphenyl)benzene :

1,3,5-Tris(4,4,5,5-tetramethyl-1,3,2-dioxaborolan-2-yl)benzene (1.8 g, 4.4 mmol) and methyl 2-methoxy-4-bromon-benzoate (4.2 g, 17.1 mmol), dioxane 50 mL and water 50 mL were added into two neck bottles. The mixture was degassed by three freeze-pump-thaw cycles and protected under argon atmosphere. The Cesium fluoride (5.4 g, 36 mmol) and [1,1'-Bis(diphenylphosphino)ferrocene]dichloropalladium(II) (0.22 g, 0.30 mmol) were added into the mixture. The system was degassed by three freeze-pump-thaw cycles and finally protected under argon atmosphere. Then, the system was refluxed for three days. Then, the system was cooled down to room temperature, and extracted three times with ethyl acetate, dried with anhydrous Na_2SO_4, removed all the solvent under evaporation, purified by column chromatography on silica by using methylene chloride to give light yellow solid, and washed by little ethanol to give a white solid (yield, 77%). ^{1}HNMR (400 MHz, $CDCl_3$): δ = 7.94 (d, 3 H), 7.78 (s, 3 H), 7.28-7.30 (dd, 3 H), 7.22 (d, 1 H), 6.90 (d, 1 H), 4.93 (s, 9 H), 3.93 (s, 9 H) ppm.

1,3,5-tris(3`-methoxy-4`-hydrazinecarbonylphenyl)benzene (TMHzcB) :

1,3,5-tris(3`-methoxy-4`-methoxycarbonylphenyl)benzene (1.0 g, 1.75 mmol) and hydrazine monohydrate (0.5 mL, 10.5 mmol) was added into ethanol 60 mL. The mixture was refluxed for 48 hours and cooled down to room temperature at 2 hours. The white solid was filtered and washed by ethanol (yield, 88%). ^{1}HNMR (400 MHz, DMSO): δ = 9.02 (s, 3 H), 8.03 (s, 3 H), 7.84

(d, 3 H), 7.52-7.55 (m, 6 H), 6.90 (d, 3 H), 4.58 (s, 6 H), 4.01 (s, 9 H) ppm.

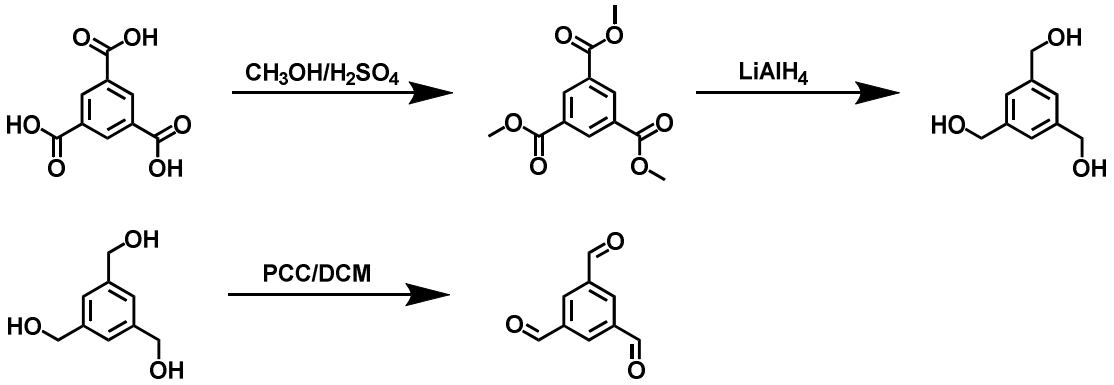

Scheme 8. Synthesis of 1,3,5-triformylbenzene (TFB).[6a]

Trimethyl benzene-1,3,5-tricarboxylate： The 1,3,5-Benzenetricarboxylic acid (1.50 g, 7.14 mmol) was added into in methanol 20 mL. The concentrated sulfuric acid (0.5 mL) was added dropwise and the mixture was refluxed for 24 hours. After cooling to room temperature, the saturated sodium bicarbonate was slowly added into the system. The precipitate was washed with plenty of water and methanol for three times to give the product as a white solid (1.76 g, 98%). ^{1}H NMR ($CDCl_3$, 400 MHz): δ = 3.98 (s, 9H), 8.86 (s, 3H) ppm.

1,3,5-tris-(hydroxymethyl)benzene： Lithium aluminum hydride (2.0 g, 5.2 mmol) in anhydrous THF (70 mL) was added into trimethyl benzene1,3,5-tricarboxylate (3 g, 1.2 mmol) at room temperature. The mixture was refluxed overnight. After cooling to room temperature, the potassium hydrogen sulfate and Celite were added into the system. The solution was filtered and washed with methanol for three times. The solvent was evaporated and the residue was purified by column chromatography on silica gel to give the white powder (1.5 g, 74%). ^{1}H NMR (DMSO, 400 MHz): δ = 4.47 (s, 6H), 7.12 (s, 3H) ppm.

1,3,5-triformylbenzene (TFB)： 1,3,5-tris-(hydroxymethyl)benzene (1.0 g, 5.95 mmol), Pyridinium chlorochromate (7.7 g, 35.7 mmol) and Celite (2.0 g) were added into anhydrous dichloromethane for 24 hours at room temperature. The mixture was filtered and washed with dichloromethane for three times. The solvent was removed by rotary evaporation. The crude product was purified by column chromatography on silica gel and the final product was washed by methanol to give a white solid (0.79 g, 82%). ^{1}H NMR ($CDCl_3$, 400 M): δ = 8.64 (s, 3H), 10.21 (s, 3H) ppm.

2.6 References

1. (a) G. Férey, C. Serre, T. Devic, G. Maurin, H. Jobic, P. L. Llewellyn, G. D. Weireld, A. Vimont, M. Daturi, J. Chang. Why hybrid porous solids capture greenhouse gases. *Chem. Soc. Rev.* **2011**, *40*, 550-562. (b) J. Liu, P. K. Thallapally, B. P. McGrail, D. R. Brown, J. Liu. Progress in adsorption-based CO_2 capture by metal-organic frameworks. *Chem. Soc. Rev*. **2012**, 41, 2308-2322. (c) D. Wu, F. Xu, B. Sun, R. Fu, H. He, K. Matyjaszewski. Design and preparation of porous polymers. *Chem. Rev.* **2012**, *112*, 3959-4015.
2. (a) X. Feng, X. Ding, D. Jiang. Covalent organic frameworks. *Chem. Soc. Rev.* **2012**, *41*, 6010-6022. (b) P. J. Waller, F. Gándara, O. M. Yaghi. Chemistry of covalent organic frameworks. *Acc. Chem. Res*. **2015**, *48*, 3053-3063. (c) N. Huang, P. Wang, D. Jiang. Covalent organic frameworks: a materials platform for structural and functional designs. *Nat. Rev. Mater*. **2016**, *1*, 16068. (d) C. S. Diercks, O. M. Yaghi. The atom, the molecule, and the covalent organic framework. *Science*, **2017**, *355*, 923.
3. (a) A. P. Côté, A. I. Benin, N. W. Ockwig, A. J. Matzger, M. O'Keeffe, O. M. Yaghi. Porous, crystalline, covalent organic frameworks. *Science*. **2005**, *310*, 1166-1170. (b) J. W. Colson, A. R. Woll, A. Mukherjee, M. P. Levendorf, E. L. Spitler, V. B. Shields, M. G. Spencer, J. Park and W. R. Dichtel. Oriented 2D covalent organic framework thin films on single-Layer graphene. *Science*. **2011**, *332*, 228-231.
4. L. Ascherl, T. Sick, J. T. Margraf, S. H. Lapidus, M. Calik, C. Hettstedt, K. Karaghiosoff, M. Do¨blinger, T. Clark, K. W. Chapman, F. Auras, T. Bein, Molecular docking sites designed for the generation of highly crystalline covalent organic frameworks. *Nat. Chem.* **2016**, *8*, 310-316.
5. E. Jin, M. Asada, Q. Xu, S. Dalapati, M. A. Addicoat, M. A. Brady, H. Xu, T. Nakamura, T. Heine, Q. Chen, D. Jiang. Two-dimensional sp^2

carbon–conjugated covalent organic frameworks. *Science*. **2017**, *357*, 673-676.

6. (a) Z. Li, X. Feng, Y. Zou, Y. Zhang, H. Xia, X. Liu and Y. Mu. A 2D azine-linked covalent organic framework for gas storage applications. *Chem. Commun*. **2014**, *50*, 13825-13828. (b) Z. Li, Y. Zhi, X. Feng, X. Ding, Y. Zou, X. Liu, Y. Mu. An azine-linked covalent organic framework: synthesis, characterization and efficient gas storage. *Chem. Eur. J*. **2015**, *21*, 12079-12084. (c) N. Huang, R. Krishna, D. Jiang, Tailor-made pore surface engineering in covalent organic frameworks: systematic functionalization for performance screening. *J. Am. Chem. Soc*. **2015**, *137*, 7079-7082. (d) N. Huang, X. Chen, R. Krishna, D. Jiang, Two-dimensional covalent organic frameworks for carbon dioxide capture through channel-wall functionalization. *Angew. Chem. Int. Ed*. **2015**, *54*, 2986-2990. (e) Y. Zeng, R. Zou, Y. Zhao. Covalent organic frameworks for CO_2 capture. *Adv. Mater.* **2016**, *28*, 2855-2873.
7. Y. Zhang, X. Shen, X. Feng, H. Xia, Y. Mu, X. Liu. Covalent organic frameworks as pH responsive signaling. *Chem. Commun*. **2016**, *52*, 11088-11091.
8. F. J. Uribe-Romo, C. J. Doonan, H. Furukawa, K. Oisaki, O. M. Yaghi. Crystalline covalent organic frameworks with hydrazone linkages. *J. Am. Chem. Soc*. **2011**, *133*, 11478-11481.
9. L. Stegbauer, K. Schwinghammer, B. V. Lotsch. A hydrazone-based covalent organic framework for photocatalytic hydrogen production. *Chem. Sci*. **2014**, *5*, 2789-2793.
10. Z. Kang, Y. Peng, Y. Qian, D. Yuan, M. A. Addicoat, T. Heine, Z. Hu, L. Tee, Z. Guo, and D. Zhao. Mixed matrix membranes (MMMs) comprising exfoliated 2D covalent organic frameworks (COFs) for efficient CO_2 separation. *Chem. Mater.* **2016**, *28*, 1277-1285.
11. H. Furukawa, O. M. Yaghi, Storage of hydrogen, methane, and carbon dioxide in highly porous covalent organic frameworks for clean energy

applications. *J. Am. Chem. Soc*. **2009**, *131*, 8875-8883.

12. Kahveci, T. Lslamoglu, G. A. Shar, R. S. Ding, H. M. EI-Kaderi, Targeted synthesis of a mesoporous triptycene-derived covalent organic framework. *CrystEngComm*. **2013**, *15*, 1524-1527.
13. M. G. Rabbani, A. K. Sekizkardes, Z. Kahveci, T. E. Reich, R. S. Ding, H. M. EI-Kaderi. A 2D mesoporous imine-linked covalent organic framework for high pressure gas storage applications. *Chem. Eur. J*. **2013**, *19*, 3324-3328.
14. L. Zhai, N. Huang, H. Xu, Q. Chen, D. Jiang. A backbone design principle for covalent organic frameworks: the impact of weakly interacting units on CO_2 adsorption. *Chem. Commun*. **2017**, *53*, 4242-4245.
15. Y. Zhang, H. Furukawa, N. Ko, W. Nie, H. J. Park, S. Okajima, K. E. Cordova, H. Deng, J. Kim, O. M. Yaghi. Introduction of functionality, selection of topology, and enhancement of gas adsorption in multivariate metal-organic framework-177. *J. Am. Chem. Soc.* **2015**, *137*, 2641-2650.

Chapter 3

Design of Luminescent Hydrazone-Linked Covalent Organic Frameworks

Abstract:

Covalent organic frameworks (COFs) can be predesigned to offer high-order π structures for developing light-emitting materials. However, high luminescence COFs are still a challenging goal. Here, I reported the designed synthesis of a series of hydrazone-linked COFs that possess good porosity and stability. The pore size was tuned from 1.6 to 3.7 nm by using different linkers and knots. Moreover, I reported that these hydrazone-linked COFs can be designed to tune emission colors by integrating different functional groups such as methoxy and methyl groups to change the emission color broadly from blue to green.

3.1 Introduction

Luminescent materials are widely used in our daily life and industrial manufacture. Nowadays, luminescence materials are also used in the fields of dyes, photo oxidants, chemical and biochemical sensor, solar traps, drug tracers and so on.[1-2] The development of fluorescent materials has a great significance for industrial production and life.

COFs are a novel class of crystalline porous organic polymers with high-ordered π structures. These outstanding merits give a platform for light-emitting materials. Nowadays, various luminescence COFs have been reported. [3-11] However, most COFs showed simple and poor luminescence, and it is very difficult to achieve controllable luminescence owing to rare functional building units. Most luminescence COFs were constructed by B-Oand C-N as linkage. However, B-O based COFs can be usually decomposed in humidity. C-N based COFs including azine, imine, and hydrazone, showed excellent chemical stability,[12-15] which provides a platform for functional luminescence COFs.

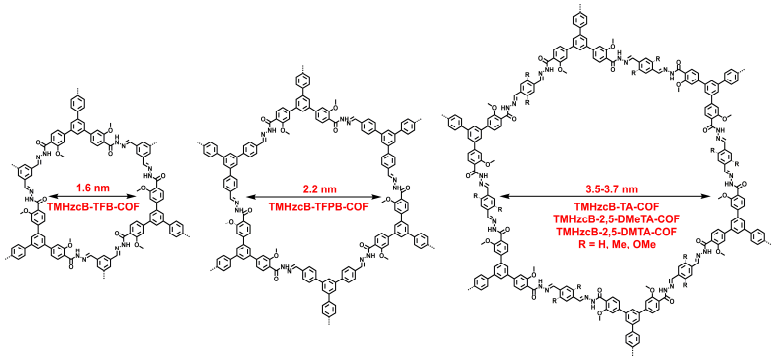

Scheme 1. Structure of designed hydrazone-linked COFs.

The hydrazone based COFs can give non-planar linkages that can weaken fluorescence quenching through strong π-π interaction of adjacent layers, which is beneficial to develop light-emitting frameworks. Moreover, different building units with different lengths and modify functional groups can be further

applied to exploit tunable luminescence COFs. Here, I designed a series of light-emitting hydrazone-linked COFs adjusted by functional linker and vertex afforded various luminescence from blue to green. The pore size of hydrazone-linked frameworks can be controlled from micropores (1.6 nm) and mesopores (3.7 nm) by using different building units (Scheme 1), which also broaden the structures of hydrazone-linked COFs.

3.2 Synthesis of COFs and Model Compounds

3.2.1 Structures of TMHzcB-TFB-COF

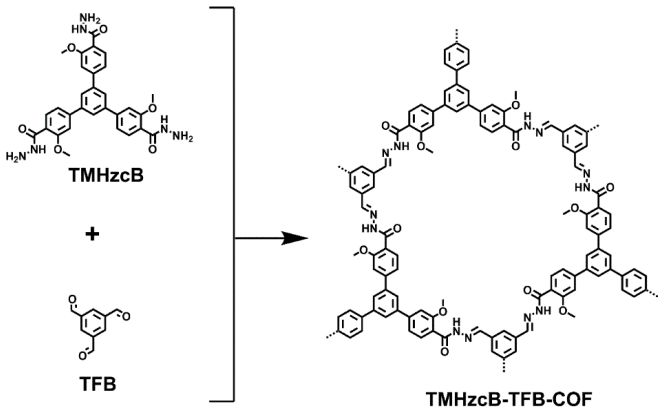

Scheme 2. Synthesis and structure of TMHzcB-TFB-COF.

TMHzcB-TFB-COF: The specific synthesis procedure can be referred to in chapter II.

3.2.3 Synthesis of TMHzcB-TFPB-COF

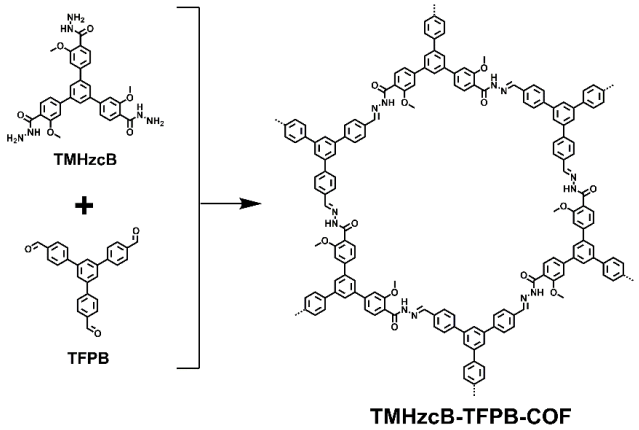

Scheme 3. Synthesis and structure of TMHzcB-TFPB-COF.

TMHzcB-TFPB-COF: A 10 mL Pyrex tube was charged with TMHzcB (15 mg, 0.026 mmol), 1,3,5-tris(4-formylphenyl) benzene (TFPB) (10.3 mg, 0.026 mmol), dioxane (0.7 mL), mesitylene (0.3 mL) and AcOH (0.1 mL, 6 M), the mixture was sonicated for 2 minutes, degassed through three freeze-pump-thaw cycles, sealed under vacuum. The system was heated at 120 ºC for 168 h. The powder collected was washed with THF for three times and acetone for three times, soxhleted by THF at 12 h, dried under vacuum at 120 °C for 12 h to give the white powder (Yield: 89%).

3.2.3 Synthesis of TMHzcB-TA-COF

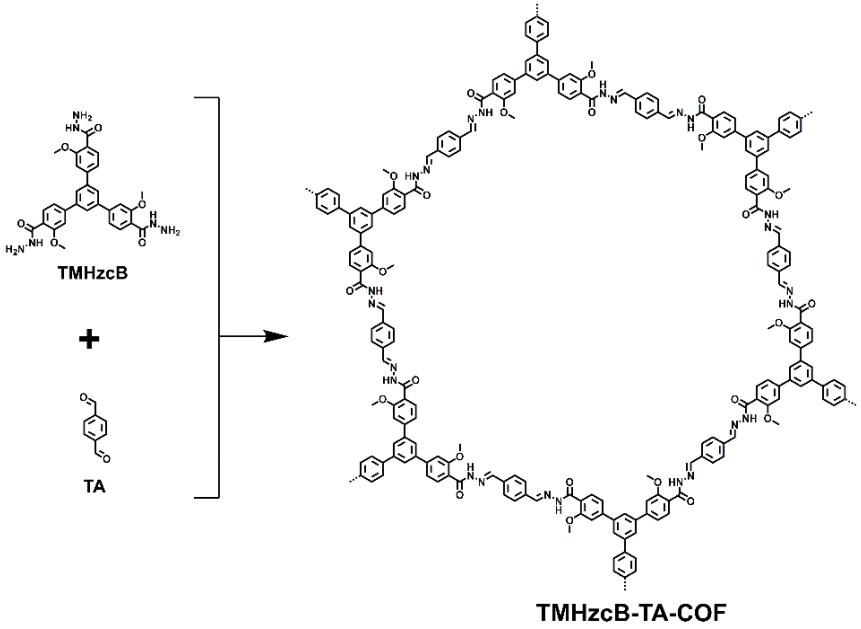

Scheme 4. Synthesis and structure of TMHzcB-TA-COF.

TMHzcB-TA-COF: A 10 mL Pyrex tube was charged with TMHzcB (18 mg, 0.032 mmol), terephthalaldehyde (TA) (6.2 mg, 0.026 mmol), dioxane (0.6 mL), mesitylene (0.4 mL) and AcOH (0.1 mL, 6 M), the mixture was sonicated for 2 minutes, degassed through three freeze-pump-thaw cycles, sealed under vacuum. The system was heated at 120 ºC for 168 h. The powder collected was washed with THF for three times and acetone for three times, soxhleted by THF at 12 h, dried under vacuum at 120 °C for 12 h to give the yellow powder (Yield: 85%).

3.2.4 Synthesis of TMHzcB-2,5-DMeTA-COF

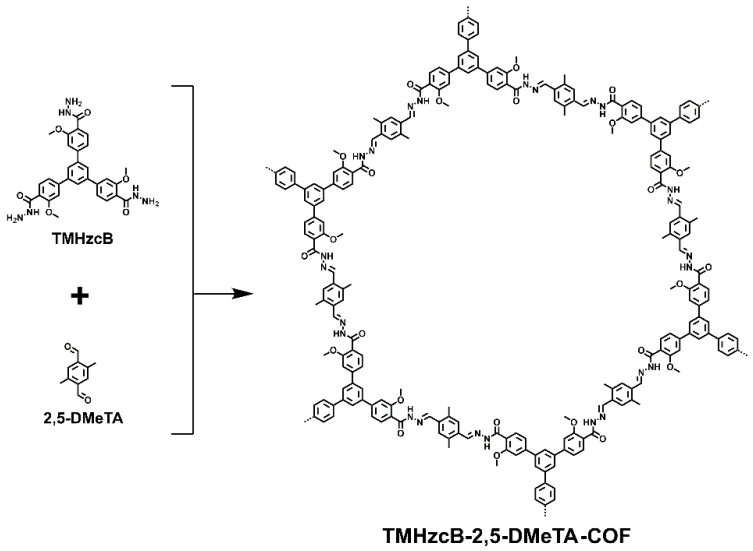

Scheme 5. Synthesis and structure of TMHzcB-2,5-DMeTA-COF.

TMHzcB-2,5-DMeTA-COF: A 10 mL Pyrex tube was charged with TMHzcB (15 mg, 0.026 mmol), 2,5-dimethylterephthalaldehyde (2,5-DMeTA) (6.4 mg, 0.039 mmol), dioxane (0.6 mL), mesitylene (0.4 mL) and AcOH (0.1 mL, 6 M), the mixture was sonicated for 2 minutes, degassed through three freeze-pump-thaw cycles, sealed under vacuum. The system was heated at 120 ºC for 168 h. The powder collected was washed with THF for three times and acetone for three times, soxhleted by THF at 12 h, dried under vacuum at 120 °C for 12 h to give the light-yellow powder (Yield: 93%).

3.2.5 Synthesis of TMHzcB-2,5-DMTA-COF

TMHzcB-2,5-DMTA-COF: A 10 mL Pyrex tube was charged with TMHzcB (15 mg, 0.026 mmol), 2,5-dimethoxyterephthalaldehyde (2,5-DMTA) (7.7 mg, 0.039 mmol), dioxane (0.4 mL), mesitylene (0.6 mL), and AcOH (0.1 mL, 6 M), the mixture was sonicated for 2 minutes, degassed through three freeze-pump-thaw cycles, sealed under vacuum. The system was heated at 120 ºC for 168 h. The powder collected was washed with THF for three times and acetone for three times, soxhleted by THF at 12 h, dried under vacuum at 120 °C for 12 h to give the yellow-green powder (Yield: 92%).

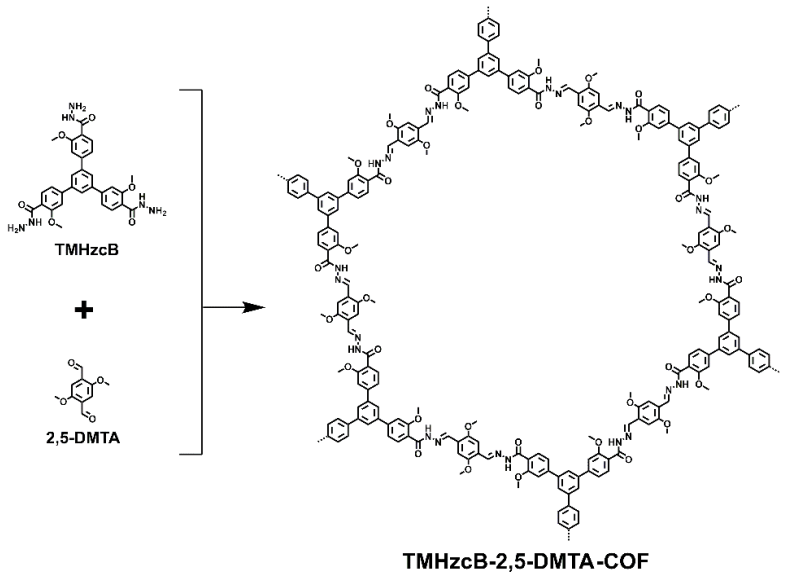

Scheme 6. Synthesis and structure of TMHzcB-2,5-DMTA-COF.

3.2.6 Synthesis of Model Compound-Me

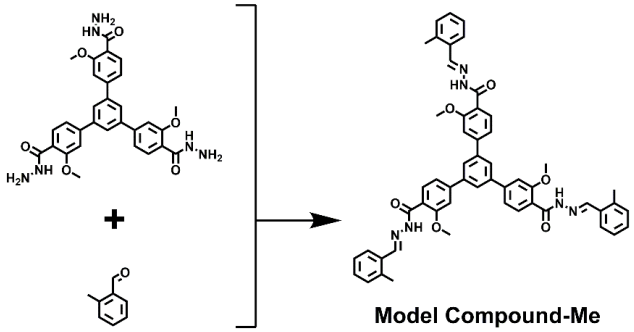

Scheme 7. Synthesis of Model Compound-Me.

Model Compound-Me: 2-methylbenzaldehyde (101 mg, 0.63 mol), TMHzcB (80 mg, 0.14 mmol), and AcOH 0.1 mL were added in methanol 15 mL and chloroform 5 mL at room temperature with vigorous stirring about 5 minutes. The system was refluxed at 48 hours, cooled down at room temperature, filtered and washed with methanol, dried under vacuum to afford Model Compound-Me as a white-yellow powder in 83% yield (101 mg).^{1}H NMR ($CDCl_3$, 400 MHz): δ = 11.52 (s, 3H), 8.68 (s, 3H), 7.29-8.11 (m, 24H), 4.08 (s, 9H), 2.47 (s, 9H) ppm. ^{13}C NMR ($CDCl_3$, 400 MHz): δ = 162.50, 157.79, 146.70, 141.62, 137.42, 132.83, 131.39, 131.24, 126.67, 126.57, 122.88, 120.19, 111.54, 56.80, 19.63 ppm.

3.2.7 Synthesis of Model Compound-OMe

Model Compound-OMe: 2-methoxybenzaldehyde (101 mg, 0.84 mol), 1,3,5-tris(3`-methoxy-4`-hydrazinecarbonylphenyl)benzene (**TMHzcB**) (80 mg, 0.14 mmol), AcOH 0.1 mL were added in methanol 10 mL and chloroform 5 mL at room temperature with vigorous stirring about 5 minutes. The system was refluxed at 48 hours, cooled down at room temperature, filtered and washed with methanol, dried under vacuum to afford Model Compound-OMe as a white powder in 85% yield (104 mg).^{1}H NMR ($CDCl_3$, 400 MHz): δ = 11.54 (s, 3H), 8.71 (s, 3H), 8.09-7.04 (m, 24H), 4.06 (s, 9H), 3.88 (s, 9H) ppm. ^{13}C NMR ($CDCl_3$, 400 MHz): δ = 162.57, 158.22, 157.74, 143.29, 132.00, 131.08, 126.11, 123.22, 122.87, 121.23, 120.08, 112.23,111.45, 56.61, 56.15 ppm.

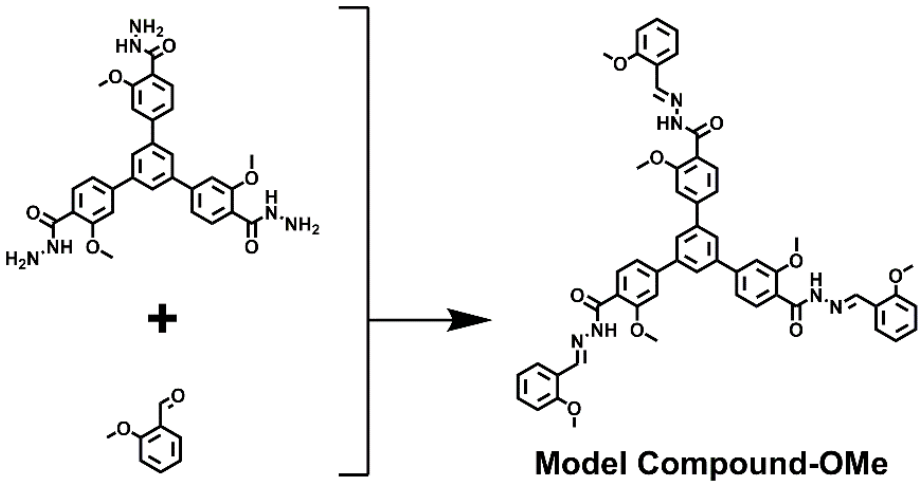

Scheme 8. Synthesis of Model Compound-OMe.

3.3 Results and discussions

3.3.1 Characterizations

These luminescent hydrazone-linked COFs were new frameworks and fully characterized by using Fourier transform infrared spectroscopy, ultraviolet-visible spectroscopy, elemental analysis, high-emission field emission scanning electron microscopy, thermogravimetric analysis, powder X-ray diffraction analysis and nitrogen adsorption.

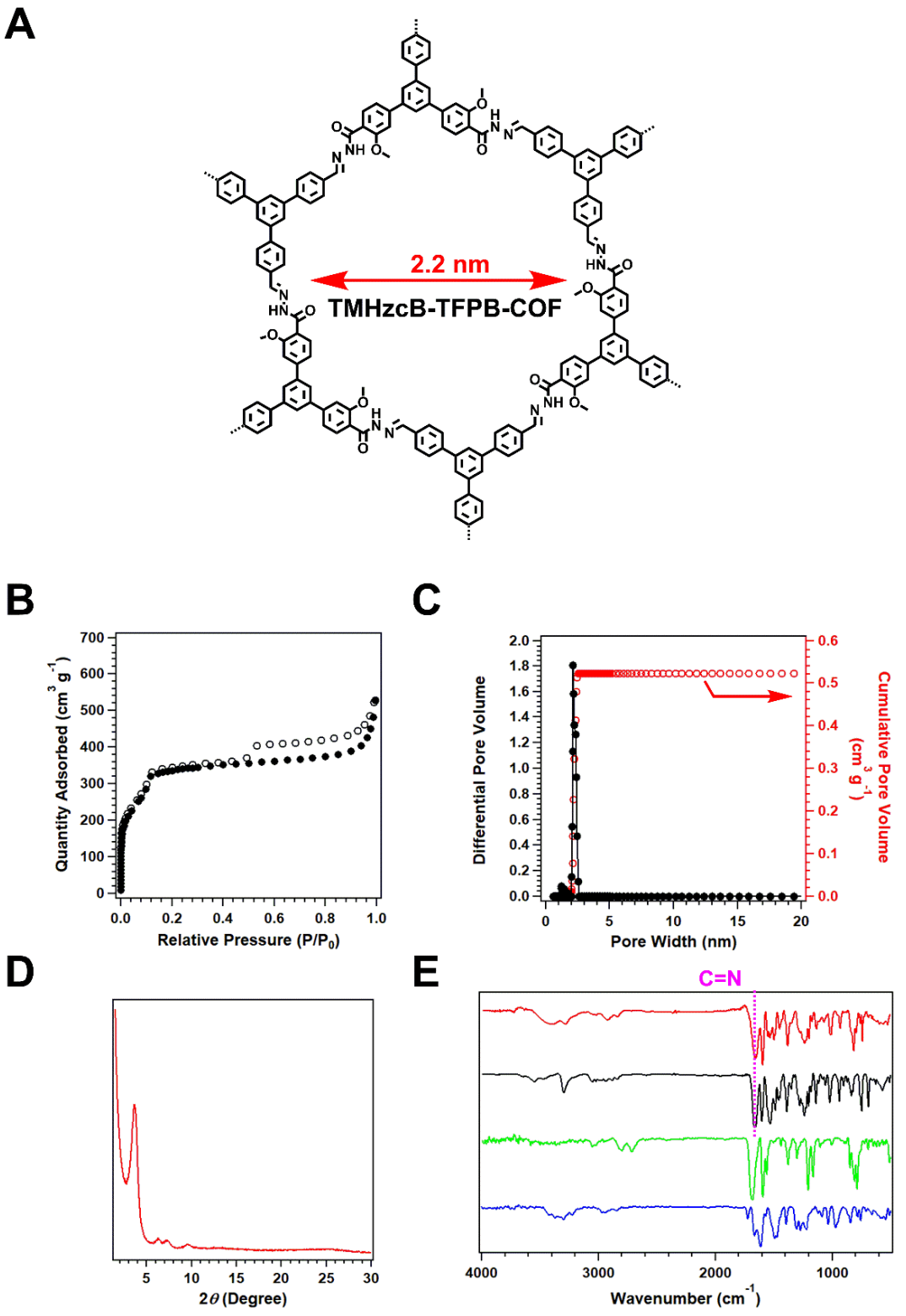

Figure 1 (A) The structure of TMHzcB-TFPB-COF. (B) Nitrogen sorption isotherm curve of TMHzcB-TFPB-COF measured at 77 K (○: desorption, ●: adsorption). (C) Pore size (black dots and curve) and pore width distribution (red dots) of TMHzcB-TFPB-COF. (D) PXRD patterns of experimentally observed. (E) FT-IR spectra of TMHzcB-TFPB-COF (red curve), Model Compound-H (black curve), TFPB (green curve), and TMHzcB (blue curve).

Firstly, I check the porosity of TMHzcB-TFPB-COF, which is evaluated by Nitrogen (N_2) adsorption-desorption isotherms at 77 K. TMHzcB-TFPB-COF exhibited type-IV sorption curves (Figure 1B and 1 C), which are typical of the micropores and exhibited BET surface area of 1116 m^2 g^{-1} with pore volume of 0.52 cm^3 g^{-1} (Figure 1C). The pore size distribution was calculated by the nonlocal density functional theory method. The pore size of TMHzcB-TFPB-COF was calculated at 2.2 nm. The powder X-ray diffraction (PXRD) was measured to determine the crystalline structure of the new COF. TMHzcB-TFPB-COF showed excellent crystallinity and exhibited strong PXRD peaks at 3.56°, 6.28°, 7.22°, and 9.56°, which were assigned to the (100), (110), (200), and (210) facts, respectively (Figure 1D, red curve). FT-IR spectrum (Figure 1E), the aldehyde group of TFPB showed stretching vibration band at 1690 cm^{-1} (green curve). Model Compound-H was constructed through condensation of TMHzcB and benzaldehyde. It exhibited the imine vibration band at 1667 cm^{-1}. Comparing TFPB and Model Compound-H, TMHzcB-TFPB-COF showed no signal of aldehyde units and the stretching vibration band of the imine (C=N) bond at 1667 cm^{-1} was clearly observed, which further confirmed the character of TMHzcB-TFPB-COF.

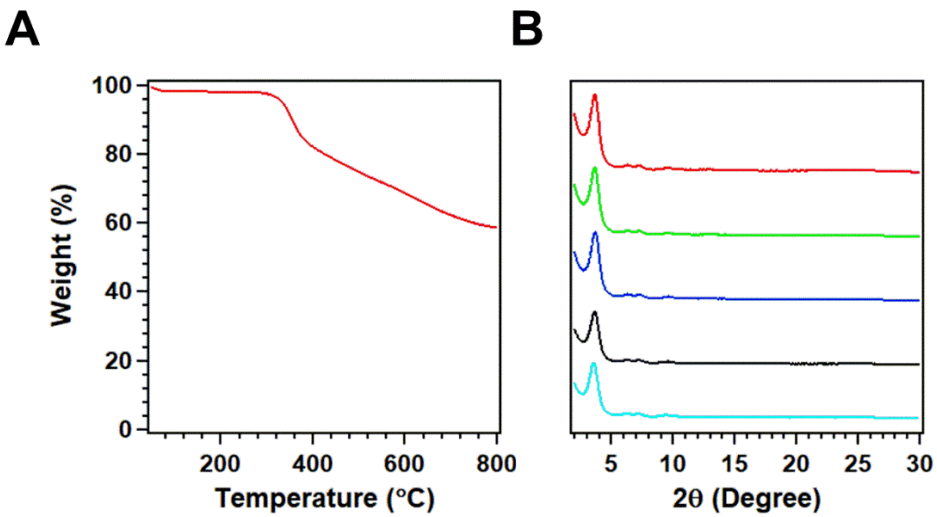

Figure 2. (A) TGA curve of TMHzcB-TFPB-COF under nitrogen atmosphere. (B) PXRD patterns, of TMHzcB-TFPB-COF upon 24 h treatment in different conditions. As-synthesized material (red line); THF (green line); water (blue line);1M HCl (black line);1 M NaOH (sky-blue line).

I investigated thermogravimetric analysis (TGA) under nitrogen atmosphere for TMHzcB-TFPB-COF to check physical stability. TMHzcB-TFPB-COF can keep integrity up to 300 °C without any decomposition (Figure 2A). The chemical stability of new COF in different solvents, including tetrahydrofuran (THF), water, aqueous HCl (1 M) and NaOH (1 M) solutions were checked at room temperature for 24 h. All samples were collected by filtered, washed with THF and water for six times, dried under vacuum for 24 h. From the PXRD patterns of COFs in different conditions, all the samples can remain diffraction peaks in PXRD patterns without any change in the peak position (Figure 2B).

I also checked the elemental analysis for TMHzcB-TFPB-COF. TMHzcB-TFPB-COF showed that the C, H, and N contents were 75.06, 4.73, and 8.12%, respectively, which were close to the calculated values of 75.25, 3.86, and 9.75% (Table 1). The H content in the observed value is higher than the calculated value. This main reason may be the COFs sample contacted with water vapor in the air during the test, which leads to an increase in H content. Another reason is some defects of frameworks, which also cause little error between observed and calculated values.

Table 1：Elemental analysis of the TMHzcB-TFPB-COF.

	C (%)	N (%)	H (%)
Observed Value	75.06	8.12	4.73
Calculated Value	75.25	9.75	3.86

The morphology of TMHzcB-TFPB-COF was observed by field-emission scanning electron microscopy (FE SEM). The TMHzcB-TFPB-COF adopted aggregated micrometer-scale particles (Figure. 3A and 3B).

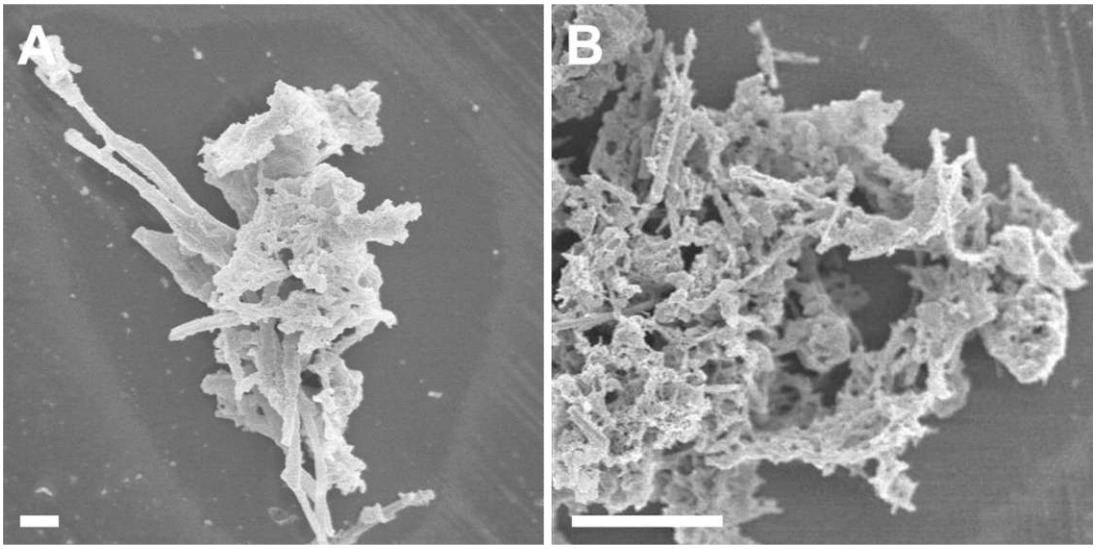

Figure 3. FE SEM Images of TMHzcB-TFPB-COF (A: scale bar: 1 um; B: scale bar: 10 um).

TMHzcB (blue curve), TFPB (green curve) and model compound (black curve) at the solid state exhibited absorption peaks at 327, 357 and 366 nm, respectively. The absorption band of TMHzcB-TFPB-COF occurred an obvious red-shift and had an electronic absorption peak at 398 nm (Figure 5A, red curve).

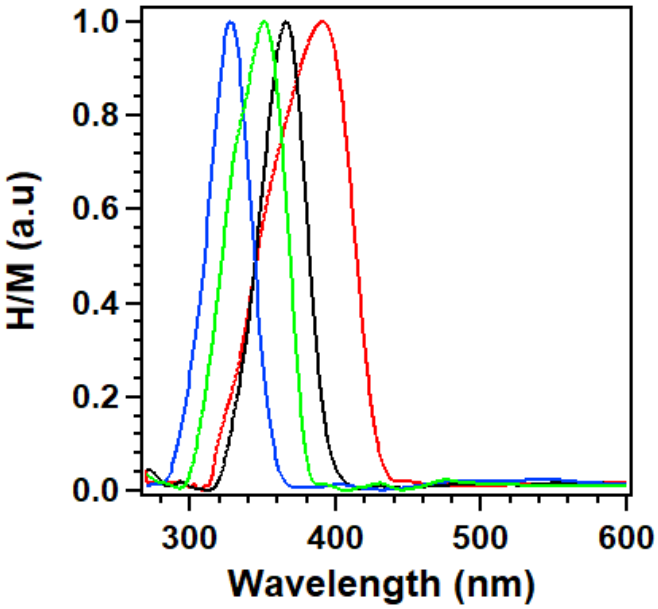

Figure 4. Solid-state electronic absorption spectra of TFPB (green curve), TMHzcB (blue curve), Model Compound-H (black curve), and TMHzcB-TFPB-COF (red curve),

TMHzcB-TA-COF showed BET surface area of 471 m^2 g^{-1} with pore volume of 0.26 cm^3 g^{-1} (Figure 5B and 5C, red curve). The new framework showed pore size of 3.7 nm (black curve), which was calculated by the nonlocal density functional theory method. Moreover, the new COF exhibited type-IV sorption curves, which accorded with the micropore character. TMHzcB-TA-COF displayed high crystallinity and all peak was clearly observed as PXRD peaks at 2.40°, 4.10°, 6.18°, and 25.54 (Figure 1D), which were assigned to the (100), (110), (210), and (001) facts, respectively

I checked FT-IR spectrum of building units, Model Compound-H and TMHzcB-TA-COF. As showed in Figure 5E, the aldehyde group of Terephthalaldehyde (TA) showed a stretching vibration band at 1691 cm^{-1} (green curve). Comparing to TA and Model Compound-H, the TMHzcB-TA-COF showed no signal of aldehyde units and stretch vibration of imine bond at 1665 cm^{-1} (red curve), which is similar to the Model Compound-H (black curve).

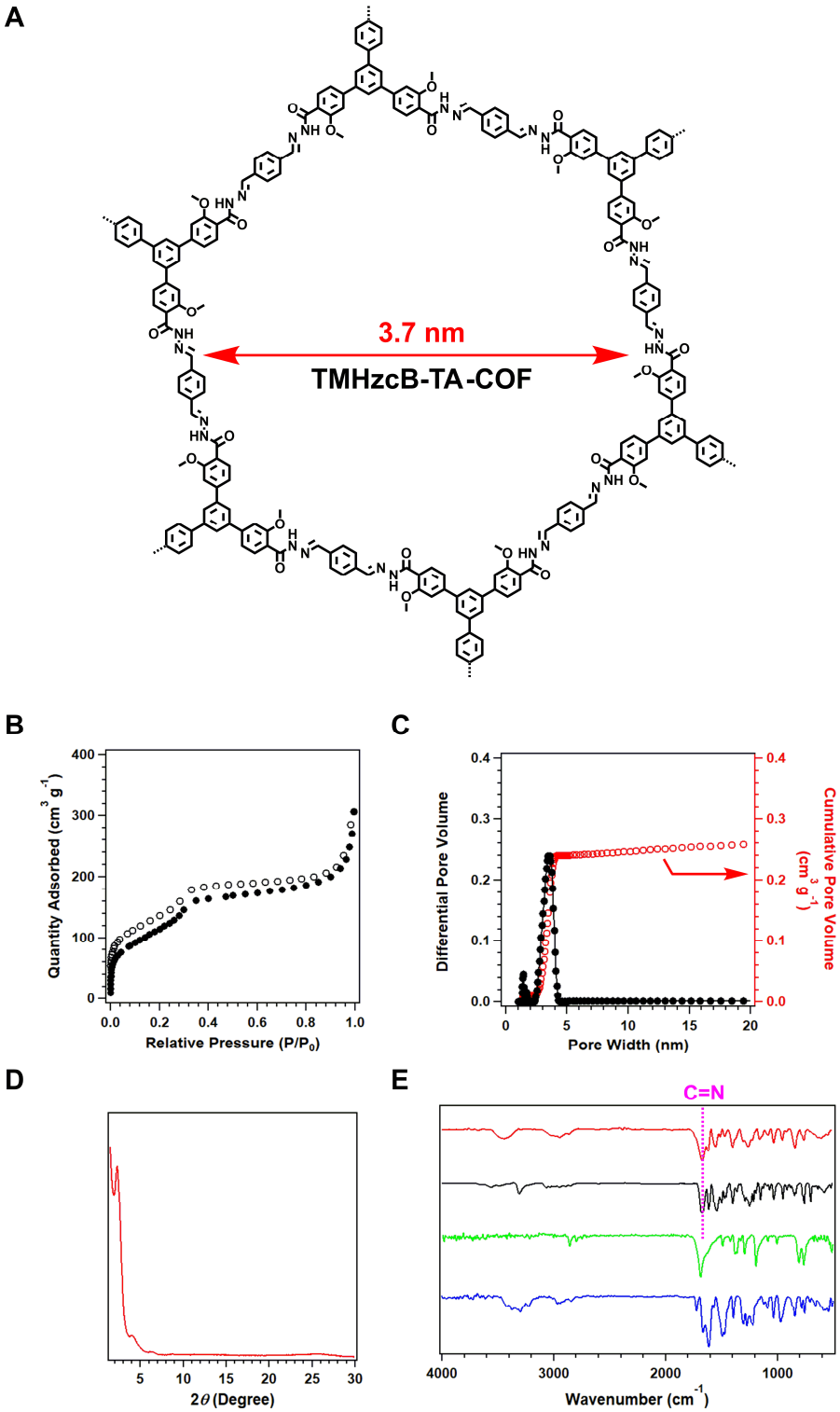

Figure 5 (A) The structure of TMHzcB-TA-COF. (B) Nitrogen sorption isotherm curve of TMHzcB-TA-COF measured at 77 K (○: desorption, ●: adsorption). (C) Pore size (black dots and curve) and pore width distribution (red dots) of TMHzcB-TA-COF. (D) PXRD patterns of experimentally observed. (E) FT-IR spectra of TMHzcB-TA-COF (red curve), Model Compound-H (black curve), TA (green curve), and TMHzcB (blue curve).

TMHzcB-TA-COF also showed good thermostability during thermogravimetric analysis (TGA) (Figure 6A). This COF also performed good chemical stability in organic solvents, water, acid and base conditions at room temperature for 24 h. From the PXRD patterns in Figure 6B, all the samples can keep strong diffraction peaks in XRD patterns without any change in the peak position (Figure 6B).

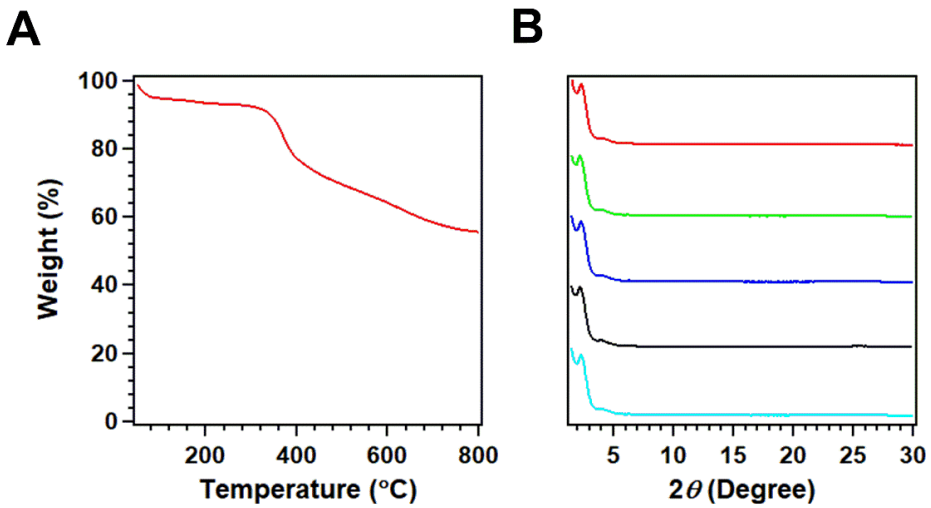

Figure 6. (A) TGA curve of TMHzcB-TA-COF under nitrogen atmosphere. (B) PXRD patterns, of TMHzcB-TA-COF upon 24 h treatment in different conditions. As-synthesized material (red line); THF (green line); water (blue line);1M HCl (black line);1 M NaOH (sky-blue line).

The elemental analysis of TMHzcB-TA-COF displayed C, H, and N contents of 68.59, 5.12, and 10.63%, respectively, which were close to the calculated values of 70.28, 4.63, and 11.71%. COF sample may be contacted with water vapor in the air during the test, which causes the observed value of H with little higher content. Another reason is that the COF sample maybe have some defects, which can also cause little error between the observed and calculated values.

Table 2： Elemental analysis of the TMHzcB-TA-COF.

	C (%)	N (%)	H (%)
Observed Value	68.59	10.63	5.12
Calculated Value	70.28	11.71	4.63

The morphology of TMHzcB-TA-COF was observed by high-emission scanning electron microscopy. The TMHzcB-TA-COF adopted aggregated micrometer-scale particles (Figure. 7A and 7B).

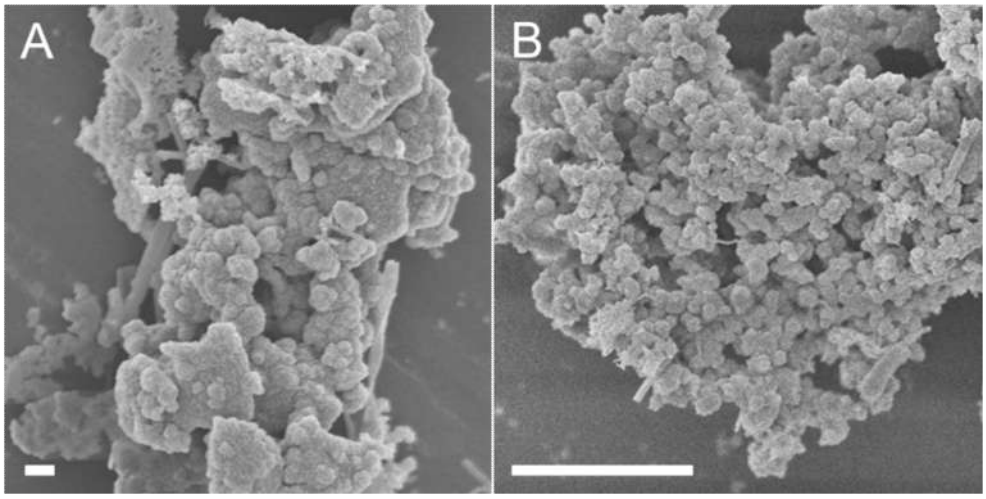

Figure 7. SEM Images of TMHzcB-TA-COF (A: scale bar: 1 um; B: scale bar: 10 um).

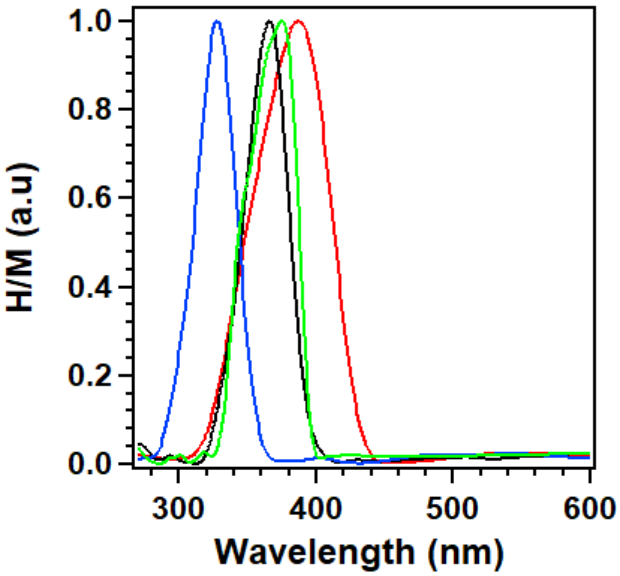

Figure 8. Solid-state electronic absorption spectra of TA (green curve), and TMHzcB (blue curve), Model Compound-H (black curve), and TMHzcB-TA-COF (red curve).

TMHzcB (blue curve), TA (green curve) and Model Compound-H (black curve) at the solid state exhibited absorption peaks at 327, 355 and 367 nm, respectively. The absorption band of TMHzcB-TA-COF occurred an obvious red-shift with an electronic absorption peak at 387 nm (Figure 8, red curve).

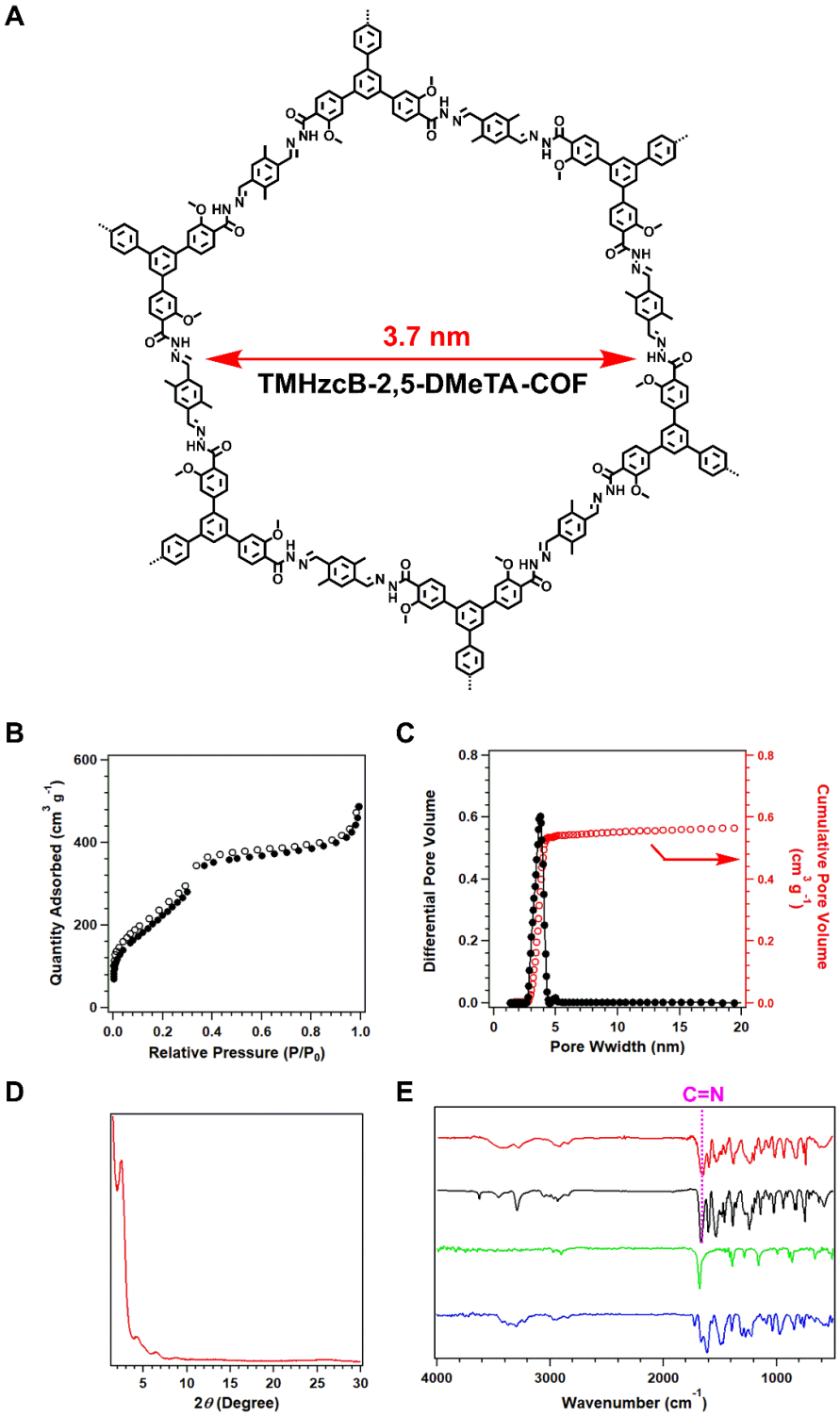

Figure 9 (A) The structure of TMHzcB-2,5-DMeTA-COF. (B) Nitrogen sorption isotherm curve of TMHzcB-2,5-DMeTA-COF measured at 77 K (○: desorption, ●: adsorption). (C) Pore size (black dots and curve) and pore width distribution (red dots) of TMHzcB-2,5-DMeTA-COF. (D) PXRD patterns of experimentally observed. (E) FT-IR spectra of TMHzcB-2,5-DMeTA-COF (red curve), Model Compound-Me (black curve), 2,5-DMeTA (green curve), and TMHzcB (blue curve).

The TMHzcB-2,5-DMeTA-COF showed high porosity and crystallinity. The BET surface area and pore volume of the new COF was 932 m^2 g^{-1} and 0.56 cm^3 g^{-1} (Figure 9B and 9C, red curve). Moreover, TMHzcB-2,5-DMeTA-COF exhibited type-IV sorption curves (Figure 9B), which are typical of the mesopore. TMHzcB-2,5-DMeTA-COF displayed strong PXRD peaks at 2.40°, 4.14°, 6.40, and 26.40°, which were assigned to the (100), (110), (210), and (001) facts, respectively (Figure 9D). To study structural features for new COFs, a similar small molecule, Model Compound-Me, was synthesized with TMHzcB and 2-methylbenzaldehyd. I checked the FT-IR spectrum of building units, Model Compound-Me and TMHzcB-2,5-DMeTA-COF. As showed in Figure 9E, the building units of 2,5-DMeTA displayed the characteristic signal of the aldehyde group at 1690 cm^{-1} (green curve). The special peaks of the aldehyde group cannot be observed in Model Compound-Me (black curve) and TMHzcB-2,5-DMeTA-COF (red curve). In contrast, Model Compound-Me and TMHzcB-2,5-DMeTA-COF displayed the same imine vibration band at 1671 cm^{-1}, which provided that condensation of the aldehyde (2,5-DMeTA) and the amino group (TMHzcB) were completed.

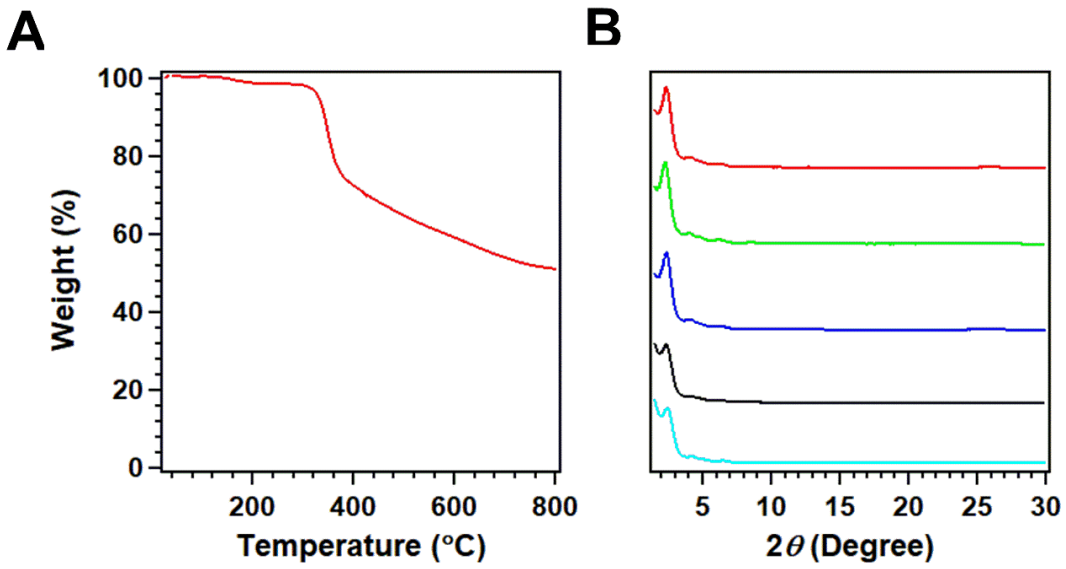

Figure 10. (A) TGA curve of TMHzcB-2,5-DMeTA-COF under nitrogen atmosphere. (B) PXRD patterns, of TMHzcB-2,5-DMeTA-COF upon 24 h treatment in different conditions. As-synthesized material (red line); THF (green line); water (blue line);1M HCl (black line);1 M NaOH (sky-blue line).

TMHzcB-2,5-DMeTA-COF also showed good thermostability and chemical stability. As showed in Figure 10A, the thermostability of TMHzcB-2,5-DMeTA-COF was testified by no decomposition under 300 °C. TMHzcB-2,5-DMeTA-COF samples were soaked in organic solvent (THF), water, acid and base conditions at room temperature for 24 h to investigate chemical stability. From the PXRD patterns in Figure 10B, all the samples can keep strong diffraction peaks in PXRD patterns without any change in the peak position.

The elemental analysis of TMHzcB-2,5-DMeTA-COF displayed C, H, and N contents of 70.89, 5.53, and 11.37%, respectively, which were very close to the calculated values of 71.11, 5.17, and 11.06% (Table 3). A very small error is between the observed value and calculated value of the TMHzcB-2,5-DMeTA-COF sample. The reason is the same as that of TMHzcB-TA-COF.

Table 3: Elemental analysis of the TMHzcB-2,5-DMeTA-COF

	C (%)	N (%)	H (%)
Observed Value	70.89	11.37	5.53
Calculated Value	71.11	11.06	5.17

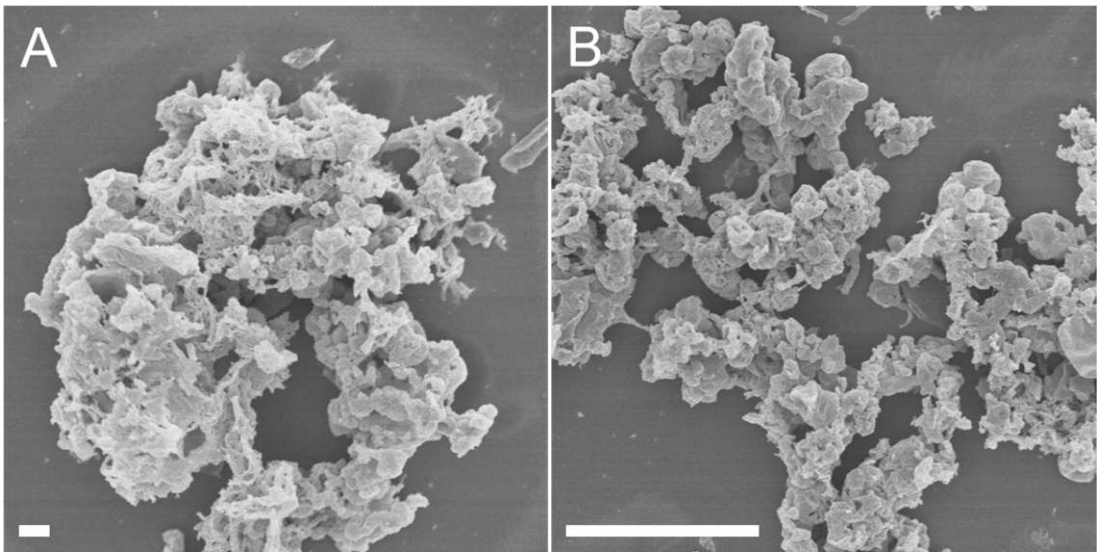

Figure 11. SEM Images of TMHzcB-2,5-DMeTA -COF (A: scale bar: 1 um; B: scale bar: 10 um).

The morphology of TMHzcB-TMHzcB-2,5-DMeTA-COF was observed by high-emission scanning electron microscopy (FE SEM). The TMHzcB-2,5-DMeTA-COF adopted aggregated micrometer-scale particles (Figure 11A and 11B).

I also investigated the solid-state electronic absorption spectra for TMHzcB, 2,5-DMeTA, Model Compound-Me, and TMHzcB-2,5-DMeTA-COF. Comparing TMHzcB (blue curve), 2,5-DMeTA (green curve), and Model Compound-Me (black curve) at the solid state that exhibited absorption bands at 327, 373 and 378 nm, respectively, the absorption band of TMHzcB-2,5-DMeTA-COF occurred an obvious red-shift and showed an electronic absorption band at 414 nm (Figure 12, red curve).

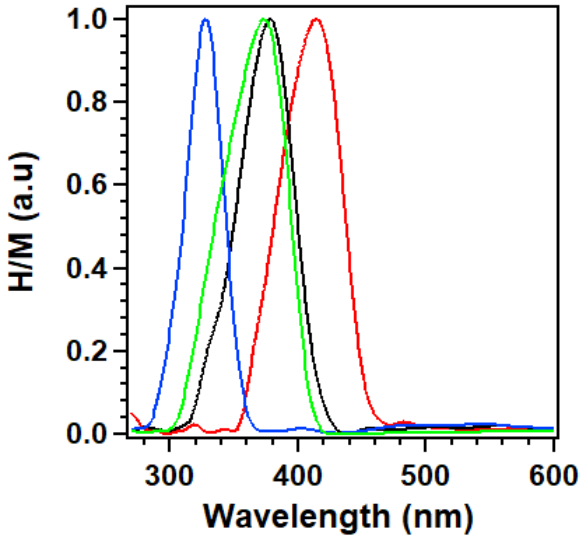

Figure 12. Solid-state electronic absorption spectra of 2,5-DMeTA (green curve), TMHzcB (blue curve), TMHzcB-2,5-DMeTA-COF (red curve), and Model Compound-Me (black curve).

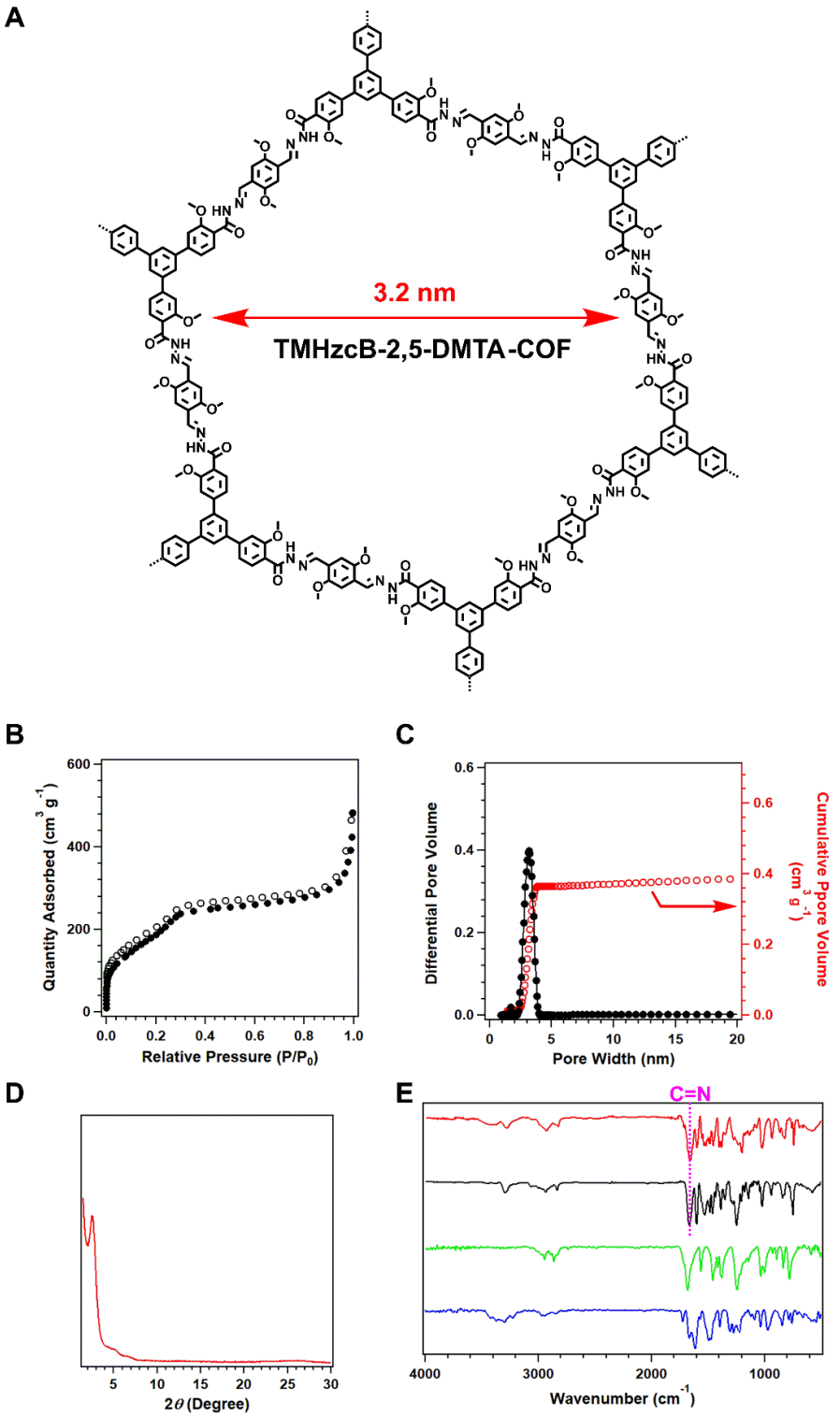

Figure 13 (A) The structure of TMHzcB-2,5-DMTA-COF. (B) Nitrogen sorption isotherm curve of TMHzcB-2,5-DMTA-COF measured at 77 K (○: desorption, ●: adsorption). (C) Pore size (black dots and curve) and pore width distribution (red dots) of TMHzcB-2,5-DMTA-COF. (D) PXRD patterns of experimentally observed. (E) FT-IR spectra of TMHzcB-2,5-DMTA-COF (red curve), Model Compound-Me (black curve), 2,5-DMTA (green curve), and TMHzcB (blue curve).

The porosity of TMHzcB-2,5-DMTA-COF can be evaluated by Nitrogen (N_2) adsorption-desorption isotherms at 77 K. TMHzcB-2,5-DMTA-COF exhibited type-IV sorption curves (Figure 13B). The BET surface area of this COF was 799 $m^2\ g^{-1}$ and the pore volume was 0.39 $cm^3\ g^{-1}$ (Figure 13C, red dots). From the pore size distribution profile, TMHzcB-2,5-DMTA-COF showed a pore width of 3.2 nm that calculated by the nonlocal density functional theory method. (Figure 13C, black dots).The crystalline structure of the new COF was determined by PXRD. TMHzcB-2,5-DMTA-COF showed excellent crystallinity (Figure 13D). To confirm structure of COF, I designed and synthesized the Model Compound-OMe. As showed in Figure 13E, TMHzcB-2,5-DMTA-COF (red curve) and Model Compound-OMe (black curve) showed very similar signals. The new COF also displayed the imine vibration bond at 1669 cm^{-1}, which is the same as Model Compound-OMe. Moreover, the aldehyde group of 2,5-DMTA at 1686 cm^{-1} was not observed in TMHzcB-2,5-DMTA-COF (red curve).

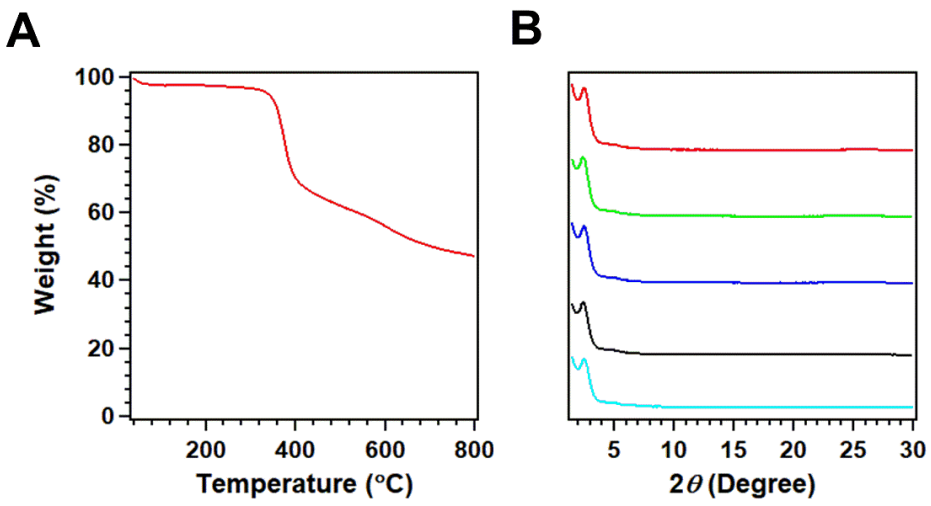

Figure 14. (A) TGA curve of TMHzcB-2,5-DMTA-COF under nitrogen atmosphere. (B) PXRD patterns of TMHzcB-2,5-DMTA-COF upon 24 h in different conditions. As-synthesized material (red line); THF (green line); water (blue line);1M HCl (black line);1 M NaOH (sky-blue line).

The thermostability and chemical stability of the material is very important for the application. From thermogravimetric analysis curves (Figure 14 A),

TMHzcB-2,5-DMTA-COF can keep stability up to 300 °C under nitrogen atmosphere. All TMHzcB-2,5-DMTA-COF samples can be stable in organic solvent (THF), water, acid and base conditions at room temperature for 24 h. As showed in Figure 14B, all samples remained high crystallinity, which is the same as as-synthesized materials.

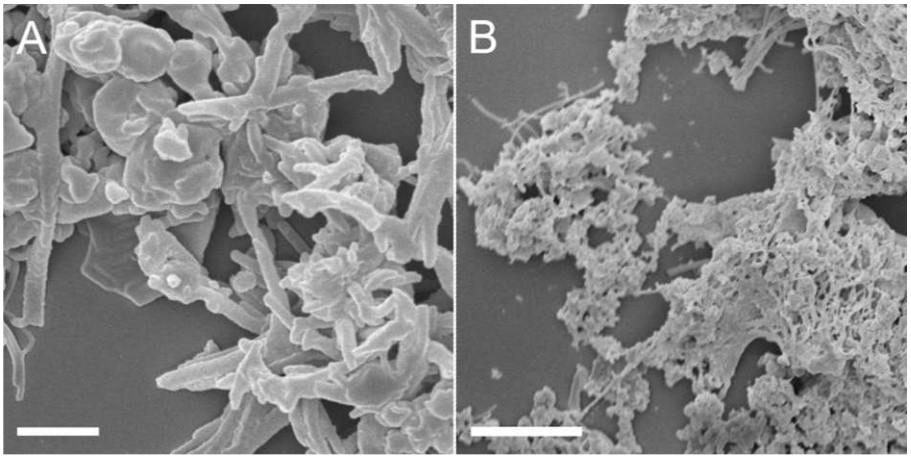

Figure 15. FE SEM Images of TMHzcB-2,5-DMTA-COF (A: scale bar: 1 um; B: scale bar: 10 um).

The field-emission scanning electron microscopy images of TMHzcB-2,5-DMTA-COF adopted aggregated micrometer-scale particles (Figure. 15A and 15B).

Table 4: Elemental analysis of the TMHzcB-2,5-DMTA-COF.

	C (%)	N (%)	H (%)
Observed Value	65.76	11.08	5.95
Calculated Value	66.91	10.04	4.87

The elemental analysis was measured for TMHzcB-2,5-DMTA-COF. The new frameworks showed C, H, and N contents of 65.76, 5.95 and 11.08%, respectively, which were close to the calculated values of 66.91, 4.87 and 10.04%.

The solid-state electronic absorption spectra for TMHzcB, 2,5-DMTA, Model Compound-Me and TMHzcB-2,5-DMTA-COF were also observed. As showed in Figure 16, TMHzcB (blue curve), 2,5-DMTA (green curve) and Model Compound-OMe (black curve) at the solid state exhibited absorption peaks at

327, 370 and 438 nm, respectively. The absorption band of TMHzcB-2,5-DMeTA-COF occurred an obvious red-shift and showed an electronic absorption peak at 442 nm (red curve).

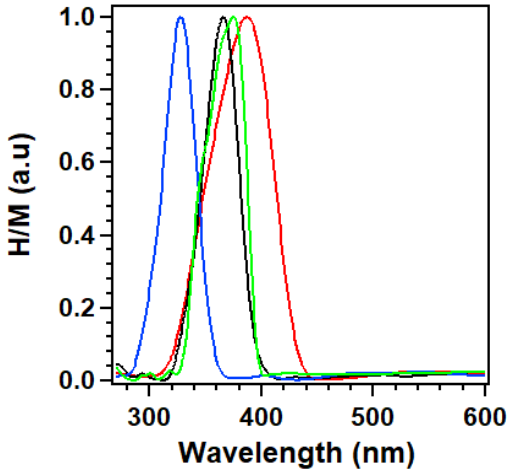

Figure 16. Solid-state electronic absorption spectra of 2,5-DMTA (green curve), TMHzcB (blue curve), Model Compound-Me (black curve), and TMHzcB-2,5-DMTA-COF (red curve),

Table 5: Porosity of TMHzcB-TFB-COF, TMHzcB-TFPB-COF, TMHzcB-TA-COF, TMHzcB-2,5-DMeTA-COF, and TMHzcB-2,5-DMTA-COF.

	BET Surface Area ($m^2\ g^{-1}$)	Pore Volume ($cm^3\ g^{-1}$)	Pore Size (nm)
TMHzcB-TFB-COF	471	0.23	1.6
TMHzcB-TFPB-COF	1116	0.52	2.2
TMHzcB-TA-COF	471	0.36	3.7
TMHzcB-2,5-DMeTA-COF	932	0.56	3.7
TMHzcB-2,5-DMTA-COF	799	0.39	3.2

These hydrazone-linked COFs showed high porosity (Table 5). However, most reported hydrazine-linked COFs were designed by using the hydrazine part as the linker, which limits the diversity of hydrazone based COFs. This study applies hydrazide units as vertices to construct frameworks. The monomers of the aromatic aldehyde group as the vertex or linker were used to synthesize various COFs. Interestingly, the pore size of these COFs can be designed and synthesized from 1.6 nm to 3.7 nm through different kinds of building units (Table 5), which can enrich structure of COFs.

3.3.2 Tunable light-emitting activity

The hydrazone-linked TMHzcB-TFB-COF was designed and constructed through condensation of 1,3,5-tris(3'-methoxy-4'-hydrazinecarbonylphenyl)benzene (TMHzcB) and 1,3,5-triformylbenzene (TFB). The non-planar structure of hydrazone linkage can weaken the fluorescence quenching through strong π-π interaction of layers. TMHzcB-TFB-COF showed a light-blue luminescence with a strong emission band at 447 nm (Figure 17). Moreover, TMHzcB-TFB-COF displayed a moderate fluorescence quantum yield of 5.1 % upon excitation at 380 nm at the solid state.

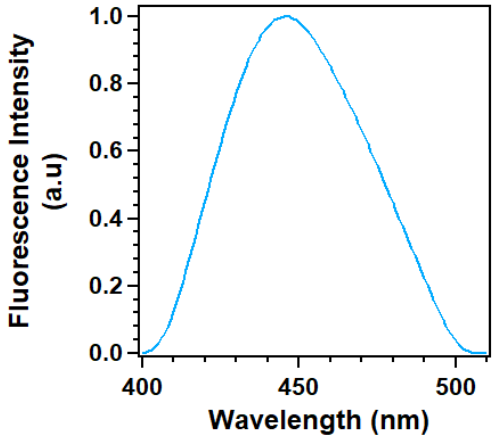

Figure 17. Fluorescence spectrum of TMHzcB-TFB-COF upon excitation at 380 nm at the solid state.

To enhance the light-emitting ability of frameworks, I used more flexible 1,3,5-tris(4-formylphenyl)benzene (TFPB) and TMHzcB to offer TMHzcB-TFPB-COF. The fluorescence spectrum of TMHzcB-TFPB-COF in the solid state at room temperature was observed in Figure 18. The new COF emitted a strong blue luminescence at 485 nm with an absolute fluorescence quantum yield of 10.7 % upon excitation at 390 nm.

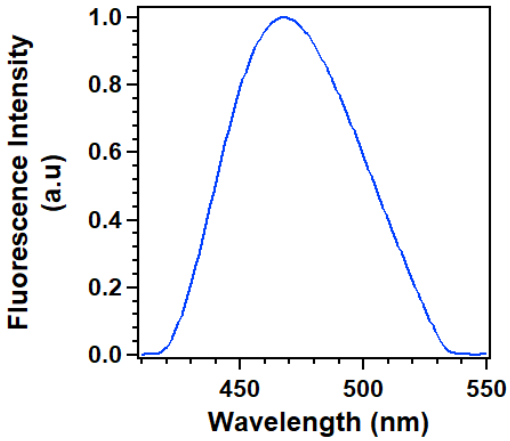

Figure 18. Fluorescence spectrum of TMHzcB-TFPB-COF upon excitation at 390 nm at the solid state.

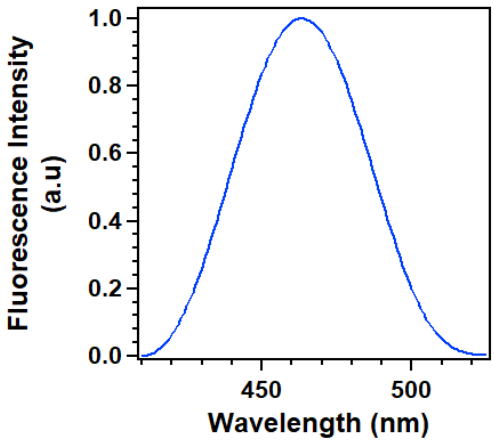

Figure 19. Fluorescence spectrum of TMHzcB-TA-COF upon excitation at 367 nm at the solid state.

Terephthalaldehyde (TA) also has much more flexibility, which can further improve light-emitting ability of frameworks. The TMHzcB-TA-COF displayed high blue luminescence and emission peak at 463 nm with a high fluorescence quantum yield of 11.7 %. With these in mind, the TMHzcB-TA-COF exhibited high luminescence activity. I modified the building blocks of TA with the addition of active autochrome group including methoxy and methyl units that can provide oxygen with two pairs of electrons when attached to a chromophore and alter both the wavelength of absorption, which can improve the wavelength and intensity of frameworks. For example, TMHzcB-2,5-DMeTA-COF with methyl group showed yellow-green luminescence and emission peak at 499 nm with high fluorescence quantum

yield of 19.5 % (Figure 19), which is higher than most reported hydrazone-linked COFs, such as COF-JLU4 (2.9 %),[4] LZU-COF-8 (3.5 %),[6a] Tf-DHzDPr (11.9%),[6b] Tf-DHzDM (8.2 %),[6b] TFPB-DHzDPr (14.4 %),[6b] Tf-DHzAll (3.9 %),[6b] TFPB-DHzDM (6.6 %),[6b] TFPB-DHzDs (16.3 %),[6b] TFPB-THz (2.4 %),[6b] TFPB-DHzDAll (3.6 %),[6b] DFDM-THz (0.4 %).[6b] Moreover, fluorescence quantum yield of new COF at the solid state is also higher than most azine, imine, based COFs, including COF-JLU3 (9.9 %)[7] and IMDEA-COF-1 (3.5 %).[16] Interestingly, light-emitting activity of this TMHzcB-2,5-DMTA-COF can also compete to AIE-Based COFs such as sp^2c-COF(14 %)[11] and 3D-TPE-COF (20 %).[17]

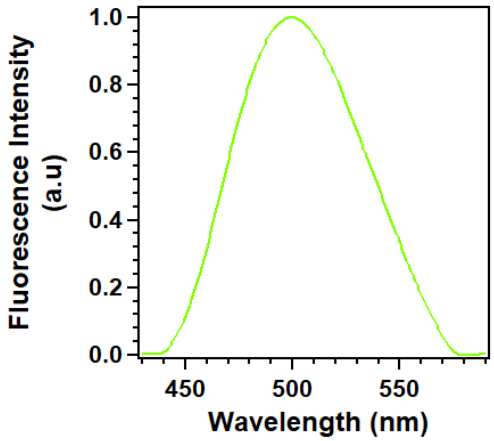

Figure 19. Fluorescence spectrum of TMHzcB-2,5-DMeTA-COF upon excitation at 390 nm at the solid state.

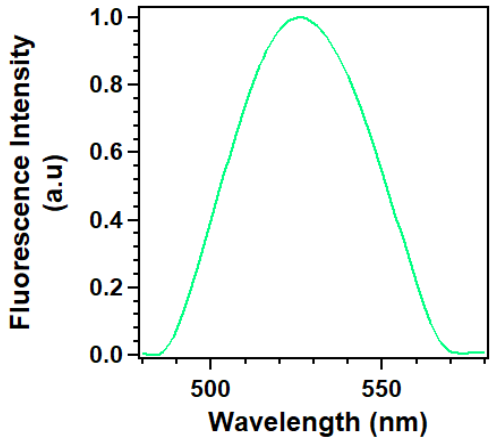

Figure 20. Fluorescence spectral change of TMHzcB-2,5-DMTA-COF upon excitation at 390 nm at the solid state.

The green fluorescence can be achieved through modified benzaldehyde

units for 2,5-dimethoxyterephthalaldehyde to obtain TMHzcB-2,5-DMTA-COF. TMHzcB-2,5-DMTA-COF showed a strong emission peak at 526 nm at the solid state upon excitation at 442 nm. The new framework also displayed high fluorescence with 19 % at the solid state (Figure 20), which is also higher than most azine, imine and hydrazone-linked COFs. [6a, 6b,16,17]

Table 6: Light-emitting activity of TMHzcB-TFB-COF, TMHzcB-TFPB-COF, TMHzcB-TA-COF, TMHzcB-2,5-DMeTA-COF, and TMHzcB-2,5-DMTA-COF.

	Emission Peak (nm)	Fluorescence Quantum Yield (%)	Pore Size (nm)
TMHzcB-TFB-COF	447	5.1	1.6
TMHzcB-TFPB-COF	485	10.7	2.2
TMHzcB-TA-COF	463	11.7	3.7
TMHzcB-2,5-DMeTA-COF	499	19.5	3.7
TMHzcB-2,5-DMTA-COF	526	19	3.2

Various luminescent COFs from blue to green were designed and synthesized. Fluorescence quantum yield of TMHzcB-TFB-COF, TMHzcB-TFPB-COF, and TMHzcB-TA-COF was enhancing with increment of their pore size, which due to the weakening of interaction from the layers. Interestingly, introducing fluorochromes group such as methyl and methoxy for the skeleton further improved the light-emitting activity.

3.3 Conclusion

A series of light-emitting hydrazone based COFs with high porosity and crystallinity were synthesized under the solvothermal method. The hydrazone-linked COFs were designed through TMHzcB as vertex and other building units as different symmetrical knots/vertexes to provide wide pore size from 1.6 nm to 3.7 nm for frameworks, which can enrich the structures of hydrazone based COFs. Moreover, these COFs displayed good stability in organic solvents, water, acid and base conditions for 24 hours at the room temperature.

The light-emitting activity of COFs can be improved through flexible building

units or functional active groups including methoxy and methyl groups. The luminescence of frameworks was tunable from blue to green luminescence as a result. Interestingly, TMHzcB-2,5-DMeTA-COF and TMHzcB-2,5-DMeTA-COF showed the highest fluorescence quantum yield over 19 % at the solid state, which is higher than most reported azine, imine and hydrazone based COFs.

3.4 Experimental section

3.4.1 Chemicals

The 2-methylbenzaldehyde, 2-hydroxybenzaldehyde and 2-methoxybenzaldehyde were obtained from TCI and Sigma-Aldrich.

3.4.2 Methods

Characterizations. The fluorescence spectra and absolute quantum yield were measured by a JASCO model FP-6600 spectrofluorometer, equipped with integral sphere. FE-SEM images were obtained on a Field-Emission Scanning Electron Microscope JEOL JSM-6701F at an electric voltage of 5 KV.

3.4.3 Synthesis of building units

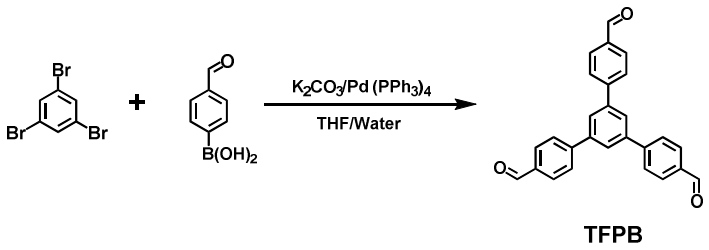

TFPB

Scheme 9. Synthesis of 1,3,5-tris(4-formylphenyl) benzene (TFPB).[18]

1,3,5-tris(4-formylphenyl) benzene (TFPB):1,3,5-Tribromobenzene (1.0 g, 3.2 mmol), 4-formylphenylboronic acid (1.7 g,11.4 mmol) and Potassium carbonate (2.65 g, 19.2 mmol) and tetrakis(triphenylphosphine)palladium (200 mg) were added into THF 50 mL and water 30 mL. The mixture was degassed for three cycles. The system was refluxed for 72 hours under Argon atmosphere. After cooling down to room temperature, the mixture was

extracted by dichloromethane for three times and the organic layer was dried over sodium sulfate, removed under the rotary evaporation. The crude product was purified through a column by using dichloromethane as eluent. The final product was washed by methanol to give white solid. (Yield, 79%).[1]H NMR (400 MHz, $CDCl_3$): δ = 10.11 (s, 3H), 8.03 (d, 6H), 7.91 (s, 3H), 7.88 (d, 6H) ppm.

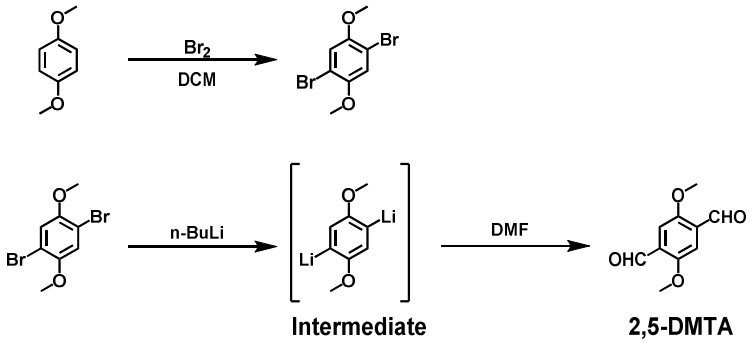

Scheme 10. Synthesis of 2,5-dimethoxyterephthalaldehyde (2,5-DMTA).[13a]

1,4-dibromo-2,5-dimethoxybenzene: To a mixture of a commercial reagent 1,4-dimethoxybenzene (10.0 g, 72.5 mmol) in dichloromethane (150 mL) was added a solution of bromine (14.6 g, 91.75 mmol) at 0 ºC. The mixture was stirred at room temperature overnight. The mixture was added dichloromethane (300 mL) washed with saturated sodium sulfite, the organic layer was dried over sodium sulfate, removed under the rotary evaporation. and washed by methanol to give the white solid (Yield, 93%). [1]H NMR (400 MHz, $CDCl_3$): δ = 7.12 (s, 2H), 3.37 (s, 6H) ppm.

2,5-dimethoxyterephthalaldehyde (2,5-DMTA): Under argon, to a solution of 1,4-dibromo-2,5-dimethoxybenzene (6.0 g, 20.0 mmol) in anhydrous THF (50 mL) was added n-BuLi (56 mL, 1.6 mol L^{-1}, 88.0 mmol) at -78 ºC, and the resulting mixture was stirred at -78 ºC for 4 hours. Then, anhydrous DMF (8.0 mL, 10.0 mmol) was added to the solution and the mixture was gradually warmed up to room temperature. After that, the mixture was stirred further at room temperature for 1 h. Subsequently, 3.0 M HCl aq. (45 mL) was added to precipitate the product, which was isolated by filtration and dried under

reduced pressure to give a crude product. The crude product was purified through a column by using dichloromethane as eluent. The final product was crystalized by acetonitrile to afford yellow crystal (Yield, 72%). ^{1}H NMR (400 MHz, $CDCl_3$): δ = 10.50 (s, 2H), 7.46 (s, 2H), 3.94 (s, 6H) ppm.

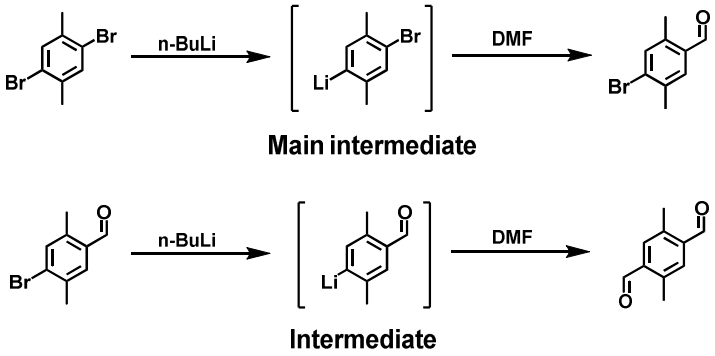

Scheme 11. Synthesis of 5-dimethoxyterephthalaldehyde (2,5-DMeTA).[19]

2,5-dimethoxyterephthalaldehyde (2,5-DMeTA): Under argon, to a solution of 1,4-dibromo-2,5-dimethylbenzene (5.0 g, 19.0 mmol) in anhydrous THF (50 mL) was added n-BuLi (18 mL, 1.6 mol L^{-1}, 28.5 mmol) at -78 ºC, and the resulting mixture was stirred at -78 ºC for 2 hours. Then, anhydrous DMF (2.2 mL, 28.5 mmol) was added to the solution and stirred at -78 ºC for 1 hour. The n-BuLi (42 mL, 1.6 mol L^{-1}, 44.0 mmol) was added into the system and stirred at -78 ºC for 2 hours. Then, anhydrous DMF (4.4 mL, 57 mmol) was added to the solution and the mixture was gradually warmed up to room temperature. Subsequently, 3.0 M HCl aq. (30 mL) was added to precipitate the product, which was isolated by filtration and dried under reduced pressure to give crude product. The crude product was purified through column by using dichloromethane as eluent. The final product was washed by methanol to afford a white solid (Yield, 67%). ^{1}H NMR (400 MHz, $CDCl_3$): δ = 10.34 (s, 2H), 7.69 (s, 2H), 2.70 (s, 6H) ppm.

3.5 References

1. T. L. Mako, J. M. Racicot, M. Levine. Supramolecular luminescent sensors. *Chem. Rev.* **2019**, *119*, 322-477.

2. Y. Cui, Y. Yue, G. Qian, B. Chen. Luminescent functional metal-organic frameworks. *Chem. Rev*. **2012**, *112*, 1126-1162.
3. (a) S. Wan, J. Guo, J. Kim, H. Ihee, D. Jiang. A belt-shaped, blue luminescent, and semiconducting covalent organic framework. *Angew. Chem. Int. Ed*. **2008**, *47*, 8826-8830. (b) S. Dalapati, S. Jin, J. Gao, Y. Xu, A. Nagai, D. Jiang. An azine-linked covalent organic framework. *J. Am. Chem. Soc*. **2013**, *135*, 17310-17313. (c) S. Dalapati, E. Jin, M. Addicoat, T. Heine, D. Jiang. Highly emissive covalent organic frameworks. *J. Am. Chem. Soc*. **2016**, *138,* 5797-5800.
4. Y. Zhang, X. Shen, X. Feng, H. Xia, Y. Mu, X. Liu. Covalent organic frameworks as pH responsive signaling scaffolds. *Chem. Commun.* **2016**, *52*, 11088-11091.
5. G. Das, B. P. Biswal, S. Kandambeth, V. Venkatesh, G. Kaur, M. Addicoat; T. Heine, S. Verm, R. Banerjee. *Chem. Sci*. **2015**, *6*, 3931-3939.
6. (a) S. Ding, M. Dong, Y. Wang, Y. Chen, H. Wang, C. Su, W. Wang. Thioether-based fluorescent covalent organic framework for selective detection and facile removal of mercury (II). *J. Am. Chem. Soc*. **2016**, *138*, 3031-3037. (b) X. Li, Q. Gao, J. Wang, Y. Chen, Z. Chen, H. Xu, W. Tang, K. Leng, G. Ning, J. Wu, Q. Xu, S. Y. Quek, Y. Lu, Kian Ping Loh. Tuneable near white-emissive two-dimensional covalent organic frameworks. *Nat. Commun.* **2018**, *9*, 2235.
7. Z. Li, Y. Zhang, H. Xia, Y. Mu, X. Liu. A robust and luminescent covalent organic framework as a highly sensitive and selective sensor for the detection of Cu^{2+} ions. *Chem. Commun*. **2016**, *52*, 6613-6616.
8. J. W. Crowe, L. A. Baldwin, P. L. McGrier. Luminescent covalent organic frameworks containing a homogeneous and heterogeneous distribution of dehydrobenzoannulene vertex units. *J. Am. Chem. Soc*. **2016**, *138*, 10120-10123.
9. G. Lin, H. Ding, D. Yuan, B. Wang, C. Wang. A pyrene-based, fluorescent three-dimensional covalent organic framework. *J. Am. Chem. Soc.* **2016**,

138, 3302-3305.

10. P. Albacete, J. I. Martínez, X. Li, A. López-Moreno, S. Mena-Hernando, A. E. Platero-Prats, C. Montoro, K. P. Loh, E. M. Pérez, F. Zamora. Layer-stacking-driven fluorescence in a two-dimensional imine-linked covalent organic framework. *J. Am. Chem. Soc*. **2018**, *140*, 12922-12929.
11. E. Jin, J. Li, K. Geng, Q. Jiang, H. Xu, Q. Xu, D. Jiang. Designed synthesis of stable light-emitting two-dimensional sp^2 carbon-conjugated covalent organic frameworks. *Nat. Commun*. **2018**, *9*, 4143.
12. (a) H. Xu, J. Guo, D. Jiang. Stable, crystalline, porous, covalent organic frameworks as a platform for chiral organocatalysts. *Nat. Chem*. **2015**, *7*, 905-912. (b) X. Chen, M. Addicoat, E. Jin, L. Zhai, H. Xu, N. Huang, Z. Guo, L. Liu, S. Irle, D. Jiang. Locking covalent organic frameworks with hydrogen bonds: general and remarkable effects on crystalline structure, physical properties, and photochemical activity. *J. Am. Chem. Soc*. **2015**, *137*, 3241-3247. (c) N. Huang, L. Zhai, H. Xu, D. Jiang. Stable covalent organic frameworks for exceptional mercury removal from aqueous solutions. *J. Am. Chem. Soc*. **2017**, *139*, 2428-2434.
13. (a) Y. Zhi, Z. Li, X. Feng, H. Xia, Y. Zhang, Z. Shi, Y. Mu, X. Liu. Covalent organic frameworks as metal-free heterogeneous photocatalysts for organic transformations. *J. Mater. Chem. A*. **2017**, *5*, 22933-22938. (b) Y. Zhi, P. Shao, X. Feng, H. Xia, Y. Zhang, Z. Shi, Y. Mu, X. Liu. Covalent organic frameworks: efficient, metal-free, heterogeneous organocatalysts for chemical fixation of CO_2 under mild conditions. *J. Mater. Chem. A*, **2018**, *6*, 374-382. (c) Z. Li, Y. Zhi, P. Shao, H. Xia, G. Lie, X. Feng, X. Chen, Z. Shi, X. Liu. Covalent organic framework as an efficient, metal-free, heterogeneous photocatalyst for organic transformations under visible light. *Applied Catalysis B: Environmental.* **2019**, *245*, 334-342.
14. (a) S. Chandra, S. Kandambeth, B. P. Biswal, B. Lukose, S. M. Kunjir, M.

Chaudhary, R. Babarao, T. Heine, R. Banerjee. Chemically stable multilayered covalent organic nanosheets from covalent organic frameworks via mechanical delamination. *J. Am. Chem. Soc*. **2013**, *135*, 17853-17861. (b) B. P. Biswal, S. Chandra, S. Kandambeth, B. Lukose, T. Heine, R. Banerjee. Mechanochemical synthesis of chemically stable isoreticular covalent organic frameworks. *J Am Chem. Soc*. **2013**, *135*, 532-5331. (c) A. Halder, M. Ghosh, A. Khayum M, S. Bera, M. Addicoat, H. S. Sasmal, S. Karak, S. Kurungot, R. Banerjee. Interlayer hydrogen-bonded covalent organic frameworks as high-performance supercapacitors. *J. Am. Chem. Soc.* **2018**, *140*, 10941-10945.

15. P. J. Waller, S. J. Lyle, T. M. O. Popp, C. S. Diercks, J. A. Reimer, O. M. Yaghi. Chemical conversion of linkages in covalent organic frameworks. *J. Am. Chem. Soc.* **2016**, *138*, 15519-15522.
16. P. Albacete, J. I. Martínez, X. Li, A. López-Moreno, S. Mena-Hernando, A. E. Platero-Prats, C. Montoro, K. P. Loh, E. M. Pérez, F. Zamora. Layer-stacking-driven fluorescence in a two-dimensional imine-linked covalent organic framework. *J. Am. Chem. Soc.* **2018**, *140*, 12922-12929.
17. H. Ding, J. Li, G. Xie, G. Lin, R. Chen, Z. Peng, C. Yang, B. Wang, J. Sun, C. Wang. An AIEgen-based 3D covalent organic framework for white light-emitting diodes. *Nat. Commun*. **2019**, *9*, 5234.
18. Y. Zhao, T. Wang, L. Zhang, Y. Cui, B. Han. Facile approach to preparing microporous organic polymers through benzoin condensation. *ACS Appl. Mater. Interfaces,* **2012**, *412*, 6975-6981.
19. N. Kuhnert, G. Rossignolo, A. Lopez-Periago. The synthesis of trianglimines: on the scope and limitations of the [3 + 3] cyclocondensation reaction between (1R,2R)-diaminocyclohexane and aromatic dicarboxaldehydes. *Org Biomol Chem*. **2003**, *1*, 1157-1170

Chapter 4

Light-Emitting Covalent Organic Frameworks: Fluorescence Improving via Pinpoint Surgery and Selective Switch-On Sensing of Anions

Abstract:

2D COFs with excellent crystallinity and porosity offer high-order π structures, which are attractive to design and develop light-emitting materials. Most COFs showed poor light-emitting activity because of aggregation-caused quenching effects. To design high luminescence COFs is challenging. In this chapter, I reported the conversion of weak emissive COFs into light-emitting materials via a pinpoint surgery on the pore walls. A hydrazone-linked COF, TFPPy-DETHz-COF was successfully constructed under solvothermal conditions. The N–H bond in linkage on the walls can be deprotonated to form anionic species, which can eliminate the nitrogen-related fluorescence quenching pathway. The fluorescence of deprotonated COF can be improved by 3.8 fold. This pinpoint N–H cleavage can be driven only by fluoride anion to switch on fluorescence. In contrast, other halogen anions, including chloride, bromide, and iodide, retained inactive. This is the first example of crystalline COFs that serve as a fluorescent sensor to detect fluoride anion at a low concentration.

4.1 Introduction

COFs are a new class of crystalline porous polymers with periodic skeletons and ordered nanopores to achieve functionalization.[1-3] Recently, COFs as multifunctional materials have achieved broad potential applications in areas including gas adsorption, catalysis, optoelectronics, molecular recognition, and toxic substance removal.[1-12] Nowadays, a variety of linkages such as B-O, C=N, C-N, and C=C have been designed and synthesized through the different condensation reaction.[1-5] The various topologies including hexagonal, trigonal, rhombic and tetragonal structures have been also developed by controlled geometry of building blocks.[1-12] Although the abundant reactions and building units can design and construct diversity and availability of skeletons and pores structure, yet functional light-emitting framework is very rare.

Light-emitting materials of 2D COFs is highly dependent on the building units and linkages.[12] Owing to strong π-π interaction between the adjacent layers of frameworks, the luminescence frameworks can be strongly affected by the aggregation-enhanced and/or quenched natures of the vertices and linkers, which can be managed by stacking or exfoliation.[12] The linkage is an important part of frameworks that presents in both single layer and stacked frameworks; layer exfoliation or stacking can hardly change its role in luminescence. In some cases, luminescence of COFs was governed by the linkages. Especially, due to the linkages that can cause the dissipation of excitation energy via photoinduced electron transfer, the photoluminescence of COFs is deactivated; this is the reason why most COFs are less emissive.

Among various linkages of COFs, the hydrazone linkage containing active N–H sites can be easily deprotonated by fluoride anion through acid-base reaction.[13] The pinpoint surgery on the nitrogen site of the hydrazone linkage by scissoring the N–H bond upon deprotonation into an N^- anion so that the

fluorescence quenching pathway can be eliminated, which can enhance luminescence of COFs.

Comparing to organic molecules, polymers can enlarge signals owing to the π structures, which can lower the detection line. Porous polymers showed quick adsorption for the guest molecule, which can easily interact to target. COFs with high-order structure showed high crystallinity and porosity, which can combine these features. In this way, the pinpoint surgery for COF can be as a switch-on sensor to recognize fluoride anion with higher sensitivity and lower detection limit.

N-H can be also deprotonated by alkaline ions through an acid-base reaction, which can improve the light-emitting activity of frameworks. Acidic ion can be recognized by N^- anion on the skeleton through the fluorescent quenching. TFPPy-DETHz-COF can also as a fluorescence off-on sensor for alkaline/ acidic ions.

4.2 Design and synthesis of TFPPy-DETHz-COF and model compound

4.2.1 Synthesis of TFPPy-DETHz-COF

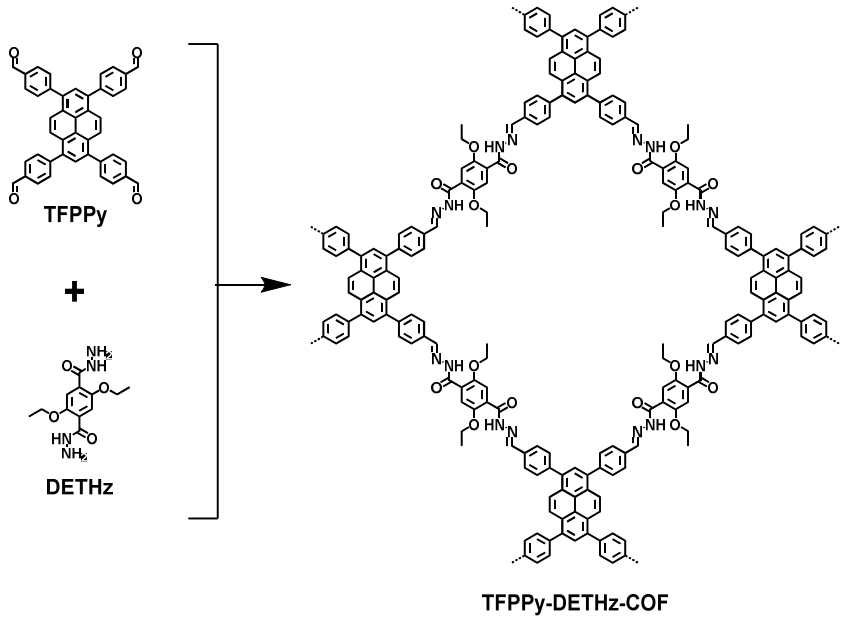

Scheme 1. Synthesis and structure of TFPPy-DETHz-COF.

TFPPy-DETHz-COF: A 10 mL Pyrex tube was charged with 1,3,6,8-Tetrakis(4-formylphenyl)pyrene, TFPPy, (18 mg, 0.029 mmol), 2,5-dithoxyterephthalohydrazide, DETHz, (16.4 mg, 0.058 mmol), dioxane (0.5 mL), mesitylene (0.5 mL) and AcOH (0.2 mL, 6 M), the mixture was sonicated for 2 minutes, degassed through three freeze-pump-thaw cycles, sealed under vacuum. The reaction was heated at 120 ºC for 72 h. The powder collected was washed with THF for three times and acetone for another three times, soxhleted with THF for 12 h, dried under vacuum at 120 °C for 12 h to afford yellow powder in 86% isolated yield.

4.2.2 Synthesis of Py-azine COF

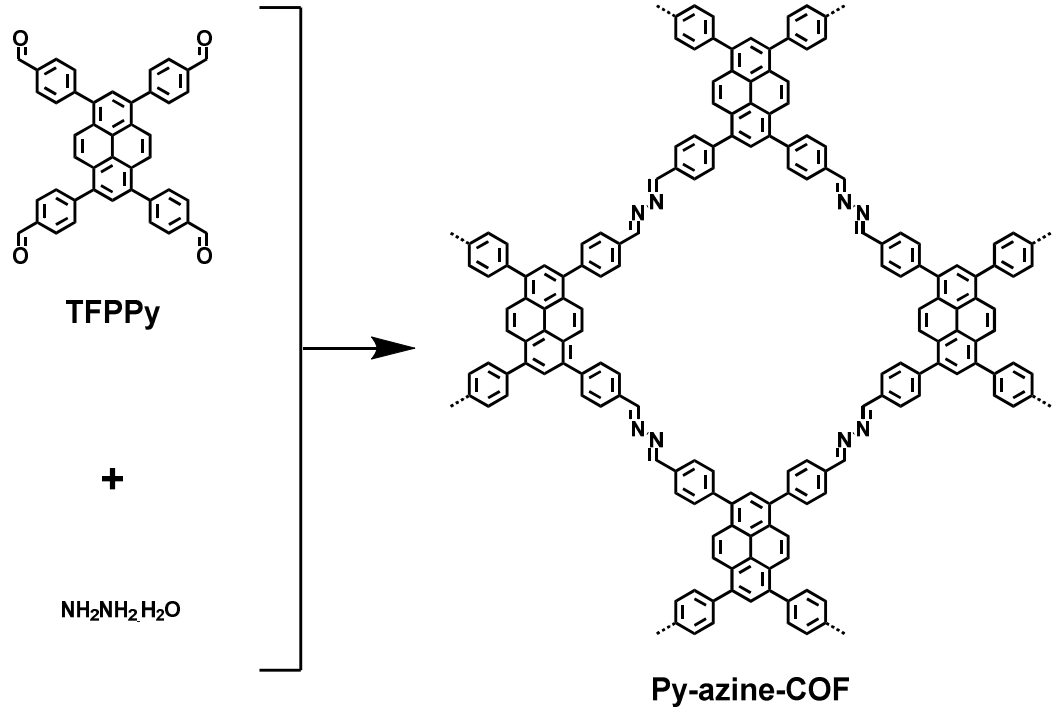

Scheme 2. Synthesis and structure of Py-Azine-COF.

Py-Azine COF: TFPPy (15.0 mg, 0.024 mmol), o-DCB 1.9 mL and n-BuOH 0.1 mL, hydrazine hydrate (2.35 μL, 0.048 mmol) and 0.2 mL AcOH (6 M) were added into a 10-mL Pyrex tube. The system was sonicated for 2 min, degassed through three freeze-pump-thaw cycles, sealed under vacuum, heated at 120 °C for 168 h. The system was cooled to room temperature. The

powder was collected and washed with THF, $CHCl_3$ and acetone for 5 times, and dried under vacuum at 120 °C for 24 h to obtain yellow powder (77%).[12b]

4.2.3 Synthesis of model compound

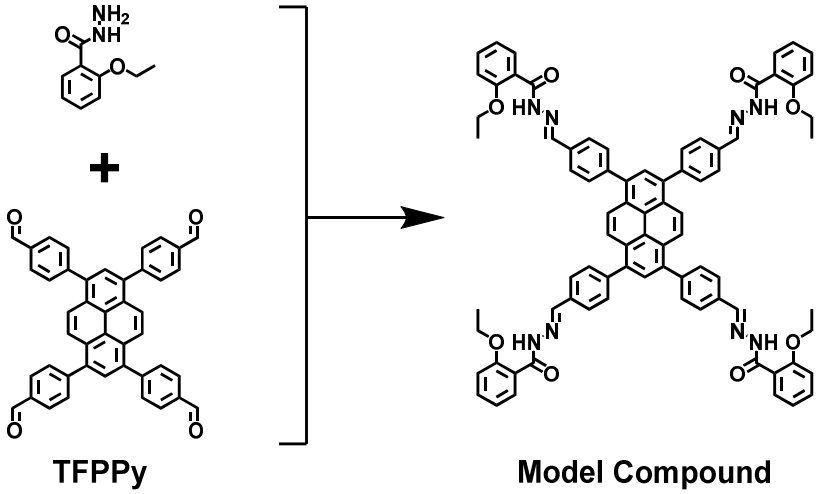

Scheme 3. Synthesis of Model Compound.

Model compound:1,3,6,8-tetrakis(4-formylphenyl) pyrene (TFPPy) (100 mg, 0.16 mmol) and 2-ethoxybenzohydrazide (174 mg, 0.97 mol) was added in 10 mL methanol at room temperature with vigorous stirring over several minutes. The system was heated overnight, cooled down at room temperature, filtered and washed with methanol, and recrystallized from methanol and chloroform, dried under vacuum to afford model compound as yellow powder in 63% yield (129 mg). ^{1}H NMR ($CDCl_3$, 500 MHz): δ = 7.45-7.47 (m, 6H, Ar-H), 7.84-7.87 (m, 24H, Ar-H), 8.67 (S, 2H, CH=N) ppm. ^{13}C NMR ($CDCl_3$, 500 MHz): δ = 162.16, 156.66, 147.21, 142.96, 136.79, 133.48, 133.12, 131.01,130.25, 128.26, 127.86, 127.73, 121.76, 120.43, 112.39, 65.17, 15.00 ppm.

4.3 Results and discussions

4.3.1 Characterizations

The TFPPy-DETHz-COF was fully characterized by using Fourier transform infrared spectroscopy, ultraviolet-visible spectroscopy, elemental analysis, ^{13}C solid-state NMR spectroscopy, field emission scanning electron microscopy,

thermogravimetric analysis, powder X-ray diffraction analysis and nitrogen adsorption.

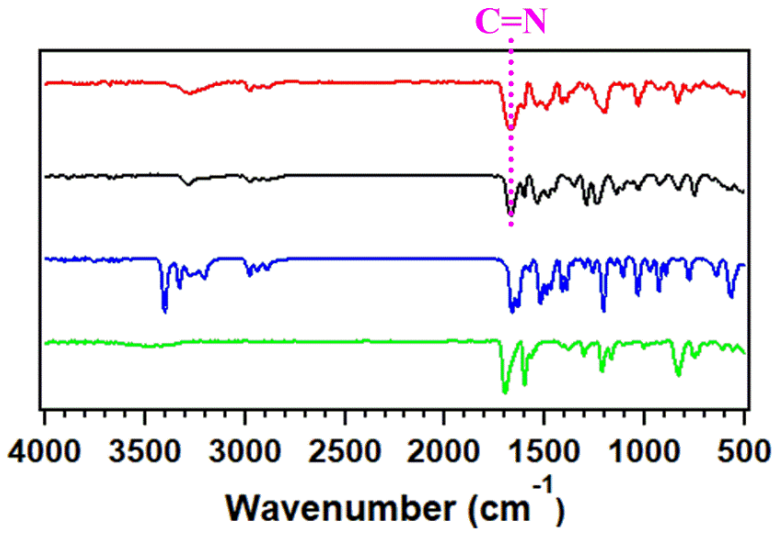

Figure 1. FT-IR spectra of TFPPy-DETHz-COF (red curve), model compound (black curve), DETHz (blue curve) and TFPPy (green curve).

The FT-IR spectrum of TFPPy-DETHz-COF showed a stretching vibration band at 1672 cm^{-1} that belonged to the imine (C=N) bond, which is the same as model compound (Figure 1). From this picture, TFPPy-DETHz-COF showed no stretching vibration band of the aldehyde group at 1698 cm^{-1}, which offers further evidence that condensation of monomers was very completed. Since the reaction is completed, the material can be provided with the high yield of 86%.

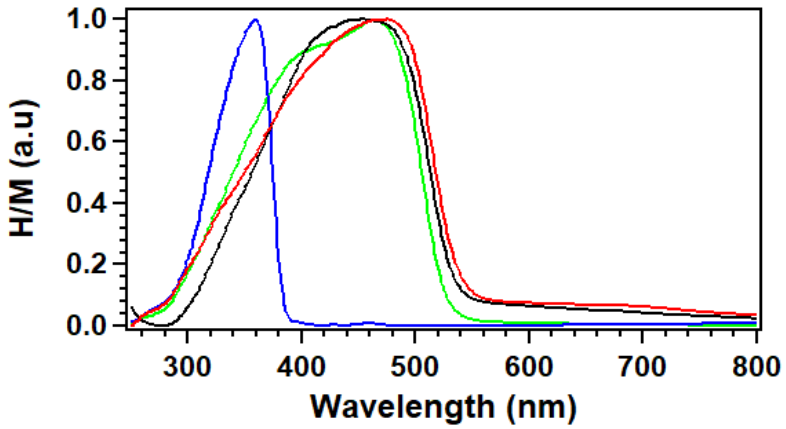

Figure 2. Solid-state electronic absorption spectra of TFPPy-DETHz-COF (red curve), TFPPy (green curve), DETHz (blue curve), and model compound (black curve).

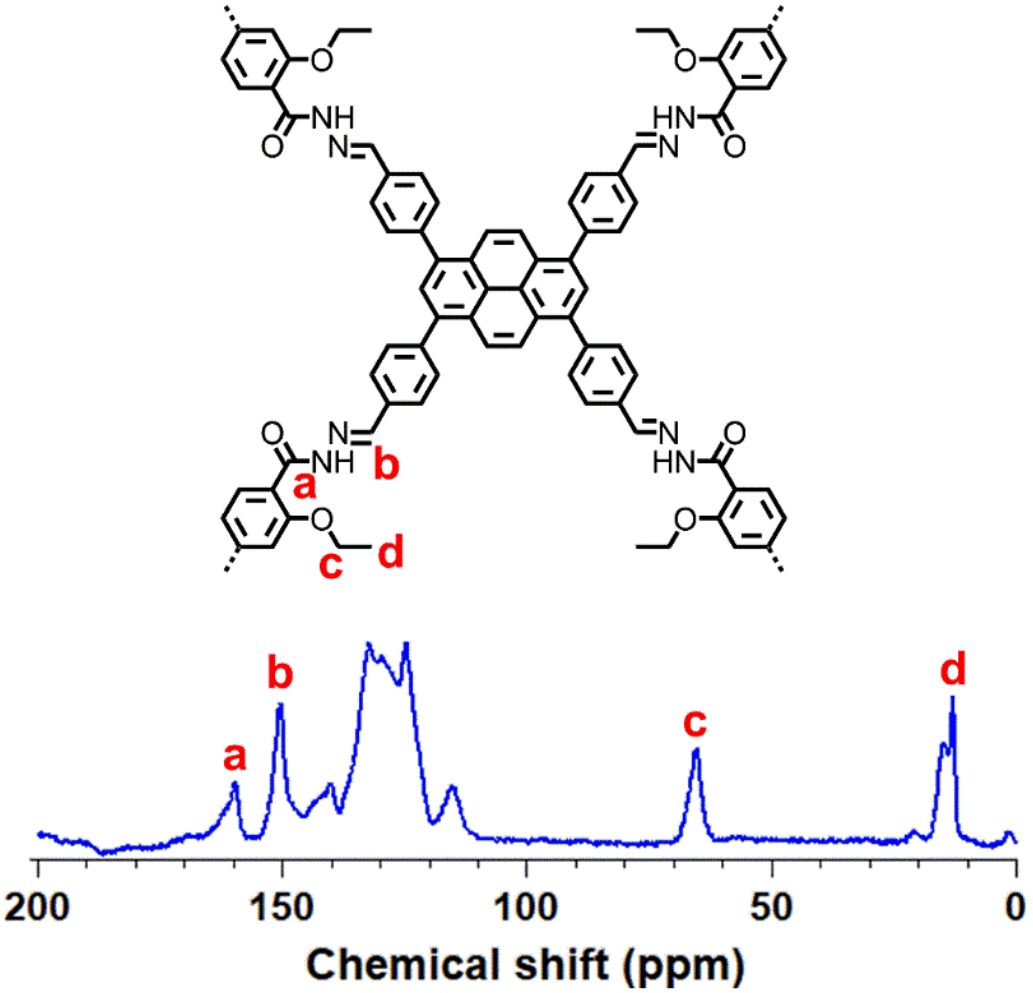

Figure 3. Solid state ^{13}C NMR spectra of TFPPy-DETHz-COF.

Compared with monomers and model compound, the absorption band of TFPPy-DETHz-COF occurred an obvious red-shift (Figure 2). Furthermore, the ^{13}C NMR peak at 150 ppm corresponds to the carbon atom of the imine bond, the formation of which is characteristic for the condensation reaction of monomers. The carbonyl carbon atoms of hydrazone linkage showed strong signals at 160 ppm. The high-field peaks at 13-15 and 65 ppm can be assigned to methyl and methylene groups of the aromatic rings. The signals at 140, 132, 125 and 115 ppm can be assigned to the carbon atoms of the phenyl groups (Figure 3). Field emission scanning electron microscopy (FE SEM) revealed micrometer-scale long rods (Figure 4).

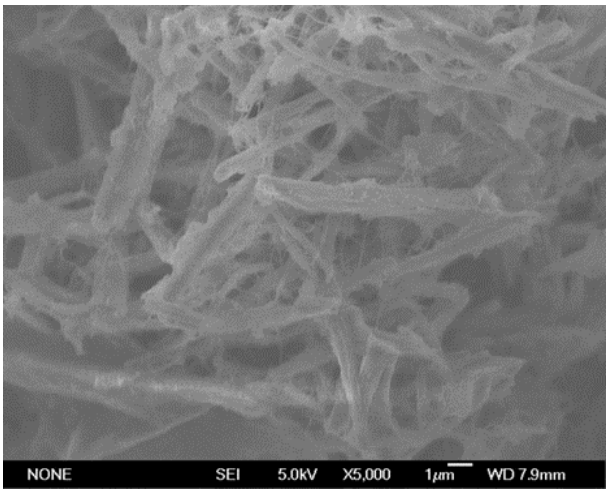

Figure 4. FE SEM Image of TFPPy-DETHz-COF.

Elemental analysis displayed that the C, H, and N contents of the TFPPy-DETHz-COF were 64.62, 5.40, and 23.67%, respectively, which were close to the calculated values of 69.22, 3.87, and 26.91% (Table 1). The C content of the observed value is not very close to the calculated value. This main reason may be the COFs sample contacted with water molecules during the test, which leads to an increment in H content and a decrease in C content. Another reason is some defects of frameworks, which can also cause little error between observed and calculated values.

Table 1： Elemental analysis of the TFPPy-DETHz-COF

	C (%)	N (%)	H (%)
Observed Value	64.62	23.67	5.40
Calculated Value	69.22	26.91	3.87

I used the nitrogen adsorption-desorption isotherms to evaluate the porosity of the TFPPy-DETHz-COF. This crystalline material exhibited type-IV sorption curves (Figure 5A), which are typical of the mesopores and exhibited BET surface area of 1090 $m^2 g^{-1}$ and pore volume of 0.5 $cm^3 g^{-1}$ (Figure 5B). The pore size distribution was calculated by the nonlocal density functional theory method. Moreover, TFPPy-DETHz-COF showed a uniform pore width of 2.1 nm, which was in good agreement with the pore size predicted from their crystal structure.

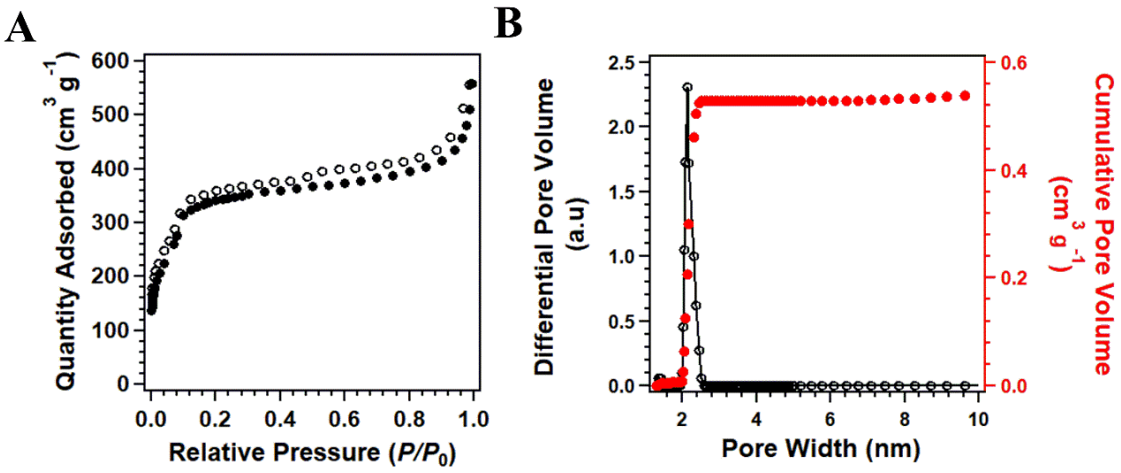

Figure 5. (A) Nitrogen sorption isotherm curves of TFPPy-DETHz-COF measured at 77 K (○: desorption, ●: adsorption). (B) Pore size (black dots and curve) and pore width distribution (red dots) of TFPPy-DETHz-COF.

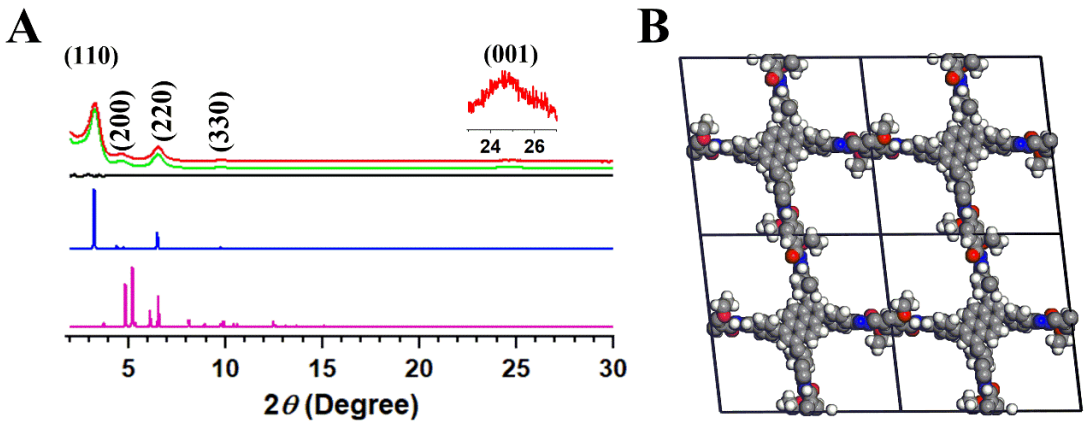

Figure 6. (A) PXRD patterns of experimentally observed (green), Pawley refined (red), and their difference (black), simulated from the eclipsed AA-stacking mode (blue), and staggered AB-stacking mode (purple). (B) Unit cell of TFPPy-DETHz-COF.

The crystalline structure of the TFPPy-DETHz-COF was determined by powder X-ray diffraction (PXRD) measurements. TFPPy-DETHz-COF exhibited PXRD peaks at 3.34°, 4.58°, 6.54°, 9.84°, and 24.52°, which were assigned to the (110), (200), (220), (330), and (001) facets, respectively (Figure 6A, red). The Pawley refined pattern (green) confirmed the diffraction peak assignments with the negligible difference (black). Among various possible stacking modes, the AA stacking mode is the most stable form in energy (Table 1). The AA stacking mode adopts a *P*1 space group with *a* = 28.1936 Å, *b* = 28.9188 Å, *c* = 4.3122 Å, and *α* = 78.3453°, *β* = 92.9836°, and *γ*

= 96.5509°, yielding a PXRD pattern that agrees with the experimentally observed profile (blue). By contrast, the staggered AB mode (purple) could not meet the experimental results.

Table 1. The total DFTB energies, Lennard-Jones contributions (LJ), and the crystal stacking energies per monolayer as well as the corresponding HOMO-LUMO energy gap for the TFPPy-DETHz-COF.

Stacking	Total DFTB Energy [a.u.]	LJ energy [a.u.]	Per unit crystal stacking energy [kcal.mol^{-1}]	HOMO-LUMO gap [eV]
monolayer	-182.321276	-0.215171		1.883
AA	-182.635083	-0.348912	-196.917076	2.325
AB	-182.471596	-0.765096	-94.327012	1.749

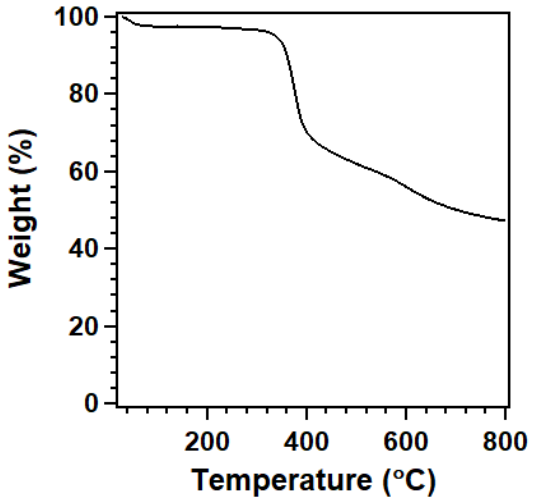

Figure 7. TGA curve of TFPPy-DETHz-COF under nitrogen atmosphere.

The stability is very important and necessary for materials. Thermogravimetric analysis (TGA) was investigated under nitrogen atmosphere. TFPPy-DETHz-COF showed excellent thermal stability and it can keep stable up to 300 °C without any decomposition (Figure 7).In addition, the chemical stability of the novel crystalline polymer was also investigated. The materials were treated in different solvents, including tetrahydrofuran (THF), water, aqueous HCl (1 M) and NaOH (1 M) solutions at room temperature for 24 h. All samples were collected by filtered, washed with THF and water, dried under vacuum for 24 h and tested by and FT-IR (Figure 8A), PXRD

measurements (Figure 8B) and N_2 sorption isotherm measurement (Figure 8C). All COF samples kept the same vibration bands that are the same as those of as-synthesized COF from the FT-IR profiles (Figure 8A), which indicates that the structure of TFPPy-DETHz-COF can be retained in harsh conditions. All the samples exhibit strong diffraction peaks in PXRD patterns without a change in the peak position, indicating that the high crystallinity is retained in the TFPPy-DETHz-COF samples (Figure 8B). Moreover, the COF samples retained the mesoporous characters from N_2 absorption and desorption curves (Figure 8C and 8D). The TFPPy-DETHz-COF showed excellent chemical stability, which can provide a good platform for functionalization.

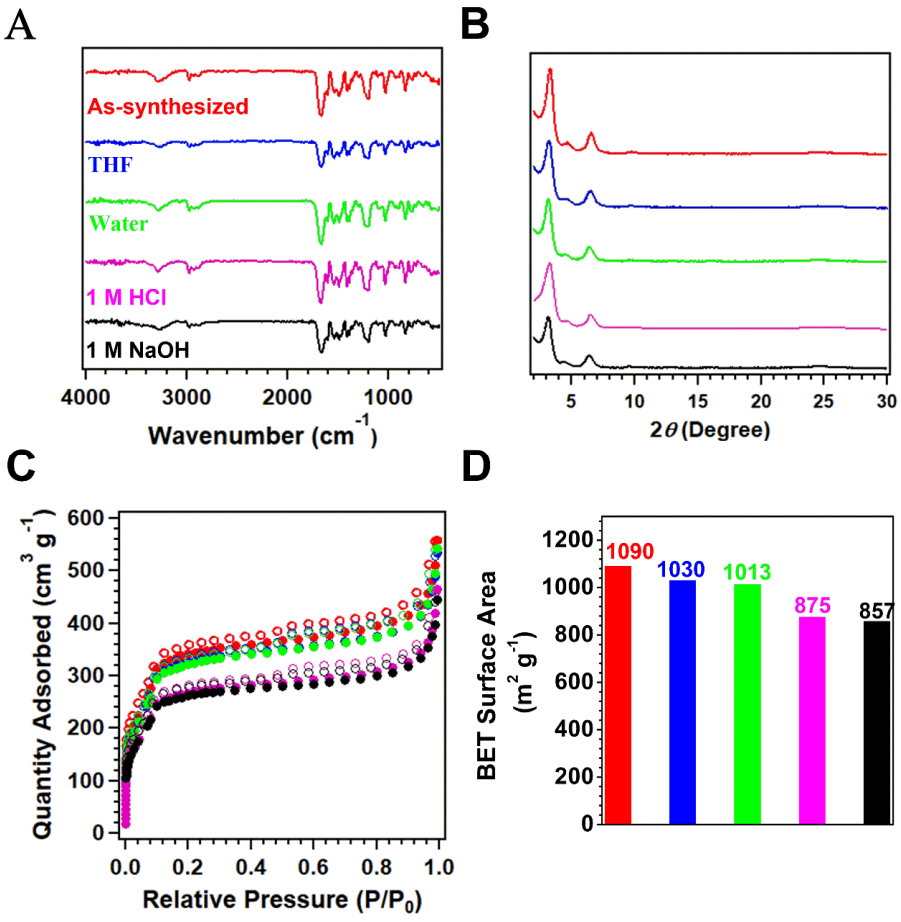

Figure 8. (A) FT IR profiles, (B) PXRD patterns, (C) Nitrogen sorption isotherm curve and (D) BET surface area of TFPPy-DETHz-COF upon 24 h treatment in different conditions. As-synthesized material (red); THF (blue); water (green);1M HCl (purple);1M NaOH (black).

4.3.2. Fluorescence characteristics and fluoride anion detection

The fluorescence spectra of TFPPy-DETHz-COF and monomers in THF at room temperature were observed. DETHz and TFPPy showed emission bond at 374 nm and 457 nm in THF at 25 °C (Figure 9A), respectively. Comparing the fluorescence spectra of monomers, TFPPy-DETHz-COF showed the red shift and emitted a weak green-yellow luminescence at 540 nm with absolute fluorescence quantum yield of 4.5% upon excitation at 460 nm.

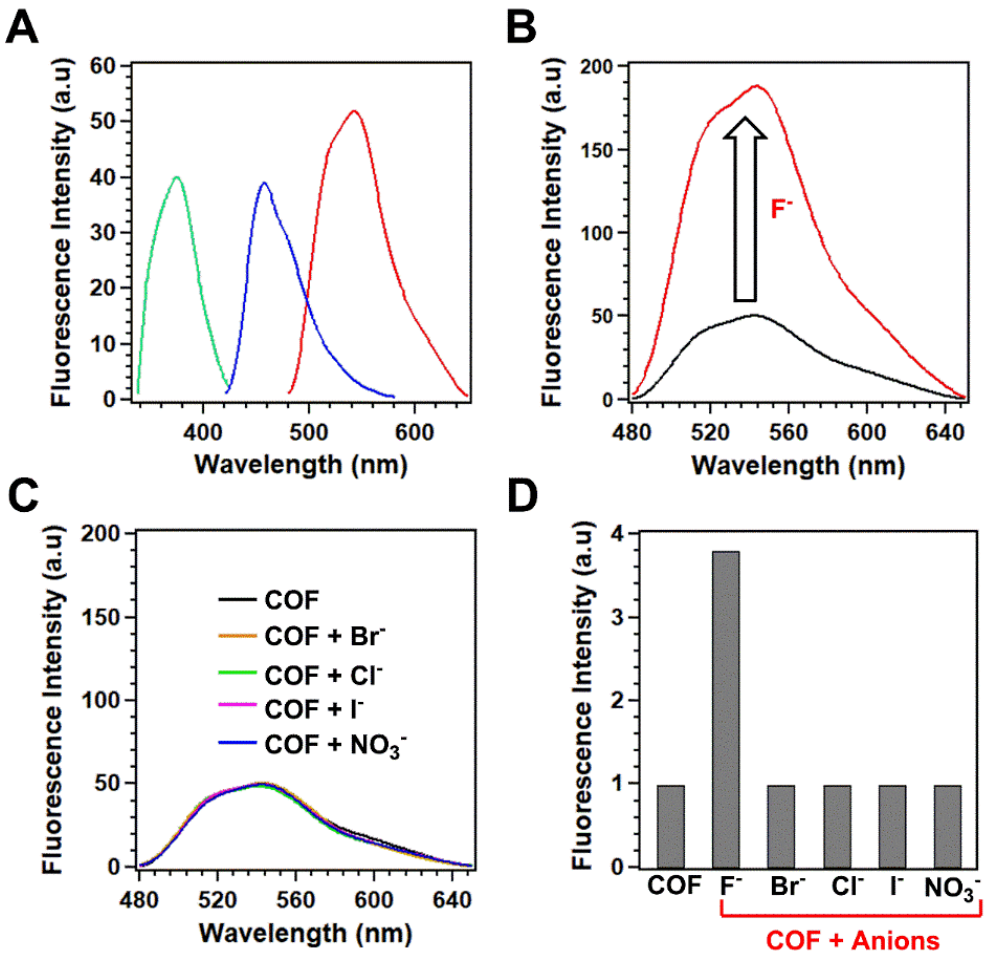

Figure 9. (A) Fluorescence spectra of DETHz (green curve), TFPPy (blue line) and TFPPy-DETHz-COF (red curve) samples in THF. (B) Fluorescence spectral change of TFPPy-DETHz-COF with addition of F^- anions. (C) Fluorescence spectra of TFPPy-DETHz-COF with addition of Cl^-, Br^-, I^-, and NO_3^-. (D) Relative fluorescence intensity of TFPPy-DETHz-COF with addition of different anions (All anions are tetrabutylammonium salts).

The TFPPy-DETHz-COF samples were simply immersed in THF solutions of tetrabutylammonium compound containing different anions (F^-, Cl^-, Br^-, I^-, and NO_3^-, respectively). Surprisingly, fluoride anion mixed with the TFPPy-DETHz-COF in THF causes a prominent enhancement of luminescence (Figure 9B). The fluorescence intensity of the ordered polymer in THF does not show any change upon the addition of Cl^-, Br^-, I^-, and NO_3^- anions (Figure 9C and 9D). The fluoride anion increases fluorescence intensity to 3.8-fold that of the original one, leading to an absolute fluorescence quantum yield of 17% (Figure 9B and 9D). These results indicate that the novel TFPPy-DETHz-COF can serve as an excellent fluorescence sensor for fluoride anion with high selectivity.

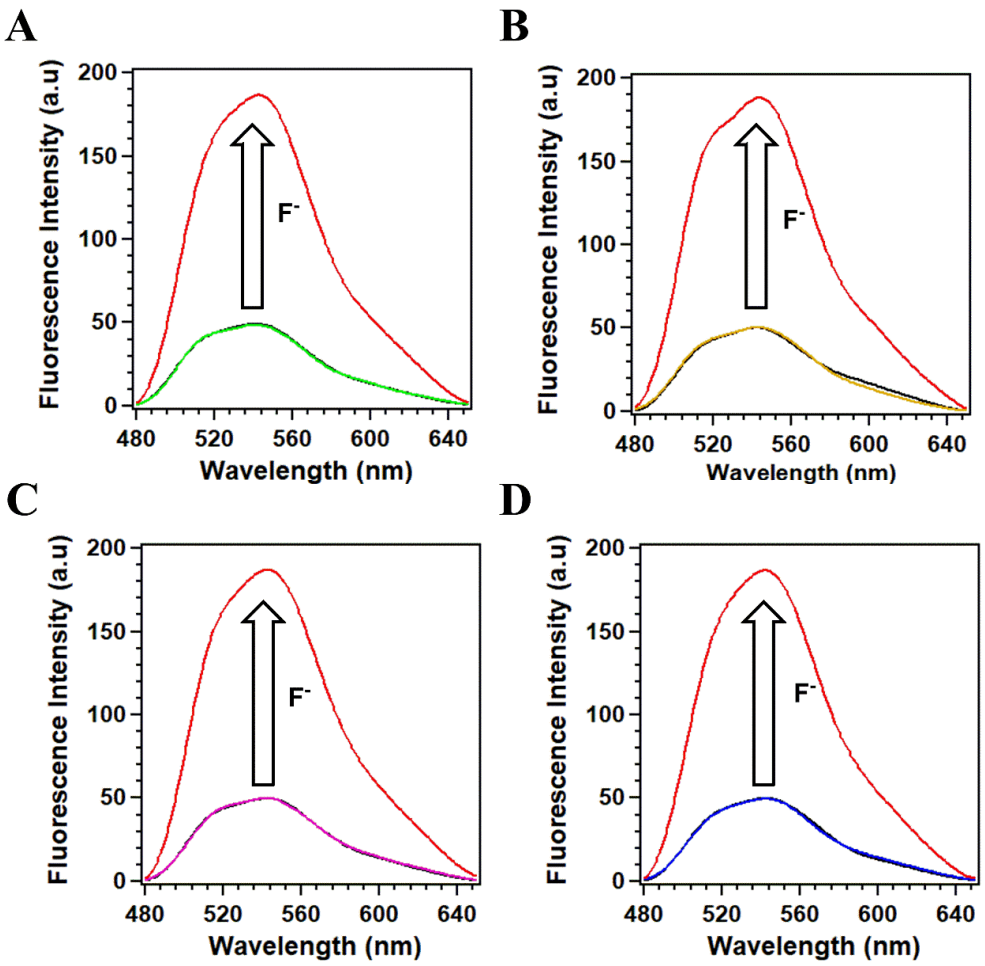

Figure 10. Fluorescence spectra of TFPPy-DETHz-COF with addition of Cl^- (A, green curve), Br^- (B, orange curve), I^- (C, purple curve), and NO_3^- (D, blue curve), followed by addition of F^- (red curves). Original COFs are black curves.

Sensitivity is significant for the fluorescent sensor. Further, I inspected the sensitivity of TFPPy-DETHz-COF toward fluoride ion, interference experiments were conducted to research the influence of other anions such as Cl^-, Br^-, I^-, and NO_3^-. The fluorescence intensity of the COF was also 3.8 times enhanced by mixing fluoride ion with other various anions, which is the same as that reacted by fluoride anion alone (Figure 9C, 9D and 10). These results implied that other anions are very little disturbance to the selective recognizing fluoride ion.

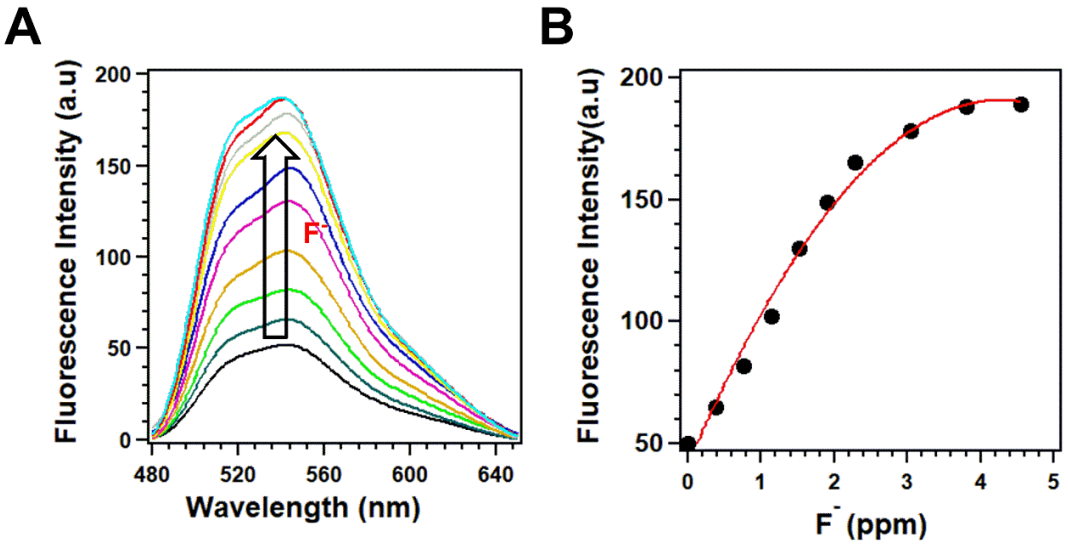

Figure 11. (A) (B) fluorescence emission spectra and fluorescence intensity of TFPPy-DETHz-COF in THF suspensions containing different concentrations of fluoride ion (0 to 5 ppm).

The luminescence spectra of the TFPPy-DETHz-COF in anhydrous tetrahydrofuran containing different concentrations of fluoride ion was observed. With the addition of fluoride anion, fluorescence intensity was enhanced (Figure 11A and 11B). The fluorescence intensity increased in a linear proportion to the concentration of the F^- anion and saturated after 4 ppm (Figure 11B). Moreover, the absolute quantum yield of the system has been increased to 4.5 % from 17 % for the original COF in THF suspension. This result is in good agreement with the luminescence spectra. Further, the fluorescence intensity showed good linearity in the range from 0 to 4 ppm and the detection limit of fluoride ion was determined as 50 ppb (Figure 11). This value

represents an excellent sensitivity toward fluoride anion detection.

The fluorescence increment effect of F^- with TFPPy-DETHz-COF has been further observed by time-resolved fluorescence spectroscopy. The fluorescence lifetime of 1.4 ns (Figure 12, black curve) for TFPPy-DETHz-COF is increased to 2.7 ns (red curve) in the presence of F^- anions. This increment indicated that the deprotonation by F^- suppresses the electron transfer from the linkage to the pyrene skeleton, which enhances the light-emitting activity of frameworks.

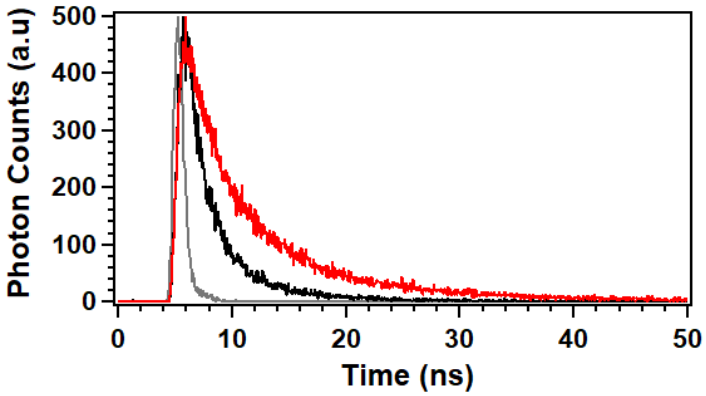

Figure 12. Fluorescence lifetime changes of TFPPy-DETHz-COF (black curve) with addition of F^- anions (red curve).

These results indicated that the F^- can deprotonate the N−H unit while other halogen anions are inactive because this process is based on an acid−base reaction mechanism.[13] The mechanism was inspected by ^1H NMR spectroscopy to confirm the reaction between F^- and the N−H unit. TFPPy-DETHz-COF is insoluble in organic solvents and water, which means it is difficult to inspect by a solution NMR spectroscopy. Therefore, the model compound that is the same as the framework's structure of TFPPy-DETHz-COF was inspected for the mechanistic study. From the ^1H NMR spectra, the peak of the N−H bond of model compound can be easily found at 11.2 ppm (Figure 13B, black curve). With the addition of fluoride anion, this peak was disappeared, which means this process is deprotonation of the N-H bond. Moreover, these results indicated that the reaction between hydrazone and fluoride anions were the acid-base reaction.

The mixture that includes F^- and TFPPy-DETHz-COF was added into trifluoroacetic acid to recover the original fluorescence. The fluorescence intensity recovered the beginning of the state. These data indicated TFPPy-DETHz-COF can be used as an alkaline sensor (F^- anions). An anionic nitrogen species of hydrazone-linked TFPPy-DETHz-COF can detect acid (H^+). In short, TFPPy-DETHz-COF can be also as for pH sensor.

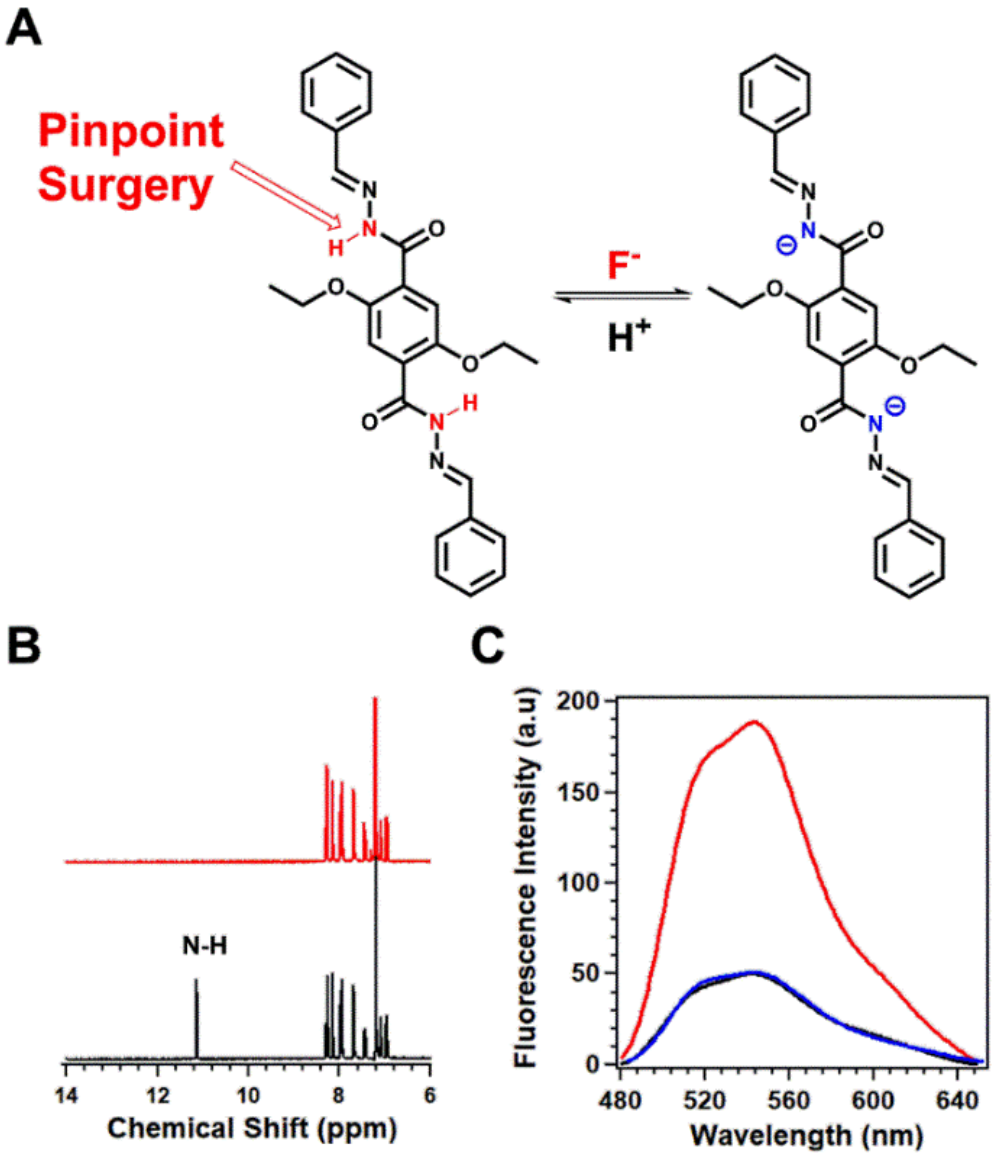

Figure 13. (A) Pinpoint surgery on the N−H unit of the hydrazone linkage through acid-base reaction with F^- and its can be regenerated by acid; (B) ^1H NMR spectral changes of the model compound (blue curve) in Chloroform-D with addition of F^- (red curve); (D) Fluorescence spectral change of TFPPy-DETHz-COF (black curve) in THF with addition of F^- (red curve) and followed by addition of trifluoroacetic acid (blue curve).

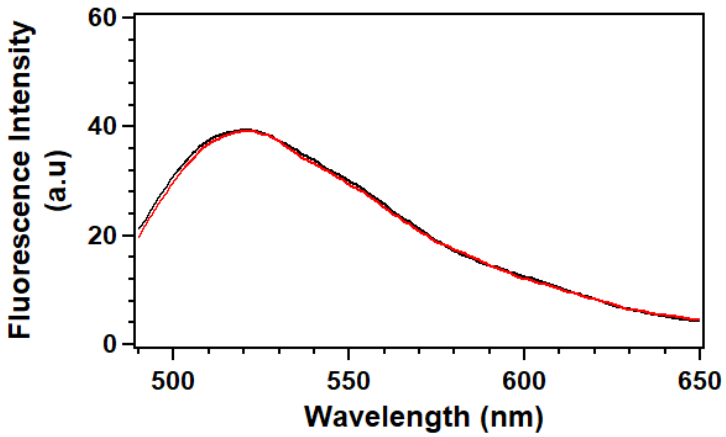

Figure 14. Fluorescence spectral change of Py-Azine COF (black curve) upon addition of F^- (red curve).

The azine-linked Py-Azine COF without active N−H units (Scheme 2) was synthesized and observed to further study the mechanism. Before and after F^- was added, the fluorescence spectra of Py-Azine COF in THF showed no any changes (Figure 14). The results further that pinpoint surgery for active N−H sites on the pore walls can trigger a great increment luminescence of frameworks.

4.4 Conclusion

In summary, a novel hydrazone-linked covalent organic framework TFPPy-DETHz-COF was successfully designed and synthesized under mild conditions. The hydrazone-linked frameworks showed permanent porosity with high BET surface area and displayed good physical and chemical stability. The pinpoint surgery on the N−H unit of the hydrazone-linked COFs and the first example of COFs for anion sensing were demonstrated. Scissoring the N−H unit upon deprotonation into N^- anion eliminates the electron transfer from the linkage to COF so that the fluorescence quenching is suppressed, enabling the improvement of light-emitting activity in a proportional fashion. Especially, the new COF showed a highly selective and sensitive response to fluoride ion. This research achieves an important step for the design of functional porous crystalline polymers.

4.5 Experimental section

4.5.1 Chemicals

The anhydrous tetrahydrofuran (stabilized with BHT), tetrabutylammonium fluoride, tetrabutylammonium chloride, tetrabutylammonium bromide, tetrabutylammonium iodide, and tetrabutylammonium nitrate, were obtained from TCI and Sigma-Aldrich. The anhydrous tetrahydrofuran was further dried over sodium/benzophenone and distilled under nitrogen prior to use. 5 1,3,6,8-Tetrakis(4-formylphenyl)pyrene (TFPPy), 2,5-dithoxyterephthalohydrazide (DETHz), 2-ethoxybenzohydrazide were synthesized using reported methods.[14-15]

4.5.2 Methods

Characterizations. The Bruker spectrometer AVANCE III 500 MH with a rotor frequency of 10 kHz was used to test the Solid-state ^{13}C CP/MAS NMR spectrum of TFPPy-DETHz-COF. Time-resolved fluorescence spectroscopy of TFPPy-DETHz-COF were recorded on a Hamamatsu model compact fluorescence lifetime spectrometer C11367 (Quantaurus-Tau).

Fluorescence spectroscopy. Firstly**,** TFPPy-DETHz-COF sample was dispersed in anhydrous tetrahydrofuran. The system was sonicated for several times to afford a transparent dispersion. Then, the fluorescence spectroscopy measurement was recorded. With the addition of fluoride anion, fluorescence spectra were recorded by time-dependent test. Each experiment was repeated at least three times to take the average.

Computational calculations. The density-functional tight-binding (DFTB) method including Grimme (D3) dispersion was used to conduct crystal structure of the TFPPy-DETHz-COF. The calculations were determined by the DFTB+ program package version 17.1.[16] DFTB is an approximate density functional theory method based on the tight binding approach and utilizes an optimized minimal LCAO Slater-type all-valence basis set in combination with

a two-center approximation for Hamiltonian matrix elements. The Coulombic interaction between partial atomic charges was determined using the self-consistent charge (SCC) formalism.[17] Grimme D3-type dispersion was employed in all calculations to describe van der Waals (vdW) and π-stacking interactions.[18] The lattice dimensions were optimized simultaneously with the geometry**.**

Pawley refinement. Molecular modeling and Pawley refinement were implemented by using Reflex, a software package for crystal determination from PXRD pattern, implemented in MS modeling version 4.4 (Accelrys Inc.).[19] At first, the DFTB calculations were applied for unit cell dimensions of TFPPy-DETHz-COF. Then, the lattice parameters were iteratively optimized by Pawley refinement until the R_P and R_{WP} values converge. Finally, a rhombic crystal system of TFPPy-DETHz-COF was deduced as a *P*1 space group with a unit cell of a = 28.1936 Å, b = 28.9188 Å, c = 4.3122 Å, and α = 78.3453°, β = 92.9836°, and γ = 96.5509°, while the final R_{WP} and R_P values were 6.04 and 4.64% for TFPPy-DETHz-COF, respectively.

4.5.3 Atomic coordinates

Table S2. Atomistic coordinates for the AA-stacking mode of TFPPy-DETHz-COF optimized by using DFTB+ method.

C	-0.20508	-0.46423	0.88243
C	-0.1033	-0.48874	1.35702
C	-0.05064	-0.48913	1.31448
C	-0.02553	0.48259	1.5579
C	-0.02562	-0.46612	1.04107
C	0.02262	0.47618	1.52989
C	0.02253	-0.47253	1.01306
C	0.04763	0.49918	1.25648
C	0.10029	0.4988	1.21394
C	0.20207	0.47429	0.68853
C	0.49167	0.20837	1.34208
C	0.48464	0.10491	1.03324
C	0.49465	0.05437	1.1655
C	0.52174	0.03935	1.44507

C	0.47215	0.01929	1.00813
C	0.52485	-0.00923	1.56287
C	0.47526	-0.02929	1.12593
C	0.50235	-0.04431	1.40549
C	0.59355	0.07183	0.68058
C	0.51236	-0.09486	1.53776
C	0.6109	0.10329	0.90022
C	0.40345	-0.06178	0.89042
C	0.3861	-0.09324	0.67078
C	0.50532	-0.19831	1.22892
C	0.512	-0.24891	1.26191
C	0.5423	-0.27377	1.49258
C	0.49097	-0.27148	1.02508
C	0.55365	-0.31842	1.45883
C	0.50075	-0.31679	0.99939
C	0.53218	-0.34095	1.22427
C	0.54231	-0.39018	1.21315
C	0.50583	-0.42866	1.26682
C	0.58863	-0.39855	1.15484
C	0.51682	-0.47542	1.25919
C	0.45807	-0.42235	1.3384
C	0.60031	-0.4441	1.14732
C	0.48017	0.48547	1.31179
C	0.56437	-0.48313	1.19913
C	0.42319	-0.45961	1.38888
C	0.6501	-0.45041	1.07525
C	0.43262	0.49318	1.37184
C	0.49116	0.43872	1.30416
C	0.57381	0.46966	1.18209
C	0.67841	-0.4797	1.29467
C	0.6691	-0.42705	0.78841
C	0.39668	0.45415	1.42365
C	0.45468	0.40023	1.35783
C	0.53892	0.4324	1.23258
C	0.7241	-0.48589	1.20918
C	0.7143	-0.43461	0.69799
C	0.40836	0.4086	1.41614
C	0.34689	0.46046	1.49572
C	0.46482	0.351	1.34672
C	0.74332	-0.46233	0.92238
C	0.31858	0.48975	1.2763
C	0.3279	0.43711	0.78256

C	0.49625	0.32685	1.5716
C	0.44334	0.32847	1.11215
C	0.2729	0.49595	1.36178
C	0.28269	0.44467	0.87298
C	0.50602	0.28153	1.54592
C	0.4547	0.28383	1.07842
C	0.25367	0.47238	0.64859
C	0.485	0.25896	1.30909
C	0.02602	0.40134	0.88657
C	0.04965	0.37881	1.18154
C	-0.02903	-0.39129	0.68439
C	-0.05266	-0.36876	1.38942
H	-0.12147	-0.47378	0.88195
H	0.11847	0.48384	0.68901
H	0.18886	0.47418	0.94109
H	0.49506	0.1915	0.60982
H	0.49708	0.12658	1.45525
H	0.45008	0.03132	0.79956
H	0.54692	-0.02126	0.77144
H	0.60312	0.03531	0.76234
H	0.61128	0.08601	1.44942
H	0.59814	0.1381	0.83128
H	0.59817	0.0876	1.13988
H	0.64968	0.1076	0.91655
H	0.38572	-0.07596	1.12158
H	0.39388	-0.02526	0.80866
H	0.49992	-0.11653	1.11575
H	0.39883	-0.07754	1.43112
H	0.39886	-0.12805	0.73972
H	0.34732	-0.09755	0.65445
H	0.50193	-0.18144	0.96118
H	0.56268	-0.25506	0.65886
H	0.4688	-0.2518	0.84241
H	0.57745	-0.33735	0.63351
H	0.48072	-0.33537	0.83126
H	0.61639	-0.36877	1.11379
H	0.45001	-0.38714	1.35694
H	0.38761	-0.45383	1.44821
H	0.60938	0.46388	1.12276
H	0.66224	0.49783	1.50333
H	0.64704	-0.4048	0.62077
H	0.54698	0.39719	1.21403

H	0.74664	0.49282	1.37968
H	0.73043	-0.41184	1.48986
H	0.38061	0.37882	1.45719
H	0.33476	-0.48777	1.06764
H	0.34996	0.41486	0.95021
H	0.51627	0.34543	0.73972
H	0.41955	0.3474	0.93747
H	0.25036	-0.48276	1.19128
H	0.26656	0.4219	1.08111
H	0.52819	0.26186	0.72859
H	0.43432	0.26512	0.91213
H	-0.01309	0.39911	0.90534
H	0.03275	0.38167	0.6976
H	0.08836	0.38445	1.16964
H	0.03945	0.39395	1.38028
H	0.0386	0.3409	1.23808
H	-0.03576	-0.37161	0.87336
H	0.01008	-0.38906	0.66562
H	-0.04246	-0.38389	1.19068
H	-0.09136	-0.3744	1.40132
H	-0.04161	-0.33085	1.33288
H	-0.04579	0.46373	0.76142
H	0.04278	-0.45368	0.80954
H	-0.19187	-0.46412	0.62987
N	-0.17856	-0.46594	1.13893
N	-0.1293	-0.46626	1.10283
N	0.12629	0.47631	1.46813
N	0.17555	0.476	1.43203
N	0.493	0.18632	1.10845
N	0.50177	0.13822	1.20994
N	0.49523	-0.12816	1.36106
N	0.50399	-0.17627	1.46255
O	-0.12178	0.49102	0.61465
O	0.11877	-0.48097	0.95631
O	0.4614	0.11424	0.77644
O	0.54292	0.07177	0.61968
O	0.45408	-0.06171	0.95132
O	0.5356	-0.10419	0.79456
O	0.04585	0.44977	0.78351
O	-0.04886	-0.43971	0.78745

Table S3. Atomistic coordinates for the AA-stacking mode of TFPPy-DETHz-COF optimized by Pawley refinement.

C	-0.20517	-0.46493	0.90611
C	-0.10339	-0.48944	1.3807
C	-0.05073	-0.48983	1.33816
C	-0.02562	0.48189	1.58158
C	-0.02571	-0.46682	1.06475
C	0.02253	0.47548	1.55357
C	0.02244	-0.47323	1.03674
C	0.04754	0.49848	1.28016
C	0.1002	0.4981	1.23762
C	0.20198	0.47359	0.71221
C	0.49158	0.20767	1.36576
C	0.48455	0.10421	1.05692
C	0.49456	0.05367	1.18918
C	0.52165	0.03865	1.46875
C	0.47206	0.01859	1.03181
C	0.52476	-0.00993	1.58655
C	0.47517	-0.02999	1.14961
C	0.50226	-0.04501	1.42917
C	0.59346	0.07113	0.70426
C	0.51227	-0.09556	1.56144
C	0.61081	0.10259	0.9239
C	0.40336	-0.06248	0.9141
C	0.38601	-0.09394	0.69446
C	0.50523	-0.19901	1.2526
C	0.51191	-0.24961	1.28559
C	0.54221	-0.27447	1.51626
C	0.49088	-0.27218	1.04876
C	0.55356	-0.31912	1.48251
C	0.50066	-0.31749	1.02307
C	0.53209	-0.34165	1.24795
C	0.54222	-0.39088	1.23683
C	0.50574	-0.42936	1.2905
C	0.58854	-0.39925	1.17852
C	0.51673	-0.47612	1.28287
C	0.45798	-0.42305	1.36208
C	0.60022	-0.4448	1.171
C	0.48008	0.48477	1.33547
C	0.56428	-0.48383	1.22281
C	0.4231	-0.46031	1.41256
C	0.65001	-0.45111	1.09893

C	0.43253	0.49248	1.39552
C	0.49107	0.43802	1.32784
C	0.57372	0.46896	1.20577
C	0.67832	-0.4804	1.31835
C	0.66901	-0.42775	0.81209
C	0.39659	0.45345	1.44733
C	0.45459	0.39953	1.38151
C	0.53883	0.4317	1.25626
C	0.72401	-0.48659	1.23286
C	0.71421	-0.43531	0.72167
C	0.40827	0.4079	1.43982
C	0.3468	0.45976	1.5194
C	0.46473	0.3503	1.3704
C	0.74323	-0.46303	0.94606
C	0.31849	0.48905	1.29998
C	0.32781	0.43641	0.80624
C	0.49616	0.32615	1.59528
C	0.44325	0.32777	1.13583
C	0.27281	0.49525	1.38546
C	0.2826	0.44397	0.89666
C	0.50593	0.28083	1.5696
C	0.45461	0.28313	1.1021
C	0.25358	0.47168	0.67227
C	0.48491	0.25826	1.33277
C	0.02593	0.40064	0.91025
C	0.04956	0.37811	1.20522
C	-0.02912	-0.39199	0.70807
C	-0.05275	-0.36946	1.4131
H	-0.12156	-0.47448	0.90563
H	0.11838	0.48314	0.71269
H	0.18877	0.47348	0.96477
H	0.49497	0.1908	0.6335
H	0.49699	0.12588	1.47893
H	0.44999	0.03062	0.82324
H	0.54683	-0.02196	0.79512
H	0.60303	0.03461	0.78602
H	0.61119	0.08531	1.4731
H	0.59805	0.1374	0.85496
H	0.59808	0.0869	1.16356
H	0.64959	0.1069	0.94023
H	0.38563	-0.07666	1.14526
H	0.39379	-0.02596	0.83234

H	0.49983	-0.11723	1.13943
H	0.39874	-0.07824	1.4548
H	0.39877	-0.12875	0.7634
H	0.34723	-0.09825	0.67813
H	0.50184	-0.18214	0.98486
H	0.56259	-0.25576	0.68254
H	0.46871	-0.2525	0.86609
H	0.57736	-0.33805	0.65719
H	0.48063	-0.33607	0.85494
H	0.6163	-0.36947	1.13747
H	0.44992	-0.38784	1.38062
H	0.38752	-0.45453	1.47189
H	0.60929	0.46318	1.14644
H	0.66215	0.49713	1.52701
H	0.64695	-0.4055	0.64445
H	0.54689	0.39649	1.23771
H	0.74655	0.49212	1.40336
H	0.73034	-0.41254	1.51354
H	0.38052	0.37812	1.48087
H	0.33467	-0.48847	1.09132
H	0.34987	0.41416	0.97389
H	0.51618	0.34473	0.7634
H	0.41946	0.3467	0.96115
H	0.25027	-0.48346	1.21496
H	0.26647	0.4212	1.10479
H	0.5281	0.26116	0.75227
H	0.43423	0.26442	0.93581
H	-0.01318	0.39841	0.92902
H	0.03266	0.38097	0.72128
H	0.08827	0.38375	1.19332
H	0.03936	0.39325	1.40396
H	0.03851	0.3402	1.26176
H	-0.03585	-0.37231	0.89704
H	0.00999	-0.38976	0.6893
H	-0.04255	-0.38459	1.21436
H	-0.09145	-0.3751	1.425
H	-0.0417	-0.33155	1.35656
H	-0.04588	0.46303	0.7851
H	0.04269	-0.45438	0.83322
H	-0.19196	-0.46482	0.65355
N	-0.17865	-0.46664	1.16261
N	-0.12939	-0.46696	1.12651

N	0.1262	0.47561	1.49181
N	0.17546	0.4753	1.45571
N	0.49291	0.18562	1.13213
N	0.50168	0.13752	1.23362
N	0.49514	-0.12886	1.38474
N	0.5039	-0.17697	1.48623
O	-0.12187	0.49032	0.63833
O	0.11868	-0.48167	0.97999
O	0.46131	0.11354	0.80012
O	0.54283	0.07107	0.64336
O	0.45399	-0.06241	0.975
O	0.53551	-0.10489	0.81824
O	0.04576	0.44907	0.80719
O	-0.04895	-0.44041	0.81113

4.6 References

1. A. P. Côté, A. I. Benin, N. W. Ockwigm, M. O'Keeffe, A. J. Matzger, O. M. Yaghi. Porous, crystalline, covalent organic frameworks. *Science.* **2005**, *310*, 1166-1170.
2. E. Jin, M. Asada, Q. Xu. S. Dalapati, M. A. Addicoat, M. A. Brady, H. Xu, T. Nakamura, T. Heine, Q. Chen, D. Jiang. Two-dimensional sp^2 carbon–conjugated covalent organic frameworks. *Science.* **2017**, *357*, 673-676.
3. H. Xu, J. Guo, D. Jiang. Stable, crystalline, porous, covalent organic frameworks as a platform for chiral organocatalysts. *Nat. Chem*. **2015**, *7*, 905-912.
4. X. Feng, X. Ding, D. Jiang. Covalent organic frameworks. *Chem. Soc. Rev*. **2012**, *41*, 6010-6022.
5. N. Huang, P. Wang, D. Jiang. Covalent organic frameworks: a materials platform for structural and functional designs. *Nat. Rev*. *Mater*. **2016**, *1*, 16068.
6. (a) F. J. Uribe-Romo, J. R. Hunt, H. Furukawa, C. Klöck; M. O'Keeffe; O. M. Yaghi. A Crystalline imine-linked 3D porous covalent organic framework. *J. Am. Chem. Soc*. **2009**, *131*, 4570-4571. (b) H. Li; Q. Pan; Y. Ma, X. Guan, M. Xue, Q. Fang, Y. Yan, V. Valtchev, S. Qiu. Three-dimensional covalent organic frameworks with dual linkages for bifunctional cascade catalysis. *J. Am. Chem. Soc.* **2016**, *138*, 14783-14788. (c) Y. Ma, Z. Li, L. Wei, S. Ding, Y. Zhang, W. Wang. A dynamic three-dimensional covalent organic framework. *J. Am. Chem. Soc*. **2017**, *139*, 4995-4998. (d) X. Han, J. Huang, C. Yuan, Y. Liu, Y. Cui. Chiral 3D covalent organic frameworks for high performance liquid chromatographic enantioseparation. *J. Am. Chem. Soc.* **2018**, *140*, 892-895.

7. Q. Fang, Z. Zhuang, S. Gu, R. B. Kaspar, J. Zheng, J. Wang, S. Qiu, Y. Yan. Designed synthesis of large-pore crystalline polyimide covalent organic frameworks. *Nat. Commun*. **2014**, *5*, 4503.

8. (a) Q. Sun, B. Aguila, L. D. Earl, C. W. Abney, L. Wojtas, P. K. Thallapally, S. Ma. Covalent organic frameworks as a decorating platform for utilization and affinity enhancement of chelating sites for radionuclide ssequestration. *Adv. Mater*. **2018**, *30*, 1705479. (b) Q. Sun, B. Aguila, J. Perman, L. D. Earl, C. W. Abney, Y. Cheng, H. Wei, N. Nguyen, L. Wojtas, S. Ma. Postsynthetically modified covalent organic frameworks for efficient and effective mercury removal. *J. Am. Chem. Soc*. **2017**, *139*, 2786-2793.

9. (a) Y. Zhang, X. Shen, X. Feng, H. Xia, Y. Mu, X. Liu. Covalent organic frameworks as pH responsive signaling scaffolds. *Chem. Commun*. **2016**, *52*, 11088-11091. (b) P. Wang, Q. Xu, Z. Li, W. Jiang, Q. Jiang. Exceptional iodine capture in 2D covalent organic frameworks. *Adv. Mater*. **2018**, *30*, 1801991.

10. (a) S. Wang, Q. Wang, P. Shao, Y. Han, X. Gao, L. Ma, S. Yuan, X. Ma, J. Zhou, X. Feng, B. Wang. Exfoliation of covalent organic frameworks into few-layer redox-active nanosheets as cathode materials for lithium-ion batteries *J. Am. Chem. Soc.* **2017**, *139*, 4258-4261. (b) Y. Zhu, S. Wan, Y. Jin, W. Zhang. Desymmetrized vertex design for the synthesis of covalent organic frameworks with periodically heterogeneous pore structures. *J. Am. Chem. Soc*. **2015**, *137*, 13772-13775. (c) D. Bessinger, L. Ascherl, F. Auras, T. Bein. Spectrally switchable photodetection with near-infrared-absorbing covalent organic frameworks. *J. Am. Chem. Soc*. **2017**, *139*, 12035-12042. (e) C. Qian, Q. Qi, G. Jiang, F. Cui, Y. Tian, X. Zhao. Toward covalent organic frameworks bearing three different kinds of pores: the strategy for construction and COF-to-COF transformation via heterogeneous linker exchange. *J. Am. Chem. Soc.* **2017**, *139*, 6736-6743.

11. (a) H. Li, A. D. Chavez, H. Li, W. R. Dichtel, J. Breda. Nucleation and growth of covalent organic frameworks from solution: the example of COF-5. *J. Am. Chem. Soc.* **2017**, *139*, 16310-16318. (b) S. Karak, S. Kandambeth, B. P. Biswal, H. S. S, S. Kumarr, P. Pachfule, R. Banerjee. *J. Am. Chem. Soc.* **2017**, *139*, 1856-1862. (c) H. Ma, B. Liu, B. Li, L. Zhang; Y. Li, H. Tan, H. Zang, G. Zhu. Cationic covalent organic frameworks: a simple platform of anionic exchange for porosity tuning and proton conduction. *J. Am. Chem. Soc*. **2016**, *138*, 5897-5903. (d) C. M. Thompson, G. Occhialini, G. T. McCandless, S. B. Alahakoon, V. Cameron, S. O. Nielsen, R. A. Smaldone. Computational and experimental studies on the effects of monomer planarity on covalent organic framework formation. *J. Am. Chem. Soc*. **2017**, *139*, 10506-10513.

12. (a) S. Wan, J. Guo, J. Kim, H. Ihee, D. Jiang. A belt-shaped, blue luminescent, and semiconducting covalent organic framework. *Angew. Chem. Int. Ed.* **2008,** 47, 8826-8830. (b) S. Dalapati, S. Jin, J. Gao, Y. Xu, A. Nagai, D. Jiang. An azine-linked covalent organic framework. *J. Am. Chem. Soc.* **2013**, *135*, 17310-17313. (c) G. Das, B. P. Biswal, S. Kandambeth, V. Venkatesh, G. Kaur, M. Addicoat, T. Heine, S. Verm, R. Banerjee. *Chem. Sci.* **2015**, *6*, 3931-3939. (d) S. Ding, M. Dong, Y. Wang, Y. Chen, H. Wang, C. Su, W. Wang. Thioether-based fluorescent covalent organic framework for selective detection and facile removal of mercury (II). *J. Am. Chem. Soc*. **2016**, *138*, 3031-3037. (e) Z. Li, Y. Zhang, H. Xia, Y. Mu; X. Liu. A robust and luminescent covalent organic framework as a highly sensitive and selective sensor for the detection of Cu^{2+} ions. *Chem. Commun*. **2016**, 52, 6613-6616. (f) S. Dalapati, E. Jin, M. Addicoat, T. Heine, D. Jiang. Highly emissive covalent organic frameworks. *J. Am. Chem. Soc.* **2016**, *138*, 5797-5800. (g) J. W. Crowe, L. A. Baldwin, P. L. McGrier. Luminescent covalent organic frameworks containing a homogeneous and heterogeneous distribution of

dehydrobenzoannulene vertex units. *J. Am. Chem. Soc*. **2016**, *138*, 10120-10123. (h) G. Lin, H. Ding, D. Yuan, B. Wang, C. Wang. A pyrene-based, fluorescent fhree-dimensional covalent organic framework. *J. Am. Chem. Soc*. **2016**, *138*, 3302-3305.

13. Y. Zhou, J. Zhang, J. Yoon. Fluorescence and colorimetric chemosensors for fluoride-ion detection. *Chem. Rev.* **2014**, *114*, 5511-5571.
14. M. G. Rabbani, A. K. Sekizkardes, Z. Kahveci, T. E. Reich, R. Ding, H. M. El-Kaderi. A 2D mesoporous imine-linked covalent organic framework for high pressure gas storage applications. *Chem. Eur. J*. **2013**, *19*, 3324-3328.
15. M. Maha, N. H. Ismail, S. Imran, E. H. Anouar, M. Selvarad, W. Jamilf, M. Ali, S. M. Kashif, F. Rahim, K. M. Khan, M. I. Adenan. Synthesis and molecular modelling studies of phenyl linked oxadiazole-phenylhydrazone hybrids as potent antileishmanial agents. *Eur. J. Med. Chem.* **2017**, *126*, 1021-1033.
16. B. Aradi, B. Hourahine, T. Frauenheim. DFTB+, a sparse matrix-based implementation of the DFTB method. *Phys. Chem. A.* **2007**, *111*, 5678-5684.
17. M. Elstner, D. Porezag, G. Jungnickel, J. Elsner, M. Haugk, T. Frauenheim, S. Suhai, G. Seifert. Self-consistent-charge density-functional tight-binding method for simulations of complex materials properties. *Phys. Rev. B.* **1998**, *58*, 7260-7268.
18. M. Kubillus, T. Kubař, M. Gaus, J. Řezáč, M. Elstner. Parameterization of the DFTB3 Method for Br, Ca, Cl, F, I, K, and Na in organic and biological systems. *J. Chem. Theory Comput.* **2015**, *11*, 332-342.
19. Accelrys, Material Studio Release Notes, Release 4.4, Accelrys Software, San Diego **2008**.

Chapter 5
Summary and Perspectives

COFs are novel porous crystalline materials that allow the precisely integration of building units into high-ordered 2D and 3D frameworks. From a synthetic point of view, COFs can be constructed through different chemical reaction to give various linkage. The hydrazone linkage showed many advantages. Here, I summarized my research project in the three years on designed and synthesis of functional hydrazone-linked COFs for carbon dioxide absorption and anions sensing.

In chapter 1, I summarized the COFs field including the general principle of the skeleton design and the synthetic methods. This chapter elaborates the typical function of COFs including carbon dioxide, catalyst, and chemical sensing.

In chapter 2, I synthesized two micropores hydrazone-linked COFs, TMHzcB-TFB-COF and TMHzcB-TFP-COF, through condensation of 1,3,5-tris(3'-methoxy-4'-hydrazinecarbonylphenyl)benzene (TMHzcB) and 1,3,5-triformylbenzene (TFB) / triformylphloroglucinol (TFP) under solvothermal conditions. The new COFs showed high crystallinity, permanent micropores, excellent thermal and chemical stability, and abundant heteroatom activated sites on the walls. These two COFs exhibited remarkable CO_2 uptake capacity. Interestingly, the capacity of TMHzcB-TFP-COF can reach up to 14.4 wt% at 273 K and 1 bar.

In chapter 3, I synthesized a series of light-emitting COFs. These COFs not only showed excellent porosity, but also displayed good stability in organic solvents, water, acid and base conditions for 24 hours at the room temperature. I designed and synthesized hydrazone-linked COFs with wide pore size from. 1.3 nm to 3.7 nm by different symmetrical linkers or knots. The light-emitting activity of COFs can be improved through flexible building units or functional active groups including methoxy and methyl. The luminescence can be tunable from blue to green luminescence as a result. Interestingly, COF-TMHzcB-2,5-DMeTA and COF-TMHzcB-2,5-DMTA showed the highest fluorescence quantum yield over 19.5 % at the solid state, which is higher than

most reported azine, imine, and hydrazone based COFs.

In chapter 4, the hydrazone-linked TFPPy-DETHz-COF was successfully constructed through Schiff-base condensation reaction under solvothermal conditions. The N-H bond in linkage on the walls can be deprotonated to form an anionic species, which can eliminate the nitrogen-related fluorescence quenching pathway. Interestingly, the N-H bond can be cleaved by fluoride anion via an acid-base reaction. Owing to the fact that the N-H sites in TFPPy-DETHz-COF locate on the pore walls and are accessible to fluoride anion. The addition of fluoride anion eliminates the photoinduced electron transfer pathway and directly improves light emitting activity. Surprisingly, the emission is switched on in the presence of fluoride anion and its intensity is enhanced in a linear proportion to the amount of fluoride anion. The absolute fluorescence quantum yield increases to 17%, which is 3.8-fold as high as that of as-synthesized TFPPy-DETHz-COF. In contrast, other halogen anions, including chloride, bromide, and iodide, retain inactive. Interestingly, this switch-on COF can detect a ppb level of fluoride anion, which is lower than most hydrazone based detector. This is the first crystalline COF that can serve as a functional fluorescent sensor for detecting trace amounts of fluoride anion.

Through the three years, I synthesized various novel hydrazone-linked COFs including hexagonal and tetragonal structure. The COFs showed good porosity. The pore size of COFs can be adjustable from micropores (1.6 nm) and mesopores (3.7 nm), which is a very wide distribution. This work not only provides rich pore size but also enriches the diversity of the structure. The N-H units of linkage can be used for the application. For example, microporous COFs with N-H sites on the walls showed higher carbon dioxide uptake. The non-planar structure of hydrazone linkage can reduce strong interaction of adjacent layers, which can afford luminescence materials. The light-emitting activity of COFs can be tunable through various building units and linkage. In chapter 2, various luminescence with high light-emitting activity can be

controllable by building blocks. In chapter 3, high fluorescence COFs can be achieved by changing the N-H of linkage into nitrogen anions. In this way, these COFs can also detect fluoride anion with high sensitivity and selectivity. The investigated results displayed in this thesis demonstrated functional hydrazone-linked COFs that open a new phase for not only high adsorptive media but also light-emitting materials for chemical sensing.

List of Publications

Papers:

First author:

1. **Zhongping Li**, Ning Huang, Ka Hung Lee, Yu Feng, Shanshan Tao, Qiuhong Jiang, Yuki Nagao, Stephan Irle and Donglin Jiang. Light-emitting covalent organic frameworks: fluorescence improving via pinpoint surgery and selective switch-on sensing of anions. *J. Am. Chem. Soc.* **2018**, *140*, 12374.

Co-author:

1. Ping Wang, Qing Xu, **Zhongping Li**, Weiming Jiang, Qiuhong Jiang and Donglin Jiang. Exceptional iodine capture in two-dimensional covalent organic framework. *Adv. Mater*. **2018**, *30*, 1801991.
2. Xinyi Chen, Keyu Geng, Ruoyang Liu, Ke Tian Tan, Yifan Gong, **Zhongping Li**, Shanshan Tao, Qiuhong Jiang and Donglin Jiang. Covalent organic frameworks: chemical approaches to designer structures and built-in functions. *Angew. Chem. Int. Ed*. **2019**, 10.1002/anie.201904291.

Presentation in Conference:

1. Design and light-emitting functions of hydrazone-linked covalent organic frameworks. 日本化学会北陸地区講演会と研究発表会. **Dec. 2017**, Ishikawa, Japan. Style of Presentation: Poster.
2. Design and light-emitting functions of hydrazone-linked covalent organic frameworks. The 98th Annual Meeting. **Mar. 2018**, Funabashi, Japan. Style of Presentation: Oral.
3. Design and light-emitting functions of hydrazone-linked covalent organic frameworks. 10th Singapore International Chemistry Conference 2018 (SICC-10). **Dec. 2018**, Singapore. Style of Presentation: Poster.
4. Designing covalent organic frameworks for light emitting and anion sensing. The 99th Annual Meeting. **Mar. 2019**, Kobe, Japan Style of Presentation: Oral.

Acknowledgements

I wrote my thesis to express my gratitude to people who helped and supported me during the last three years in my research.

Firstly, my supervisors, Prof. Donglin Jiang, gave me profound academic thoughts and keen insights in the three years of study and life at Japan Advanced Institute of Science and Technology (JAIST) and National University of Singapore (NUS). Prof. Jiang also helped me to expand my thinking, and encouragement for my research. In short, many thanks to Prof. Jiang gave a profound influence to me on my career.

Then, I want to show my gratitude to Prof. Yuki Nagao. At June, 2018, I study in NUS as a visiting student following Prof. Jiang to continue my PhD research. During this period, Prof. Nagao patiently helped me with all the complicated issues that required by JAIST and NUS. Without his kindly help, I could not smoothly complete my research project on time.

I also thank to Prof. Noriyoshi Matsumi and Prof. Tatsuo Kaneko from JAIST, who help me finish minor research project. In particular, I would like to express sincere appreciation to Prof. Xiaoming Liu, Dr. He Li, Dr. Sigen A, Dr. Yuwei, Zhang, Mr. Yongfeng Zhi, Mr. Ziping Li, Ms. Xiaochen Shen, and Ms. Songjie Han from Jilin University, who gave me their support in measurements and daily life. I also want to show my gratitude to Prof. Stephan Irle and Mr. Ka Hung Lee form Oak Ridge National Laboratory (United States), who help me to calculate crystal structure of COFs. Moreover, Dr. Ning Huang and Mr. Chao Yang in our group contributed to PXRD simulation.

I also appreciate my friends and my lab mates Dr. Qiuhong Jiang, Dr. Yu Feng, Dr. Juan Li, Dr. Guangtong Wang, Dr. Ning Huang, Dr. Sasanka Dalapati, Dr. Enquan Jin, Dr Lipeng Zhai, Dr. Shanshan Tao, Dr. Ping Wang, Dr. Qing Xu, Dr. Ting He, Mr. Chao Yang, Mr. Weiming Jiang, Mr. Zhanzhao Li, Mr. Xiaozhu Zhong, Mr. Kengyu Geng, Mr. Ruoyang Liu, Mr. Mohammad Mahmudul Hasan, Mr. Xiaoyi Xu, Mr. Dishen Zhang, Mr. Yuze Yao, Mr. Gang Du, Mr. Yongdong

Chen, Ms.Yuan Zhao, Ms. Yuta Komatsu, Mr. Kester TEO cheng hao, Ms. Umme Salma, Ms. Athchaya suwansoontron, Ms. Xinyi Chen, Ms. Ke Tian Tan, Ms. Yifan Gong, Ms. Dongjin, Wang, Ms. Miaomiao Liu, Ms. Wei Zhou, Ms. Xi Zhang and Ms. Yue Liang, who helped me a lot in the past three years.

I was fortunate to receive the financial supporting from Japan Student Services Organization (JASSO) for six months and Japan Society for the Promotion of Science (JSPS) for two years.

Last but not least, I must thank my family, grandmother, father, mother, uncle, aunt, brother, sister, and my dear friends in china. I could not smoothly complete my research without their supports and understanding.

Zhongping LI

Jul 02, 2019